Functional Molecular Monolayers

From Heterogeneous Self-Organization to Glycan Cantilever Array Sensors

Kathrin Gruber

München 2011

Functional Molecular Monolayers

From Heterogeneous Self-Organization to Glycan Cantilever Array Sensors

Kathrin Gruber

Doktorarbeit

an der Fakultät für Physik

Ludwig-Maximilians-Universität München

Juni 2011

Erstgutachter: Prof. Dr. J. O. Rädler

Zweitgutachter: PD Dr. S. Thalhammer

Tag der mündlichen Prüfung: 7. Februar 2012

Contents

Contents i

1 Zusammenfassung 1

2 Abstract 3

3 Introduction 5

3.1 Molecular Self-Organization 5

3.2 Bio-Recognition with Cantilever Array Sensors 7

3.3 The Glycome and Carbohydrate Interactions 8

3.4 Aims of this Thesis 9

4 Theoretical Concepts 11

4.1 Tunneling – The Modified Bardeen Approach 11

4.2 Beam Deflection – The Pure Bending 17

4.3 Cantilever Bending and Surface Stress – Stoney's Formula 21

4.4 Receptor Binding and Langmuir Analysis 23

5 Materials and Methods 25

5.1 Molecules, Proteins and Bacteria 25

5.2 Substrates and Substrate Preparation 29

5.3 Scanning Tunneling Microscopy 32

5.4 Cantilever Array Sensors 34

6 Unifying Host – Guest Inclusion and Templated Polymorph Assembly in One Molecular Compound 39

6.1 Independent Host Pattern and Host – Guest Inclusion 41

6.2 The Templated Polymorph Assembly 46
6.3 Assembly Mechanism 48
6.4 Conclusions 51
7 A Novel Glycan Cantilever Array Sensor 53
7.1 Specific Carbohydrate – Protein Detection Demonstrated with Concanavalin A in Nanomolar Sensitivity 54
7.2 Signal Origin, Strength and Evolution 63
7.3 Conclusions 69
8 Sensitive Detection of Anti-Viral Proteins and Pathogens with Glycan Cantilever Array Sensors 73
8.1 Specific Detection of Anti-viral Cyanovirin-N down to the Picomolar Level 74
8.2 Specific Detection of *Escherichia Coli* down to a few Cells per Sample 82
8.3 Conclusions 89
9 Conclusions and Future Prospects 91
9.1 Heterogeneous Molecular Self-Organization 91
9.2 Glycan Cantilever Array Sensors 92
9.3 Anti-Viral Protein and Bacteria Detection 93
References 95
List of Figures 109
Publications 111
Acknowledgments 113

1 Zusammenfassung

Diese Dissertation beschreibt die Einigung von zwei Organisationsprinzipien der heterogenen, molekularen Selbst-Organisation sowie den ersten Glykan Cantilever Array Sensor der in der Lage ist, klinisch relevante Proteine und Bakterien spezifisch bis hinunter zu geringsten Konzentrationen zu detektieren.

Selbstorganisierte Moleküllagen bieten einen komfortablen Weg um funktionale Oberflächen herzustellen. Bis zum jetzigen Zeitpunkt mussten bei Systemen aus zwei oder mehreren Molekülsorten unterschiedliche Verbindungen gewählt werden um entweder eine Wirt – Gast Struktur oder ein polymorphes Templatsystem zu erzeugen. Ein Molekül des Fréchet Typs kombiniert nun diese beiden zuvor getrennten Kategorien. Durch die räumliche Trennung der Wechselwirkungstypen innerhalb der beiden molekularen Muster, eines Wirt – Gast System mit gesättigtem Adamantan oder einer Templatstruktur mit aromatischem Coronen, induziert der Gast eine der beiden Formen. Diese erste Beobachtung beider Mechanismen zusätzlich zu dem reinen Wirtssystems vereinigt diese vormals getrennten Motive der heterogenen, molekularen Selbst-Organisation in einer molekularen Verbindung. Dies erlaubt nun die Entwicklung von zweistufigen Abläufen innerhalb eines Protokolls.

Bis zu diesem Zeitpunkt konzentrierten sich die meisten Anwendungen von Cantilever Arrays in der Biosensorik auf Fragestellungen innerhalb des Genoms und des Proteoms, während Kohlehydratstrukturen weitestgehend vernachlässigt wurden. Die Bedeutung des Glykoms in biologischen Abläufen sowie in diagnostischen und therapeutischen Anwendung gewinnt jedoch immer mehr an Bedeutung da Synthesetechnologien und Sequenzierverfahren laufend verbessert werden. Die Etablierung eines rein auf Zuckerstrukturen basierten Glykan Cantilever Array Sensors in dieser Dissertation erlaubt nun auch mit den

Vorteilen dieser Technik die markierungsfreie und spezifische Detektion von verschiedenen Zucker bindenden Proteinen und Mikroorganismen gegen eine *in-situ* Referenz bis hin zu niedrigsten Konzentrationen. Der Sensor erkennt das Mannose spezifische Lektin Concanavalin A (ConA) auf Nonamannose und Trimannose Sensoren gegenüber einer nichtspezifischen Galaktose Referenz und unterscheidet die individuellen Kohlehydratstrukturen durch Signalgrößen entsprechend ihrer Fähigkeit multivalente und mehrseitige Bindungen einzugehen. Die beobachtete Sensitivität im nanomolaren Bereich und die ermittelte Dissoziationskonstante des Systems zeigen sich in guter Übereinstimmung mit der Literatur. Die Spezifität der Proteinbindung wurde mit Hilfe von kompetitiver Inhibition und durch eine Messung im Hintergrund von nichtspezifischem bovinem Serumalbumin (BSA) bestätigt. Diese Sensitivität, Konzentrationsabhängigkeit und Spezifität der Erkennung etablieren somit Cantilever Array Sensoren auf dem Gebiet der Zucker – Protein Wechselwirkungen.

Die Anwendung dieses Glykan Cantilever Array Sensors zur Detektion von klinisch relevanten Proteinen und Bakterien demonstriert die Nützlichkeit des Systems. Das Protein Cyanovirin-N (CV-N) zeigt starke anti-virale Aktivität gegen das Human Immunodefizienz – Virus (HI-V) und konnte bis hinunter zu pikomolaren Konzentrationen detektiert werden. Diese Sensitivität sowie die Dissoziationskonstante des Systems stimmen gut mit Literaturwerten überein. Die Spezifität der Zucker – Protein Erkennung wurde durch kompetitive Inhibition und den Vergleich mit nichtspezifischen BSA verifiziert. In einer weiteren Studie wurde die Erkennung von Pathogenen durch Messungen an den drei *Escherichia coli* (*E.coli*) Stämmen ORN178, ORN208 und ORN206 gezeigt. Dadurch wird das Detektionsvermögen des Sensors erfolgreich von Proteinen auf Bakterien erweitert. Alle drei Stämme konnten nach ihrer Fähigkeit Mannose zu binden, unterschieden und bis hinunter zu sehr geringen 20 Zellen pro Probenvolumen spezifisch detektiert werden. Zusammen führen diese Resultate die Cantilever Array Technik als sensitive und spezifische Methode für die Detektion von Zucker – Protein Wechselwirkungen und Bakterien ein. Mit den zusätzlichen Vorteilen wie markierungsfreier Detektion und kurzen Messzeiten könnte dieses System mit geringem Aufwand auf ein breites Spektrum weiterer Zucker Interaktionen für Arzneimittel Tests und diagnostische Anwendungen erweitert werden.

2 Abstract

This thesis describes the unification of two assembly principles for two dimensional heterogeneous molecular orderings as well as the first glycan cantilever array sensor that specifically detects clinically relevant proteins and bacteria down to very low concentrations.

Self-organized molecular monolayers offer a convenient way to create functional surfaces. For multi component systems, up to date different host components had to be selected for host-guest inclusion or templated polymorph assemblies. A Fréchet type molecule now combines these two previously separated forms in heterogeneous molecular self-organization. The decision which assembly form is realized thereby depends on the type of guest molecule. By spatially separating the interaction types within the pattern, a host – guest assembly with saturated adamantane or a templated structure with aromatic coronene, the guest induces one of these forms of heterogeneous assembly. This first observation of all three material functions, the pure host assembly, host – guest inclusion and templated polymorph assembly, unifies these different assembly mechanisms within one molecular compound. It now allows for the design of two-step protocols that link the previously separated motifs in heterogeneous molecular self-organization.

Up to now most applications of cantilever arrays in biosensing applications focused on questions within the genome and proteome while carbohydrates were largely neglected. The importance of the glycome in biological functions as well as diagnostic and therapeutic applications however is rapidly gaining focus as synthesis and sequencing technologies for carbohydrate structures progress. The establishment of a purely glycan based cantilever array sensor in this thesis now allows the label-free and specific detection of several carbohydrate binding proteins and microorganisms against an *in-situ* reference down to very low

concentrations. The sensor accurately recognizes the mannose specific lectin Concanavalin A (ConA) on nonamannose and trimannose functionalized cantilevers against a galactose reference and discriminates individual carbohydrate structures *via* larger and smaller signal sizes corresponding to their affinity for multivalent and multisite binding. The demonstrated sensitivity in the nanomolar range and a value for the dissociation constant compare well to literature reports. Finally, the specificity of the protein binding was validated by a competitive inhibition assay and by measuring in the background of nonspecific bovine serum albumin (BSA). This demonstrated sensitivity, concentration dependence and specificity of the recognition establish the first successful carbohydrate based cantilever array sensor.

The application of this new the glycan cantilever array sensor to clinically relevant proteins and bacteria demonstrates the feasibility of the system. The protein Cyanovirin-N (CV-N) has been shown to have potent anti-viral activity as it binds and inhibits the human deficiency virus (HI-V). CV-N detection in picomolar sensitivity and the derived dissociation constant agree well with literature reports. The specificity of the carbohydrate – protein recognition was verified *via* competitive inhibition and the comparison to nonspecific BSA. In a further study, pathogen detection was demonstrated by use of the three *Escherichia coli* (*E. coli*) strains ORN178, ORN208 and ORN206, successfully extending the sensor's detection capabilities from proteins to bacteria. All three strains could be discriminated according to their mannose binding ability and specifically detected down to about 20 cells per sample volume. These results introduce the cantilever array technique as sensitive and specific sensing tool for carbohydrate – protein and bacteria recognition. With its additional advantages of label-free detection and fast response times, this system could easily be optimized to include a wide range of further carbohydrate interactions relevant drug testing and diagnostic applications.

3 Introduction

The development of new methods and tools catalyzes progress in the biochemical sciences.[1] Coupled to advancements in biomolecular sequencing techniques and the purification of proteins with new functionalities, novel biosensing applications aim at specific target recognition at low detection limits.[2-4] Here cantilever array sensors present an innovative and label free method that transduces biomolecular recognition processes into a nanomechanical deflection of tiny silicon springs.[5] Sophisticated concepts for the creation of the active sensing layers heavily rely on the control and feasibility of the patterning approach. Bottom-up processes like self-assembly describe a convenient method to realize various such surface functionalities and tailor chosen pattern properties. Images recorded with scanning tunneling microscopy in submolecular resolution offer ideal conditions to study the intricate details of self-organized monolayers and the responsible assembly mechanisms.

3.1 Molecular Self-Organization

Self-assembly is one of nature's ways to induce order. This phenomenon describes a process by which a pattern emerges solely by the interplay of the lower-level components of a system.[6] In contrast to the top-down approach that requires advanced technologies to miniaturize a predefined structure, this so-called bottom-up approach provides an elegant way for engineering nano-patterned surfaces.

Self-organized molecular monolayers offer a variety of phenomena that are actively under study, the various fields of interest comprise surface catalysis and chirality,[7] prediction and control over pattern formation[8, 9] and the growth of active layers for biosensing.[2, 10] One recent trend in molecular self-assembly

goes to increasingly complex systems assembled from more than one molecular species.[11] Usually, one of two distinct ordering categories results from these heterogeneous molecular systems: host-guest inclusion or templated polymorph assembly.

In host-guest systems the pre-existing host pattern remains unchanged upon the addition of guest molecules and the guests are incorporated into inherent cavities of the host assembly.[12-15] This method offers control over behavior and reactivity of the included functional molecules due to selectivity and spatial confinement of the included guest species.[11]

In contrast, templated polymorph structures rearrange after the addition of the guest molecules to the host structure and thus template a previously unobserved ordering motif.[16-19] This switching into a new ordering is accompanied by changed symmetries and intermolecular distances of the molecular layer.

In the past the host structure for either selective host-guest inclusion or for conformational switching into a new templated assembly could only be realized by choosing different molecular compounds. The crucial link, a structure that combines both functionalities and allows host-guest as well as templated structures, is missing. Such a compound would allow confinement as well as switching within one molecular system and merge both functionalities in one convenient setup. Subsequent application of both processes would provide access to a variety of two step protocols within one molecular material.

One main goal in the study of heterogeneous molecular layers is to bring specific functionalities to a surface and use the molecules as an active layer for chemical and biochemical applications.[2, 7, 10, 20] For these implementations, strong chemical bonds between sensing molecules and the sensor surface are desired to robustly anchor the molecular layer. Thiol groups attached *via* a polyethylene glycol (PEG) or alkane linker provide a stable self-assembly of the functional molecular moieties on a gold coated surface. Other methods employ so-called “click-chemistry” to enable surface functionalization in a two-step process or silanization of silicon surfaces.

In the past, such functional molecular layers have been used in biosensors based on microarrays, quartz crystal microbalance (QCM) and surface plasmon resonance (SPR) and have shown their potential for high throughput sensing

applications.[2] Recently, cantilever array sensors evolved as sensitive and label free alternative sensing method.

3.2 Bio-Recognition with Cantilever Array Sensors

The cantilever sensor technique is closely related to the more widespread atomic force microscopy (AFM), using the same silicon levers of micrometer dimensions to transduce the measurement signal. Typically the AFM uses a very sharp tip attached to the end of such a lever to image a surface contour of constant force in a scanning motion. It thereby relies on exchange interactions like van der Waals, electrostatic or frictional forces[21] where the lever's bending at each point is read out by the deflection of a laser beam focused on the lever apex. Complementary to these applications such cantilevers are also employed for force spectroscopy to characterize the force – distance relationship of individual tip – substrate interactions.[21]

In 1994 R. R. Schlittler and co-workers published the first application that uses the surface of these levers itself as a sensor for chemical reactions.[22] The cantilever deflection corresponding to the respective analyte concentrations again is read out *via* beam deflection, similar as for the AFM. Some measurement setups today also utilize a pirezoresistive readout that relies on elements in the microcantilever structure changing their resistance in response to an applied strain.[23] Able to operate in vacuum, air or liquids, the cantilever technique has proven its value as very sensitive mass sensor and as powerful, label-free transducer of biomolecular recognition into a nanometer deflection signal.[24, 25]

Picomolar concentrations of mRNA in total RNA background[26] as well as a single base pair mismatch of two ssDNA strands can be detected.[27, 28] Cells,[29] microorganisms[30], various pathogens[31] and lipids[32] have been investigated using cantilever sensors. Antibiotic-peptide recognition has been probed[33] while immunosensors detect the specific recognition of prostate-specific antigen (PSA) in the presence of human serum albumin.[34] While the majority of these results focuses on the genome and the proteome, the glycome and studies investigating specific carbohydrate – ligand interactions are still largely neglected.

3.3 The Glycome and Carbohydrate Interactions

Many carbohydrate structures in nature occur as glycoconjugates in the form of glycoproteins, proteoglycans and glycolipids and as such are mainly found on the cell surface of organisms.[35] There these cell surface glycans regulate the interactions of the cell with the extracellular environment. In particular carbohydrate – protein interactions are crucial to most mammalian physiological processes as mediators of cell adhesion and signal transduction, and organizers of protein interactions.[36-38] Interestingly, also the surfaces of bacteria, viruses and parasites are decorated with carbohydrates and specific glycans have been localized on the surface of many infectious agents and also cancer cells.[39] Several of these carbohydrate structures are recognized by the immune system and consequently glycans possess an enormous but underexplored potential for eukaryotes, prokaryotes and viruses as both diagnostic and therapeutic targets.[40, 41]. Many carbohydrate structures are unique, which could indicate the possibility of undiscovered biological properties. In addition, these unusual glycans show promise as a safe, fast and reliable means to screen for the presence of cancer cells and pathogens.[39]

Recent advances in technologies for sequencing and synthesizing carbohydrate structures revealed the structural complexity of the glycome to be more diverse than that of the genome and proteome.[42, 43] However the functions of many glycans are as yet unknown. To gain insight into the biological significance of these carbohydrates, more than the pure knowledge about glycan structures is necessary and glycan behaviors have to be analyzed in detail both biochemically and microbiologically. In recent years, pioneering glycobiologists have developed sophisticated technologies to efficiently measure carbohydrate – protein interactions, such as glycan microarrays.[44-48] However, further complementary technologies with fast response time and low cost are necessary to identify specific carbohydrate binding partners for successful progress in the emerging field of functional glycomics. Here the cantilever array technique with advantages like label-free detection and short measurement times could offer valuable input if a glycan sensor for clinical relevant protein and pathogens could be established.

3.4 Aims of this Thesis

In light of the above discussed state of scientific research, the following scientific goals could be envisioned:

- *A combination of host-guest inclusion and the templated ordering motif for Fréchet dendron assemblies.*

To this end, guest molecules of differing assembly properties should be chosen for heterogeneous assemblies with a Fréchet type dendron. The resulting patterns would be observed with STM and analyzed with complementary computational modeling techniques. The resulting observations on the pattern formation should be examined according to the type of included guest molecule and lead to a general rule for the assembly process.

- *An application of the cantilever array technique in functional glycomics.*

Various carbohydrate assemblies could be tested and optimized as active layers for cantilever array sensing. As a crucial indicator for a sensor's quality, the sensitivity, concentration dependence and specificity of the binding should be established. Complementary measurements with nonspecific binding partners and additional test assays could aid to verify the quality of the cantilever array sensor setup and the specificity of the biomolecular recognition.

- *The specific and sensitive recognition of clinically or biologically relevant proteins and pathogens with a glycan cantilever array sensor.*

To be of value, the previously established glycan cantilever array sensor would need to prove its capabilities for the detection of relevant biomolecular interactions. Here again the sensitivity, concentration dependence and specificity of the binding need to be tested to ensure the usefulness and quality of the sensor setup.

4 Theoretical Concepts

The pattern formation of self-organized molecular monolayers is studied with scanning tunneling microscopy (STM). This technique is based on the quantum mechanical tunnel effect. Aiming at a more realistic description, the Modified Bardeen Approach (MBA) adds perturbation theoretical contributions to the calculated tunneling current to account for the interaction of substrate and tip.

The detection of carbohydrate interactions with cantilever array sensors can be considered on the basis of three theoretical concepts. In a first approach the nanomechanical deflection of a cantilever sensor can be described as pure bending of a straight beam. Then, Stoney's equation gives a relation between the measured deflection and the surface stress generated on the cantilever surface due to the recognition of the sample substance. Finally, the degree of cantilever deflection in dependence on the sample concentration can be evaluated by a Langmuir isotherm analysis.

4.1 Tunneling – The Modified Bardeen Approach

A typical STM measurement is performed with very short tip – substrate distances of about 1-10 angstrom (Å) from mechanical contact. To provide an accurate theory of the tunneling phenomenon, van der Waals forces between tip and substrate as well as the exchange interaction itself have to be considered. The modification of the undisturbed wave functions of tip and substrate by the van der Waals force can be treated by a stationary-state perturbation calculation. Following the method of Oppenheimer and Bardeen,[49] the process of quantum transmission can then be treated by time-dependent perturbation theory.

An energy schematic of the tip-substrate system is depicted in figure 4.1. For the perturbation calculations describing the van-der-Waals force, a separation surface is drawn between tip and substrate. The potentials for the two subsystems of substrate (S) and tip (T), U_S and U_T, are then defined to satisfy the following two conditions: First, the sum of the potentials of the two subsystems equals the potential U of the combined system

$$U_S + U_T = U. \tag{4.1}$$

Outside of the interaction region where the potential barrier is substantially lowered, the potential equals the reference point of energy, the vacuum level. Thus, second, the product of the two potentials of the two subsystems equals zero in the entire space

$$U_S\, U_T = 0 \tag{4.2}$$

Figure 4.1 c) shows the free and disturbed potentials of the substrate, U_{S0} and U_S, respectively. If the perturbation potential $V_S = U_{S0} - U_S$ is known in terms of the free and disturbed potentials of the substrate, U_{S0} and U_S, respectively, time-independent perturbation theory can be applied to derive the perturbed wave functions ψ_μ. In principle though, the wave functions are solutions of the Schrödinger equation

$$(T + U_S)\psi_\mu = E_\mu \psi_\mu \tag{4.3}$$

where $T = -(\frac{\hbar}{2m})^2 \nabla^2$ denotes the kinetic energy operator.
The same is true for the tip with the free and distrurbed potentials U_{T0} and U_T, respectively, see figure 4.1 d). Again the Schrödinger equation delivers the stationary states, here called χ_ν

$$(T + U_T)\chi_\nu = E_\nu \chi_\nu \tag{4.4}$$

Knowing the modified wave functions ψ_μ and χ_ν, the two subsystems can once again be brought together. As a first step the time-dependent Schrödinger equation provides the wave function of the complete system. Using time-dependent perturbation theory the transition probability can then be determined from its expansion coefficients. In first-order perturbation theory this transition probability is also known as Fermi's Golden Rule.

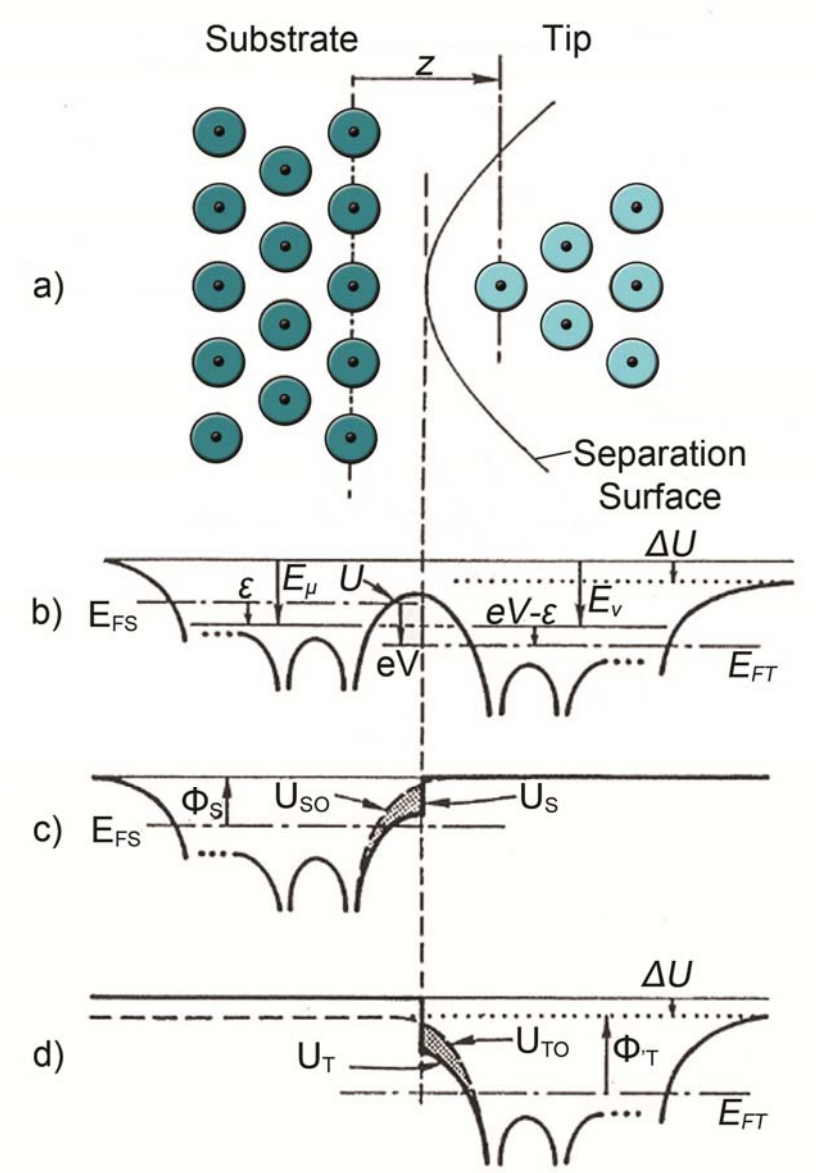

Figure 4.1. Perturbation Approach at the Tip-Sample Interface. a) Atoms of the tip and surface subsystems with b) corresponding energy scheme depicting the potential surface of the complete system. Here E_{FS} and E_{FT} refer to the Fermi level, E_μ and E_v to the energy levels of substrate and tip, respectively. U denotes the potential of the complete system. c-d) Disturbed and undisturbed potentials of substrate and tip, respectively.

At the beginning of the calculation each subsystem is in its disturbed but stationary state, as described above. Without loss of generality, the following considerations are conducted from the perspective of the surface. At $t > 0$ the

perturbation potential of the tip U_T is switched on and the complete system starts to evolve according to the time-dependent Schrödinger equation

$$i\hbar\frac{\partial\Psi}{\partial \mathrm{t}} = (T + U_S + U_T)\Psi \tag{4.5}$$

Since the tip wave functions constitute a complete and orthogonal set of states, the time-dependent wave function Ψ of the combined system can be expanded in terms of the χ_ν:

$$\Psi = \sum_\nu a_\nu(t)\chi_\nu e^{-\frac{iE_\nu t}{\hbar}} \tag{4.6}$$

At t = 0, the state of the system still should be ψ_μ, thus the expansion coefficients will have to be

$$a_\nu(t) = \langle\chi_\nu|\psi_\mu\rangle e^{-\frac{i(E_\mu - E_\nu)t}{\hbar}} + c_\nu(t) \tag{4.7}$$

with $c_\nu(0) = 0$. Substituting eq. (4.7) for eq. (4.6) then leads to the following form of the wave function Ψ of the combined system:

$$\Psi = \psi_\mu e^{-\frac{iE_\mu t}{\hbar}} + \sum_\nu c_\nu(t)\chi_\nu e^{-\frac{iE_\nu t}{\hbar}} \tag{4.8}$$

The first term describes how Ψ would evolve if U_T would not have been switched on, the second term describes the aberration induced by U_T.
Finally, to get an expression for the $c_\nu(t)$, eq. (4.8) again has to be substituted for eq. (4.5), resulting in the term

$$i\hbar\dot{c}_\nu(t) = \langle\chi_\nu|U_T|\psi_\mu\rangle e^{-\frac{i(E_\mu - E_\nu)t}{\hbar}} + \sum_\lambda\langle\chi_\nu|U_S|\chi_\lambda\rangle c_\lambda(t)e^{-\frac{i(E_\lambda - E_\nu)t}{\hbar}} \tag{4.9}$$

The transition probability from a state ψ_μ of the substrate to a state χ_ν of the tip, $P_{\mu\nu}$, can now be derived from the expansion coefficients $c_\nu(t)$:

$$P_{\psi_\mu\to\chi_\nu} = P_{\mu\nu} = \left|\int_0^t \dot{c}_\nu(t)dt\right|^2 \tag{4.10}$$

Finally, the transition rate $\omega_{\mu\nu}$ in first order perturbation theory is given by P/τ and its calculation leads to Fermi's Golden Rule

$$\omega_{\mu\nu}^{(1)} = \frac{2\pi}{\hbar}\left|M_{\mu\nu}\right|^2\frac{dN}{dE} \tag{4.11}$$

with the tunneling matrix element

$$M_{\mu\nu} = \left\langle \chi_\nu \middle| U_T \middle| \psi_\mu \right\rangle = \int_{V_{Tip}} \chi_\nu^* \, U_T \psi_\mu \, dV_{Tip} \qquad (4.12)$$

For the calculation of the tunneling current I all states of the tip and the substrate including their respective occupation probabilities have to be taken into account, as well as the interplay of states described by the matrix element $M_{\mu\nu}$.

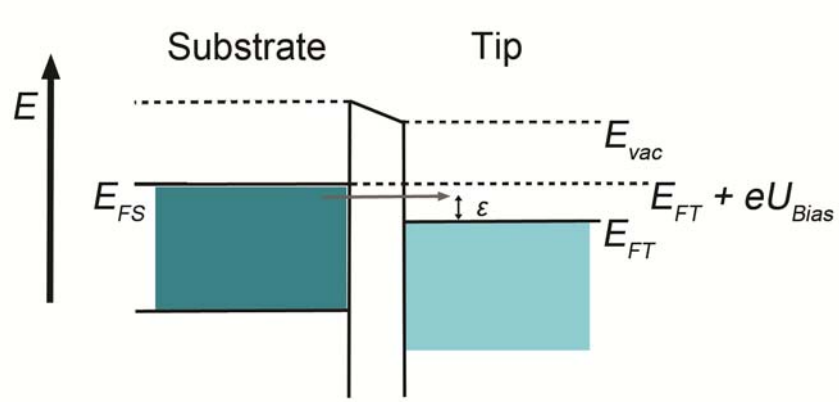

Figure 4.2. The Tunneling Current. The energy of a state is measured in reference to the Fermi level E_F of substrate (S) and tip (T). At an arbitrary energy ε, electrons can tunnel from an occupied state of the substrate into an unoccupied state of the tip, case (i), or vice versa, case (ii) (not shown).

For an arbitrary energy level ε the contribution of the states of substrate (S) and tip (T) to the tunneling current corresponds to the density of states (DOS) ρ, resulting in the factors

$$\rho_S(E_{FS} - eU + \varepsilon) \qquad (4.13)$$

$$\rho_T(E_{FT} + \varepsilon) \qquad (4.14)$$

where E_{FS} and E_{FT} denote the Fermi level E_F of the substrate and tip, respectively. To find an expression for the occupation probabilities, the tunneling current is divided into two parts: (i) transition from an occupied state of the surface to an unoccupied state of the tip, see figure 4.2, and (ii) transition from an occupied state of the tip to an unoccupied state of the surface.

If the Fermi-Energy is used as the reference level, the occupation probabilities F for (i) are then given by:

$$F_{\rightarrow} = f_S(\varepsilon - eU)[1 - f_T(\varepsilon)] \qquad (4.15)$$

with the Fermi-Dirac distribution

$$f(E) = \frac{1}{1+e^{\frac{E-E_F}{kT}}} \tag{4.16}$$

Whereas for the transition in the reverse direction (ii), the occupation probabilities are:

$$F_{\leftarrow} = f_T(\varepsilon)[1 - f_S(\varepsilon - eU)] \tag{4.17}$$

Consequently, the factor containing the total occupation probabilities from process (i) and (ii) reads:

$$F_{\rightarrow} - F_{\leftarrow} = f_S(\varepsilon - eU) - f_T(\varepsilon) \tag{4.18}$$

Finally, including the fact that there are two spin states, the expression for the total tunneling current is given by:

$$I = \frac{4\pi e}{\hbar}\int_{-\infty}^{\infty}[f_S(E_{FS} - eU + \varepsilon) - f_T(E_{FS} + \varepsilon)] \cdot \rho_S(E_{FS} - eU + \varepsilon)\rho_T(E_{FS} + \varepsilon)|M|^2 d\varepsilon \tag{4.19}$$

In good approximation the matrix element M depends exponentially on the tip-substrate distance, explaining the atomic resolution of the STM. Only the outermost atom at the apex of the tip contributes significantly to the tunneling current while adjacent atoms add little to the signal.

Assuming a simplified tip geometry, Tersoff and Hamann could apply this approach to demonstrate the ability of the STM to measure a surface of constant density of states near the Fermi level for certain metallic samples.[50] Although today there are more sophisticated approaches available,[51] for an adequate explanation of the atomic resolution of the STM, C. J. Chen expanded Tersoff and Hamann's description of the tip geometry to include so-called dangling bond states. The Modified Bardeen Approach (MBA) has since proven its value for the interpretation of scanning tunneling microscopy images of molecular adsorbates.[52]

For molecular assemblies studied with Scanning Tunneling Microscopy (STM), it is expected that electrons can tunnel from the highest occupied molecular orbital (HOMO) into the lowest unoccupied orbital of the tip or from

highest occupied orbital of the tip into the lowest unoccupied molecular orbital (LUMO) of the substrate. The direction the quantum transition is then given by the sign of the applied bias. In most cases organic molecules possess a large energy gap between the HOMO and the LUMO. When physisorbed on a metal substrate the energy resonances derived from these orbitals are usually several electron Volts (eV) below and above the Fermi level of the substrate as described by Cyr *et al*.[53] Thus their contribution to the local density of states (LDOS) at the Fermi level of the substrate usually is rather small, clearly indicating that the influence of the substrate can never be neglected for the interpretation of STM images.

The electronic structure of the adsorbate-substrate system can be calculated for a theoretical simulation of the obtained STM tunneling current. The various applied techniques include effective Hückel approximations as well as first-principle self-consistent methods, mainly based on density functional theory (DFT).[54] DFT calculations in combination with the MBA for the tunneling current were successfully applied to explain experimental STM data as is shown by C. J. Chen.[52]

4.2 Beam Deflection – The Pure Bending

In its most basic way cantilever deflection can be described as pure bending of a straight beam with no additional axial, shear, or torsional forces from an isotropic and homogeneous material.[55] This concept is valid for infinitesimal deflections under the assumption that the width and height of the beam are small compared to its length. For these conditions a kinematic hypotheses dating back to J. Bernoulli (1654-1705) applies: The cross sections perpendicular to the beam's long axis (neutral axis) stay perpendicular to the deformed axis. If this is the case, the neutral surface does not change its length by the deformation and the beam bends into an arc with radius ρ, subtending an angle $d\varphi$. Thus an element at the neutral surface retains its length ds during deformation, while the length of a second segment of this element at a distance y to the neutral surface becomes ds^*. The strain ε_z of a beam can then be calculated in terms of ds, ds^* and their respective distance y, the radius of curvature ρ and the angle $d\varphi$:

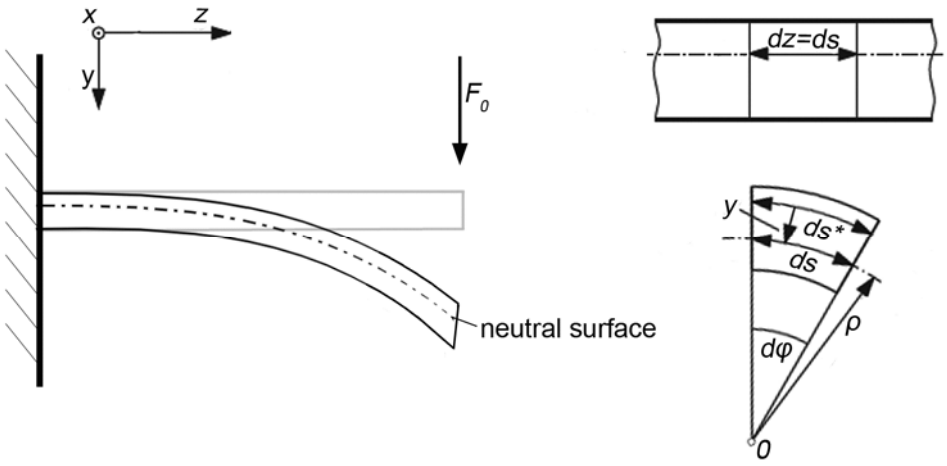

Figure 4.3. Pure Bending of a Cantilever Beam. Left: Schematic of a cantilever deflection under a force F_0. Right: Beam segment ds at radius ρ and deformation angle $d\varphi$ and segment ds* under strain. See text.

$$\varepsilon_r = \frac{ds - ds^*}{ds} = \frac{(\rho + y)d\varphi - \rho d\varphi}{\rho d\varphi} = \frac{y}{\rho} \tag{4.20}$$

For the here considered uniaxial stress σ_z Hooke's Law states:

$$\sigma_z = E\varepsilon_z \tag{4.21}$$

where E denotes the Young's modulus. Substitution equation (4.21) with (4.20) yields:

$$\sigma_z = E\frac{y}{\rho} \tag{4.22}$$

Considering that there are no longitudinal forces, the global balance of force in z-direction results in the following expression:

$$\int_A \sigma_z dA = 0$$

(4.23)

which can be converted with equation (4.22) to

$$\frac{E}{\rho}\int_A y dA = 0$$

(4.24)

since both the radius of curvature ρ and the Young's modulus E do not depend on the coordinate of distance y.

The corresponding torque M_b can be written with the help of equation (4.21) as:

$$M_b = \int_A y\sigma_z dA$$

(4.25)

Substituting equation (4.22) and considering the definition of the area moment of inertia for the x-axis $I_{xx} = \int_A y^2 dA$ leads to the following expression for the torque M_b in equation (4.25):

$$M_b = \frac{E}{\rho}\int_A y^2 = \frac{E}{\rho} I_{xx}$$

(4.26)

Finally, to link the radius of curvature ρ to the beam deflection, the relation

$$ds = \rho d\varphi$$

(4.27)

can be modified to

$$\frac{1}{\rho} = \frac{d\varphi}{ds} = \frac{\frac{d^2y}{d^2z}}{(\sqrt{1 + (\frac{dy}{dz})^2})^3}$$

(4.28)

For small deflections $\delta = -y$ compared to the beam dimensions, equation (2.28) combined with equation (4.26) yields the differential equation for the deflection curve:

$$\frac{1}{\rho} = -\frac{d^2\delta}{d^2z} = \frac{M_b}{EI_{xx}} \tag{4.29}$$

For comparison with the deflection of a cantilever sensor, the following considerations apply to a beam of length L fixed on one side when only ordinary bending is considered. Then, equation (4.29) can be simplified to:

$$EI\frac{d^2\delta}{d^2z} = -M_b \tag{4.30}$$

Now a force F_0 is applied at the free end of the beam. When the z-axis is aligned along the long axis of the beam, the corresponding torque can be written as:

$$M_b = -F_0 z \tag{4.31}$$

Substituting equation (4.31) for equation (4.30) and integrating two times with the integration constants C_1 and C_2 yields:

$$EI\frac{d\delta}{dz} = F_0\frac{z^2}{2} + C_1 \tag{4.32}$$

and

$$EI\delta = F_0\frac{z^3}{6} + C_1 z + C_2 \tag{4.33}$$

At the fixed end of the beam at $z = L$ the bending and torsion vanish:

$$\delta(L) = 0, \qquad \frac{d\delta}{dz}(L) = 0 \tag{4.34}$$

Inserting these boundary conditions in equations (4.32) and (4.33) yields the equation describing the beam deformation v at the free end of the beam at $z = 0$:

$$\delta(0) = \frac{F_0 L^3}{3EI} \tag{4.35}$$

The beam deflection δ depends on the material constants L, E and I as well as on the force F_0 applied at the free end of the beam. Any contributions from thin film coatings or thermic influences are neglected in this approach. Also, in most applications cantilever sensors are usually not subjected to a single point load at the free end.

For the detection of bio-interactions, cantilever sensors are usually coated with layer of sensing molecules and thus subjected to a uniform load when analyte binds. In this case the relation for the deflection of the free end $\delta(0)$ slightly differs from equation (4.35) and is given for a load by unit length w_0 by:[56]

$$\delta(0) = \frac{w_0 L^4}{8EI} \tag{4.36}$$

Typically this kind of bending results from surface stress that is induced by the analyte bending. A relation for the surface stress to the measured cantilever deflection is expressed by Stoney's Formula.

4.3 Cantilever Bending and Surface Stress – Stoney's Formula

For cantilever array sensors operated in the static mode, the deflection of the cantilever beam that arises upon analyte binding is measured. Adsorption of a thin film induces a difference in surface stress between top and bottom side of the beam that the cantilever relieves by bending. For the case of a steel strip with metallic coating and based on the following two equilibrium conditions:

$$F = \int_A \sigma_z dA = 0$$

$$M_b = \int_A y\sigma_z dA = 0$$

(4.37)

under the assumption that the adsorbed film is thin compared to substrate, G. G. Stoney in 1909 derived a formula that connects the surface stress P to the resulting radius of curvature r of the beam which is independent on the adsorbed mass.[57]

$$\frac{1}{r} = 6\frac{Pt}{Ed^2}$$

(4.38)

Here P denotes the surface stress due to a one sided coating of the beam, t is the thickness of the coating and d the thickness of the beam. The formula assumes a uniform film much smaller than the cantilever thickness.

This equation also assumes a uniaxial stress in the film. However for a cantilever sensor the width of the beam, though small compared to its length, is still much larger than the thickness of the coating. Therefore the stress in the film is biaxial and equation (4.38) needs to be corrected by a factor $(1 - \upsilon)$ with υ being the Poisson's ratio of the material:[58]

$$\frac{1}{r} = 6\frac{1-\upsilon}{Ed^2}(\Delta\sigma)$$

(4.39)

As is convention in literature, in equation (4.39) the surface stress P is exchanged for the stress per unit thickness of the coating $\Delta\sigma$ in units N/m that causes the deflection.[56] By use of the geometric relation

$$\frac{1}{r} = \frac{2\delta}{L^2}$$

(4.40)

the deflection δ of the cantilever beam can then be given in terms of the unit stress $\Delta\sigma$:

$$\delta = \frac{d^2}{3L^2}\frac{E}{(1-\upsilon)}\Delta\sigma \tag{4.41}$$

The cantilevers used in this thesis are 500 µm long and about 1 µm thick. The ratio $E/(1-\upsilon)$ between Young's modulus E and Poisson ratio υ for Si(100) has been calculated to 180 GPa.[59] Thus for a typical deflection of 125 nm measured for Cyanovirin-N – nonamannose recognition (see figure 7.8 in chapter 7.2) the surface stress responsible for the cantilever bending amounts to $\Delta\sigma = 30$ mN/m, which is comparable to results from other groups detecting protein binding with cantilever sensors.[33, 60]

Stoney's Formula (equation 4.38) assumes no interaction of the adsorbed particles and is only an exact solution for a beam that is unrestrained on all sides. For a measurement principle like cantilever array sensors, reading out beam deflection due to surface stress induced by biomolecular binding, the cantilever beam needs to be rigidly clamped on one side. Therefore some corrections have been derived in literature, taking into account the necessary boundary conditions[61] or other properties, for example the influence of the active layer by separating the chemical and elastic contributions to the surface stress.[62]

4.4 Receptor Binding and Langmuir Analysis

The adsorption of proteins and other biomolecules *via* molecular receptors induces surface stress and in turn cantilever bending. A quantitative evaluation of the signal size dependence on the sample concentration allows the determination of affinity constants that characterize the analyte – receptor binding. The subsequent comparison with literature then can be used to evaluate the quality of the achieved results and the sensor design.

For cantilever sensors the binding events take place on a surface, therefore not all protein binding sites are available as would be the case in solution assays. Thus, in a minimalistic model individual analyte – receptor binding events on the cantilever surface can be considered independent and unaffected by neighboring binding events (1:1 binding model). This approach includes one site specific binding and assumes that the concentration of bound protein is negligible in

comparison to the total protein concentration. Therefore concentration of non-bound protein equals the concentration of the injected protein concentration (c[protein] bound = c[protein] total). The dissociation constant (K_d), can then be determined by a Langmuir isotherm analysis. The Langmuir isotherm states:

$$\delta = a\frac{c}{K_d + c} \tag{4.43}$$

where δ is the measured deflection (maximum differential deflection), c is the sample concentration and a is a proportionality constant.

The actual fitting of the data to the Langmuir adsorption isotherm can then be performed by suitable software like the here used GraphPad Prism (version 5.03 for Windows, GraphPad Software, San Diego California USA, www.graphpad.com). Langmuir analyses have been successfully employed in cantilever array sensing for various protein – protein or DNA detection assays.[33, 63]

5 Materials and Methods

In this chapter the materials and methods used for this thesis are grouped according to the following categories: Chapter 5.1 describes all molecular compounds, proteins and bacteria. This group comprises the Fréchet dendrons and guests for the heterogeneous self-organization discussed in chapter 6 and the mannose specific proteins and *Escherichia coli* strains detected with the glycan cantilever array sensors that are discussed in chapters 7 and 8. Chapter 5.2 describes the substrates and preparation methods. It contains paragraphs about the graphite substrate used for scanning tunneling microscopy and the cantilever arrays employed for biosensing as well as the preparation procedures required for their respective experimental applications. Finally chapters 5.3 and 5.4 discuss the working principles of scanning tunneling microscopy and cantilever array sensing, respectively, the main techniques used for this work.

5.1 Molecules, Proteins and Bacteria

A **Fréchet Dendron Type Molecule** (**1**) (methyl (3-[3,5-bis(butyloxy-phenyl)methoxy]-5-[3,5-bis(octyloxyphenyl) methoxy] benzoate)[64, 65] was used to assemble host structures for the study of self-organized heterogeneous molecular monolayers. This compound consists of three phenyl rings at its molecular core. The outer rings are decorated with two octyl and two butyl alkane chains, respectively, which allow high conformational flexibility and van der Waals interactions with adjacent molecules during self-assembly. The middle phenyl ring carries an ester termination enabling the molecule to interact *via* electrostatic forces with its environment. The synthesis of these Fréchet

dendrons was conducted in the group of Professor E. Constable at the University of Basel, Switzerland.

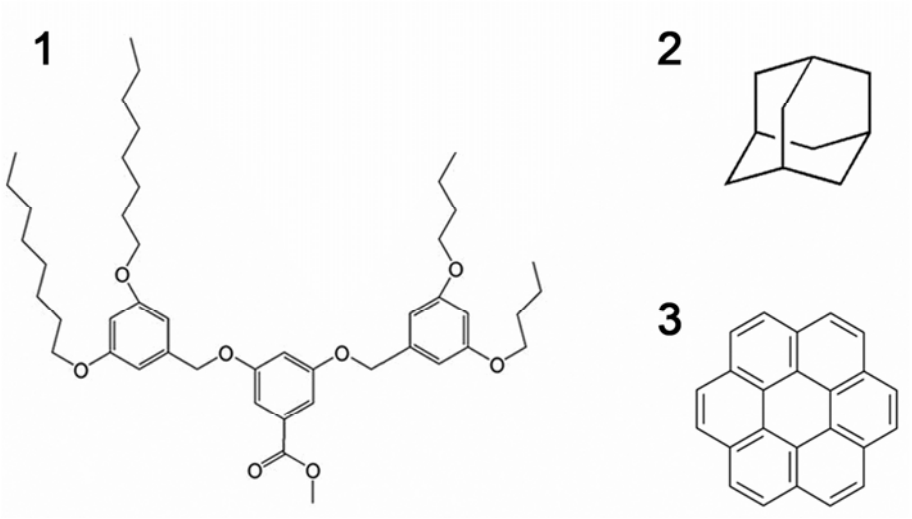

Figure 5.1. Molecular Structures for Heterogeneous Self-organization. A Fréchet type dendron (**1**) decorated with alkane chains at the outer of three phenyl rings is used to assemble the host pattern. Adamantane guests (**2**) were chosen as small saturated hydrocarbons, while coronene (**3**) represents a small aromatic hydrocarbon compound.

Adamantane[1] (**2**) and **Coronene**[1] (**2**) were chosen as guest molecules due to their small sizes and electronic properties. Adamantane is a very small diamondoid structure. As saturated hydrocarbon compound it is able to interact *via* van der Waals forces with its molecular environment in a self-organized pattern. The small coronene molecule carries aromatic hydrocarbon rings with a delocalized π-electron system. These electrons can be influenced by partial charges of adjacent molecules within the molecular monolayer. See figure 5.1 for both molecular structures.

For the coating of the cantilever array sensors, self-assembled monolayers of three different carbohydrate structures were employed to build up the sensing layers. Branched **Trimannoside** (**4**) and **Nonamannoside** (**5**) equipped with thiol linkers were chosen as specific binding partners for lectin and bacteria (see below) recognition. The nonamannose molecule contains three arms with three,

[1] Purchased from Sigma-Aldrich.

two and four mannose sugars and corresponds to a structure decorating gp120, a glycoprotein found on the surface of the Human Immunodeficiency Virus (HI-V).

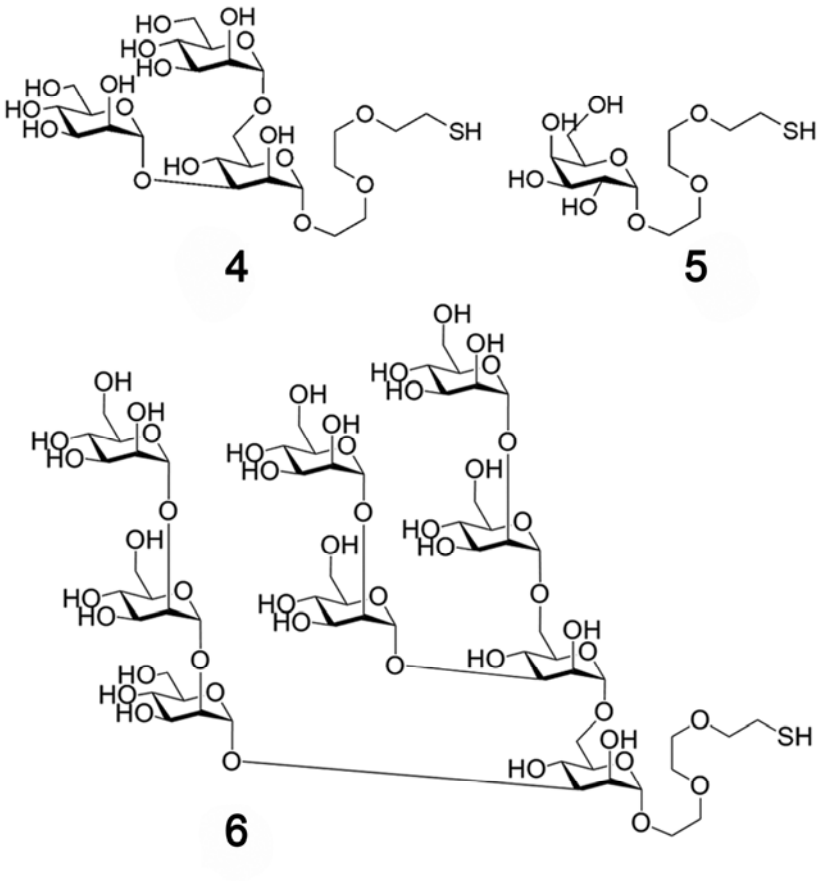

Figure 5.2. Carbohydrate Structures for Sensing Layers. A branched trimannose (**4**), a nonamannose containing three arms with three, two and four mannose sugars (**5**) and a monogalactose (**6**) structure, each equipped with a thiol linker, were used to coat the cantilever surface for specific and nonspecific binding of lectins and bacteria.

The individual mannose rings of trimannose and nonamannose are connected by glycosidic bonds. These can form between different carbon atoms of the sugar rings and as such are individually recognized by some mannose specific lectins like scytovirin,[66] see also chapter 8.1. Due to the larger structure of the nonamannose compared to the trimannose molecule, binding to more than one protein, so-called multivalent binding can occur.[67]

Galactoside (**6**) represents an ideal candidate to check nonspecific binding on the reference cantilevers as it is of similar structure but is not recognized by

mannose binding proteins. See figure 5.2 all three carbohydrate structures. The synthesis of these carbohydrate structures was conducted in the group of Professor P. H. Seeberger currently located at the Max Planck Institute of Colloids and Interfaces in Berlin, Germany.

The specificity and sensitivity of the carbohydrate sensing layers was tested with the lectins **Concanavalin A**[2] (ConA) and **Cyanovirin-N**[3] (CV-N).

The 104 kD lectin ConA was chosen as a model system due to its well characterized properties as a widely used standard protein. At neutral to basic pH values ConA has a tetrameric structure of four identical subunits. Each monomer bears one highly specific mannose binding site so that ConA can bind up to four ligands under ideal conditions.[68]

CV-N is an 11 kDa protein isolated from cyanobacteria. It has been shown to have potent anti-viral activity by recognizing mannosides on gp120, the heavily glycosylated envelope protein of the Human Immunodeficiency Virus (HIV).[69, 70] CV–N irreversibly attaches to the nonamannose arms on gp120, thus preventing the conformational changes necessary for HIV-cell fusion.[67] The CV-N protein folds in a 2-fold pseudo-symmetry with two distinct mannose binding sites that allow multi-site binding for up to two ligands.[71]

Strain	Description	Reference
ORN178	thr-1 leuB thi-1 Δ (argF-lac) U169 xyl-7 ara-13 mtl-2 gal-6 rpsL tonA2 supE44 pilG1 Pil^+ Tc^r	[72]
ORN208	thr-1 leuB thi-1 Δ (argF-lac) U169 xyl-7 ara-13 mtl-2 gal-6 rpsL tonA2 supE44 λ^r pilG1 Pil^+ except fimH::kan with adjacent tetR, Nal^r	[73]
ORN206	Δ (lac-proAB) supE thi/F´ $lacI^q$ Z Δ M15 traD36 proAB except Δ (fimBEACDFGH) and recA13 Kan^r	[74]

Table 5.1: *E. coli* bacterial strains used for specific and nonspecific carbohydrate recognition.

For the detection of microorganism three strands of *Escherichia coli* (*E. coli*) with slight modifications were employed. While strain ORN178 carries the

[2] Purchased from Sigma-Aldrich.
[3] Kind gift from B. O'Keefe, Laboratory of Drug Discovery Research and Development, Division of Basic Sciences, National Cancer Institute, Frederick, Maryland.

mannose specific protein FimH at its pilii, the deletion mutant ORN208 expresses abnormal type I pilii with the nonbinding protein FimH*. The strain ORN206 finally is completely stripped of pilii, see table 5.1. All three of these *E. coli* strains are equipped with the phosphotransferase system (PTS) for carbohydrate uptake.[75, 76] The transporters of the PTS are able to recognize mannose[77] and galactose moieties.

The *E.coli* strains ORN178, ORN208 and ORN206 were grown overnight in LB Medium at 37°C, diluted to an optical density of 0.1 and then resuspended in medium. After reaching an optical density of 1, the cultures were spun down twice for five minutes at 1900 *x* g and then resuspended in Tris buffer (10 mM Tris, pH 7.7, 100 mM NaCl, 1 mM $CaCl_2$ and 0.005% Tween-20) to inhibit further growth. The individual samples were then diluted to the desired concentrations immediately before each measurement was taken. The measurements on bacterial recognition with glycan cantilever array sensors were conducted by Andreas Mader during the course of his diploma thesis. A more detailed description about the preparation of the *E.coli* samples can be found there.[78]

5.2 Substrates and Substrate Preparation

The self-organization of heterogeneous molecular monolayers was investigated on **Highly Oriented Pyrolytic Graphite (HOPG)**. HOPG is a suitable substrate for scanning tunneling microscopy under ambient conditions since it is inert as well as conducting in these cases. It is built as a multilayer crystal with a unit cell size of 0,246 nm from hexagonal rings of sp2 hybridized carbon, stacked in an ABA sequence, that give rise to atomically flat terraces of several hundred nanometers in size. Weak π-interactions between consecutive layers allow the preparation of clean HOPG surfaces for consecutive experiments by lifting off the top layers with adhesive tape. Physisorption *via* π-stacking and van der Waals interactions of the molecules deposited on the crystal surface facilitates the self-organization process and stabilizes the molecular ordering.

The ABA stacking of the graphite layers leads to a difference in conductivity between adjacent carbon atoms which is visible in STM images. This effect results from the fact that only every second atom has a nearest neighbor in the layer below.[79] The stacking of consecutive layers can also lead to several

other defects that can disturb the measurements, the most frequently observed being the Moiré pattern.[80]

There are several methods available to apply molecular layers onto a substrate surface, these include thermal evaporation[81] and molecular film deposition by the Langmuir-Blodgett method[82] or at the liquid/solid interface.[83] A simple and elegant way requiring only millimolar molecular concentrations is **Solution Casting**, a method also suitable for experiments under ambient conditions. Dissolving the compounds in a slowly evaporating solvent, a droplet of the solution is placed on the crystal surface. The measurements are then taken only after the solvent has completely evaporated, in the best case leaving behind a molecular monolayer in the middle area of the previous droplet.[84]

Although the molecules "self-assemble" with no external help other than the chosen solvent and ambient conditions, the experience of groups working in the field of molecular self-organization often shows that the finding of the correct preparation protocols for such molecular layers is not straight forward.[4] After several weeks testing with slow and fast evaporating solvents and examining concentration ranges from 0.1 mM to 20 mM, the here the self-assembled monolayers of the Fréchet dendrons finally could be applied from solutions in hexane or toluene solvent in concentrations from 0.2 to 0.4 mM. For the host-guest inclusion, adamantane was added in in hexane (8 mM). To induce the templated polymorph assemblies, coronene was dissolved in toluene (2 mM) due to solubility. In both cases the guest molecules could be added in the same solution as the Fréchet dendrons or applied in successive, evaporating droplets with the same results.

The **Cantilever Arrays**[5] used here for biosensor experiments consist of a chip with eight individual silicon cantilevers (500 µm x 100 µm x 1 µm) on a support with spring constants of 0.05 N m^{-1}. They are coated on the upper side with a 3 nm titanium adhesion layer followed by a 20 nm layer of gold to allow the anchoring of functional molecules *via* a thiol linker.

The development of efficient protocols for the **Cantilever Functionalization** is crucial for the operation and quality of the sensor results. For new systems they are not easily transferable from established cantilever

[4] Private Communications.
[5] Purchased (with gold coating) from Concentris GmbH, Switzerland.

assays and can take considerable time. For example the successful development of the standardized DNA Detection Kit that is commercially available from Concentris GmbH, Switzerland, took about two years effort.[6] Thus unsurprisingly several months had to be dedicated at optimizing buffer salt composition and concentrations, carbohydrate concentrations, cantilever cleaning and coating procedures for the more complex system building up the glycan cantilever array sensor presented in this work.

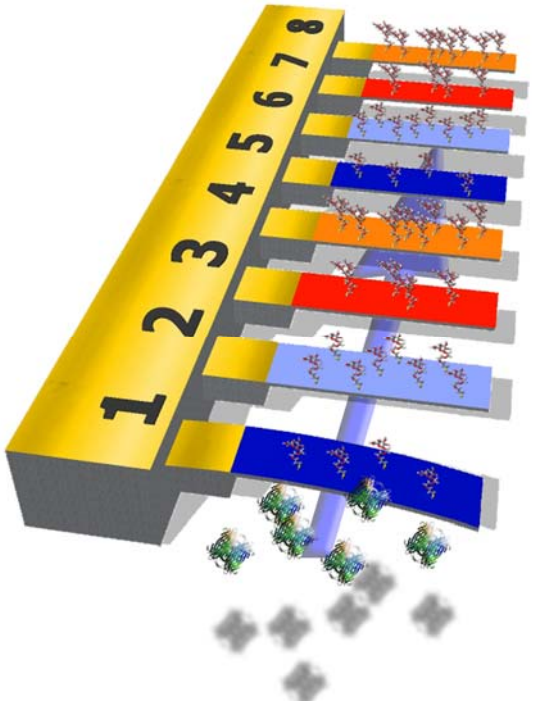

Figure 5.3. Functionalization of a Cantilever Array Sensor. Specific (reds) and nonspecific (blues) carbohydrate layers in sparse (lighter colors) and denser layers (darker colors) are employed in parallel to gain an online reference.

The following protocol for the creation of carbohydrate active layer could be established: To remove possible residues from organic molecules, all arrays were exposed to a UV-Ozone atmosphere for about 45 minutes immediately before applying the functional sensing layer. This treatment was observed to be critical for a good carbohydrate assembly and subsequent protein recognition. Under an optical microscope the individual cantilevers are inserted in glass capillaries filled with the carbohydrate solutions (40 µM in 10 mM Tris buffer,

[6] Private Communication.

pH 7.7). During times between 7 and 25 minutes the carbohydrate structures self-assemble on the cantilever surface by forming a thiol bond with the gold coating and thus effectively creating the sensing layer, see figure 5.3 for an illustration. Within these times no differences of the specific protein binding between longer and shorter incubation times, corresponding to denser and more sparse coatings, could be observed, see the discussion in chapter 7.2.

The individual cantilevers of an array are usually coated with specific (reds) and nonspecific (blues) carbohydrate coatings of lower and higher densities, compare the lighter and darker colors in figure 5.3, respectively. In this way, all eight parallel channels can be exploited to gain an *in-situ* reference. Usually the different carbohydrate coatings are applied in an alternating fashion to counteract any effects due to the time shift of sample arrival on the individual cantilevers that arises from the slow buffer flow through the measurement chamber.

Before the actual cantilever sensing experiments, all arrays were tested for quality variations due to fabrication and/or coating. Slight changes in temperature in the measurement chamber (e.g. from 22° C to 25° C) induce a deflection that is due to the bimetallic makeup of the cantilevers between the silicon array and the gold coating. The larger coefficient of thermal expansion of the gold coating on top of the silicon cantilevers should induce downwards bending when the temperature rises, and upwards bending, when the temperature drops. Thus, when all cantilevers behave in a comparable way, artifacts caused by fabrication or functionalization procedures can be excluded.[85] The behavior of the individual arrays can be monitored via optical beam deflection inside the Cantisens Research Platform as is described in chapter 5.4. Only arrays with comparable performance were then used for further detection experiments.

5.3 Scanning Tunneling Microscopy

With the invention of the scanning tunneling microscope (STM) in 1982 by G. Binnig and H. Rohrer it became possible to image surfaces at atomic resolution for the first time.[86, 87] Beyond visualization and characterization of materials and their properties like standing electron waves[88, 89] or spin polarization[90], scanning tunneling microscopy was and is employed to study

atomic and molecular adlayers,[91] the induction of chemical reactions,[92] surface chirality[93] and conformational switching.[94-96]

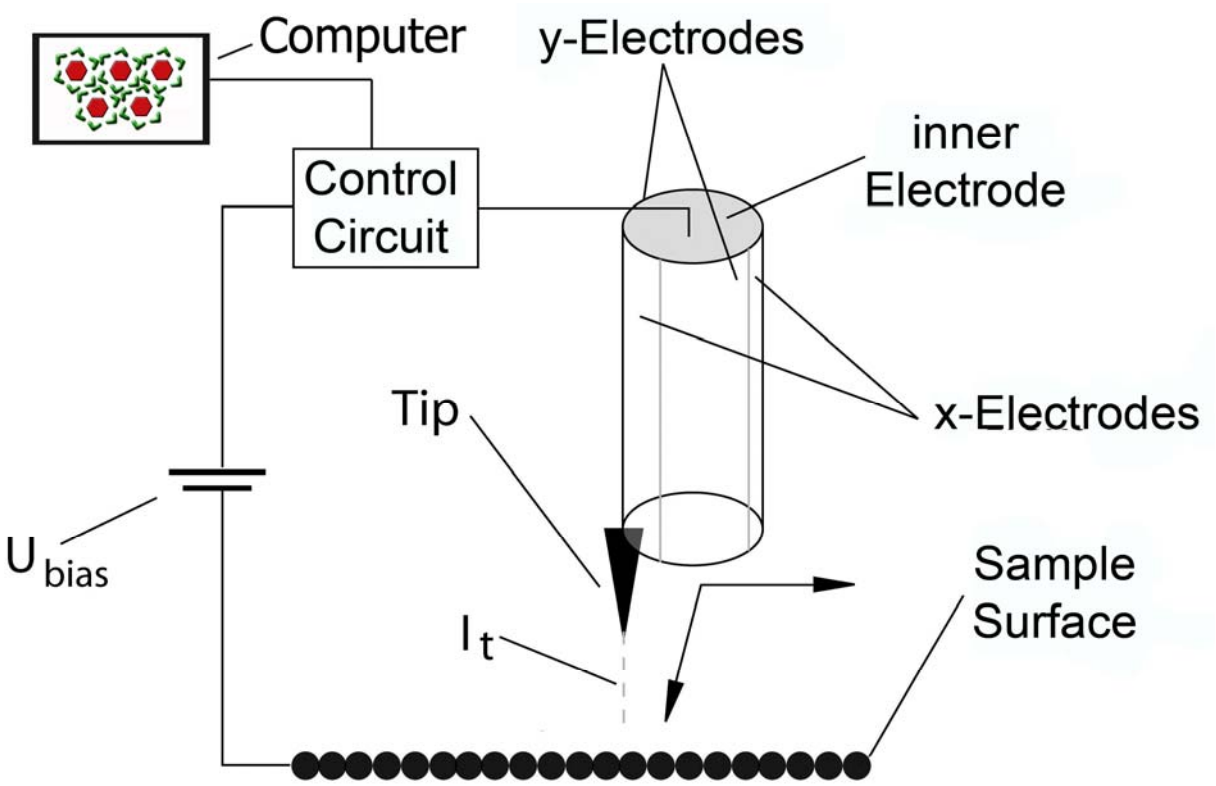

Figure 5.4. Scheme of a Scanning Tunneling Microscope. Electrons can tunnel through the small distance between the surface and the atomically sharp tip due to an applied bias voltage U_{Bias}, which results a pico ampere current I_T. To keep the tunneling current constant a feedback loop adjusts the position of the tip *via* piezo elements. The piezo movement representing the surface image is recorded and depicted on a computer screen.

The working principle of the STM is based on the quantum mechanical tunneling effect, see also chapter 4.1. This extremely short ranged interaction supplies precise height information convoluted with a contour of constant local density of electronic substrate states (LDOS) near the Fermi level.[97] The measured tunneling current between probe and surface is inversely exponential to the tip – surface distance and typically in the range of pico- to some nano-Ampère.

The positioning of the tip above the sample substrate is realized with piezo-actuators that allow sub-angstrom precision, see figure 5.4. Images

typically of the size of 512 *x* 512 pixels are then recorded by a scanning movement across the surface where values are taken at intervals of equal distance. During the measurement a feedback loop, usually a proportional-integral-derivative (PID) control circuit, is employed to correct the z-position of the tip and thus keep the tunneling current at the chosen set point.

The STM measurements for this thesis were conducted on a commercial Nanoscope III Multimode from Digital Instruments, USA, at room temperature under ambient conditions. All images were acquired with a constant tunneling current (constant current mode) with a low current scan head that in combination with a preamplifier allows tunneling currents down to the pico ampère range. The employed STM tips were mechanically cut from a Pt/Ir wire.

All acquired images were flattened to correct for the tilt of the substrate and equalized to enhance the contrast. When indicated, sections were correlation averaged and corrected for thermal drift.

5.4 Cantilever Array Sensors

Since the advent of the scanning tunneling microscope (STM) in 1982 by G. Binnig and H. Rohrer[86, 87] various spin-off developments brought to light successful techniques like the atomic force microscope (AFM) and cantilever sensors. While STM and AFM use very sharp tips to probe nanoscale features on flat materials, the cantilever sensor technique utilizes the surface of an AFM lever itself as a reaction vessel for (bio)chemical interactions. With advantages like label-free detection, fast response times, *in-situ* referencing and small sample concentrations the cantilever array technique has gained acceptance as very sensitive method for various biosensing applications,[26-34] see also chapter 3.2 for some prominent examples.

The functionalization of the cantilever surface with an active layer for sample recognition is typically done by thiol chemistry *via* self-assembly with thiolated molecules on a gold coating, see also chapter 5.2 for the arrays used in this thesis, or by silane chemistry and attachment *via* silanization on the pure silicon array.[3]

There are two typical modes of operation for cantilever sensors. In the dynamic mode, very small changes in mass due to material adsorption can be detected by the corresponding change in resonant frequency.[56] The static mode

takes advantage of the cantilever bending due to surface stress. Here the recognition of analyte by receptor molecules immobilized on the cantilever surface and the subsequent adhesion leads to steric and/or electrostatic interactions within the adsorbate layer. The resulting surface stress in turn is relieved by the cantilever bending and is measured in real-time and as a function of the amount of material adsorbed,[24] compare also chapter 4.3. In principle both the dynamic and the static mode can be operated simultaneously, however stiffness changes resulting from anlyte binding have been shown to affect the resonant frequency shift measured in the dynamic mode and need to be carefully considered.[98]

In principle cantilever sensor assays can be realized by using an AFM cantilever and the corresponding measurement setup. A more advanced approach takes advantage of an automated liquid handling system to control the buffer and sample flow. Here arrays with eight individual cantilevers are employed to gain eight parallel measurement channels for *in-situ* referencing. The Cantilever Array Sensor measurements for this thesis were performed in the static mode on a commercial Cantisens sensor platform from Concentris GmbH, Switzerland. The device contains a measurement cell of 5 µL and is operated by an automated liquid handling system under continuous buffer flow. To this end, the buffer is continuously pulled through the system by a pump with a volume of 500 µl, see figure 5.5. Using a small syringe the sample solution for each measurement is injected into a short piece of tubing called the sample loop. A valve allows switching between the buffer reservoir on the left of figure 5.5 and the sample tubing at any chosen time to introduce the sample solution to the measurement chamber. The length of time until the entire sample has passed the measurement chamber is dependent on the size and length of the sample loop and the operating speed of the pump. For this work a sample loop with a volume of 100 µL was employed.

After functionalization, the cantilever array is mounted in a sensor cartridge inside the measurement cell and kept under a continuous flow of running buffer (10 mM Tris, pH 7.7, 100 mM NaCl, 1 mM $CaCl_2$ and 0.005% Tween-20) at a speed of 0.42 µL/sec and a temperature of 22°C. An integrated temperature control with extra pre-heating stage for the injected sample maintains the temperature setpoint with a stability of 0.01°C. The array then is equilibrated under these conditions for several hours until the transient

molecular rearrangements taking place on the cantilever surface result in a constant drift of the sensor signal.[99] Only then the measurement signals due to analyte binding can be separated from these effects and be interpreted correctly.

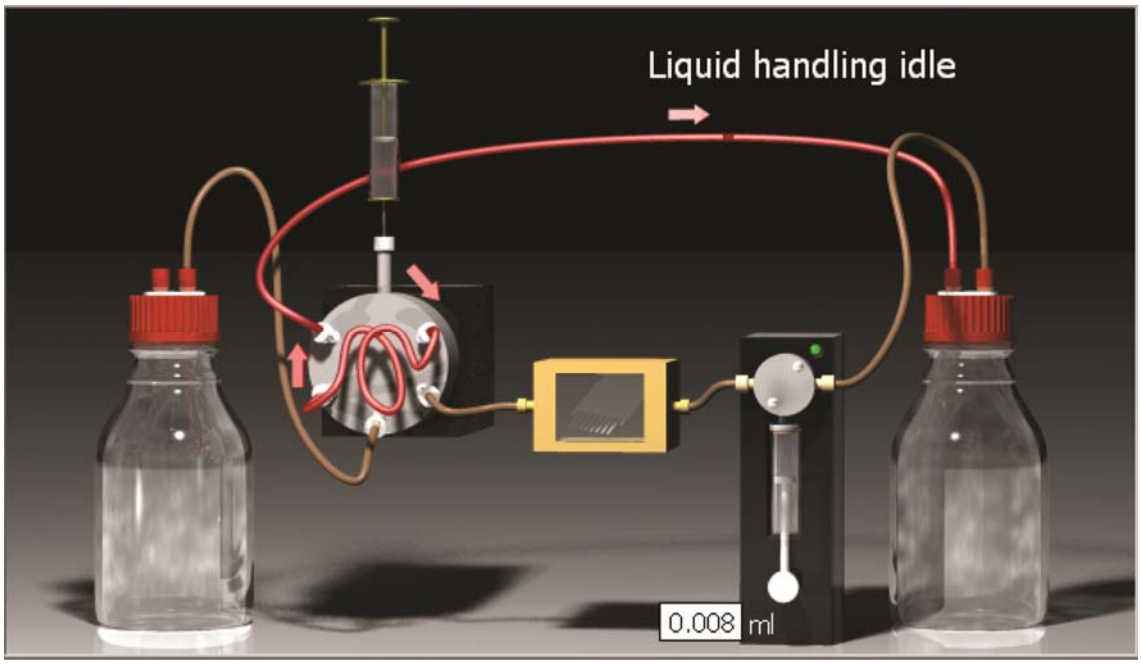

Figure 5.5. The Liquid Handling System of the Cantisens Research Platform. The buffer flow and sample injections are controlled *via* an automated liquid handling system which is operated under constant flow. The buffer is continuously pulled through the system by the pump depicted on the right before reaching the waste container. The sample solution is injected *via* a syringe into the sample loop (small red tube). A valve is employed to switch between the buffer reservoir on the left and the sample loop to introduce the sample solution to the measurement chamber. Reprinted with permission from Concentris GmbH, Switzerland.

The nanometer sized deflection of each of the eight individual cantilevers of an array upon analyte binding is detected in real time by sampling the deflection of a laser beam emitted from an array of eight parallel VCSELs (Vertical Cavity Surface Emitting Lasers) *via* a position sensitive photodetector (PSD). See figure 5.6 for a schematic of this optical readout method. For all experiments very low noise was observed, the signal-to-noise ratio remained well above 3 to 1 even for the detection of picomolar protein concentrations. A LabView™ based

software provided by Concentris GmbH, Switzerland is employed for instrument control and signal processing.

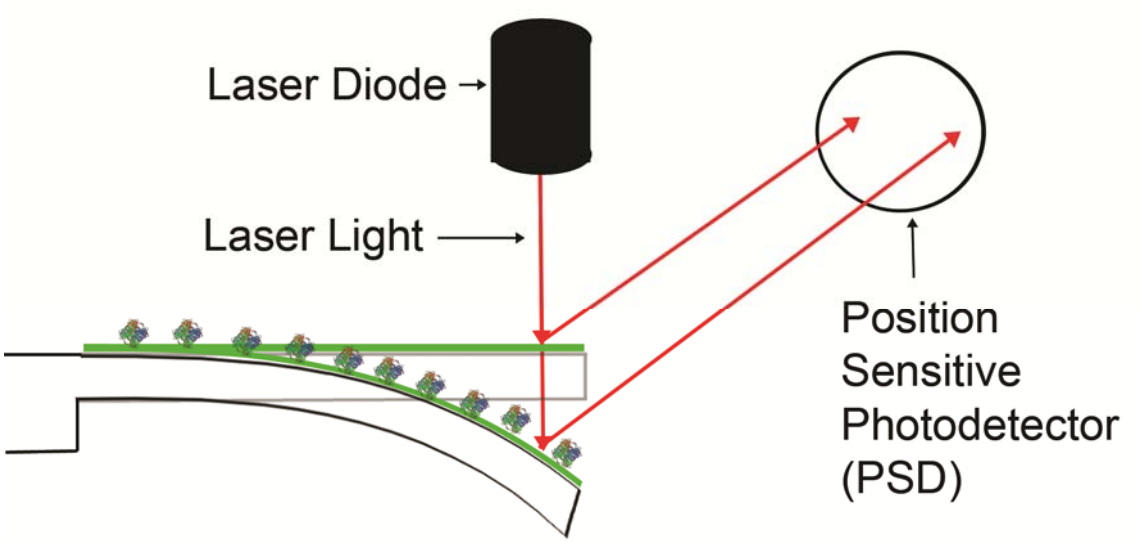

Figure 5.6. Optical Readout Method for Cantilever Deflection. The nanometer sized deflection of the cantilever beam induced by analyte binding is read out with a position sensitive photodetector (PSD) that tracks the deflection of a laser beam focused on the cantilever apex.

The signal curves depicted in chapters 7 and 8 were corrected for constant drift when needed. Where indicated, the signals of identically functionalized cantilevers were *averaged*. The *differential* signals, which are related to the specific part of the sample binding, were calculated by subtracting the nonspecific reference from the specific recognition signal.

6 Unifying Host – Guest Inclusion and Templated Polymorph Assembly in One Molecular Compound

This chapter describes the first observation of host – guest inclusion and a templated polymorph assembly from one molecular compound, unifying these two previously separated categories in heterogeneous molecular self-organization. This material functionality is explained by the Fréchet dendron molecule striving to separate the different interaction types within the two heterogeneous patterns. Parts of these results have been published.[100]

Molecular self-organization is one of the favored ways to create functional nanostructures from a bottom-up approach. Here weak intermolecular forces like van der Waals and dipole interactions allow for the high flexibility and self-healing capability needed for an efficient pattern formation. The interest in two dimensional self-assembled monolayers comprises areas such as surface catalysis, control over pattern formation and the growth of active layers for biosensing.[2, 7-10]

In our previous work we demonstrated that Fréchet dendrons assemble with the largest pattern variety observed in 2D molecular self-organization up to date. We expended substantial effort to understand the rules and mechanisms guiding the assembly process.[101] We could explain the surprising phase variety by the molecules' high conformational freedom which leads to the first occurrence of a multi-hierarchical assembly found in this field.[102] For a family of Fréchet dendron molecules with increasing structural complexity, we could

relate the resulting increasingly rugged energy landscape to the emergence of additional, transient states.[103]

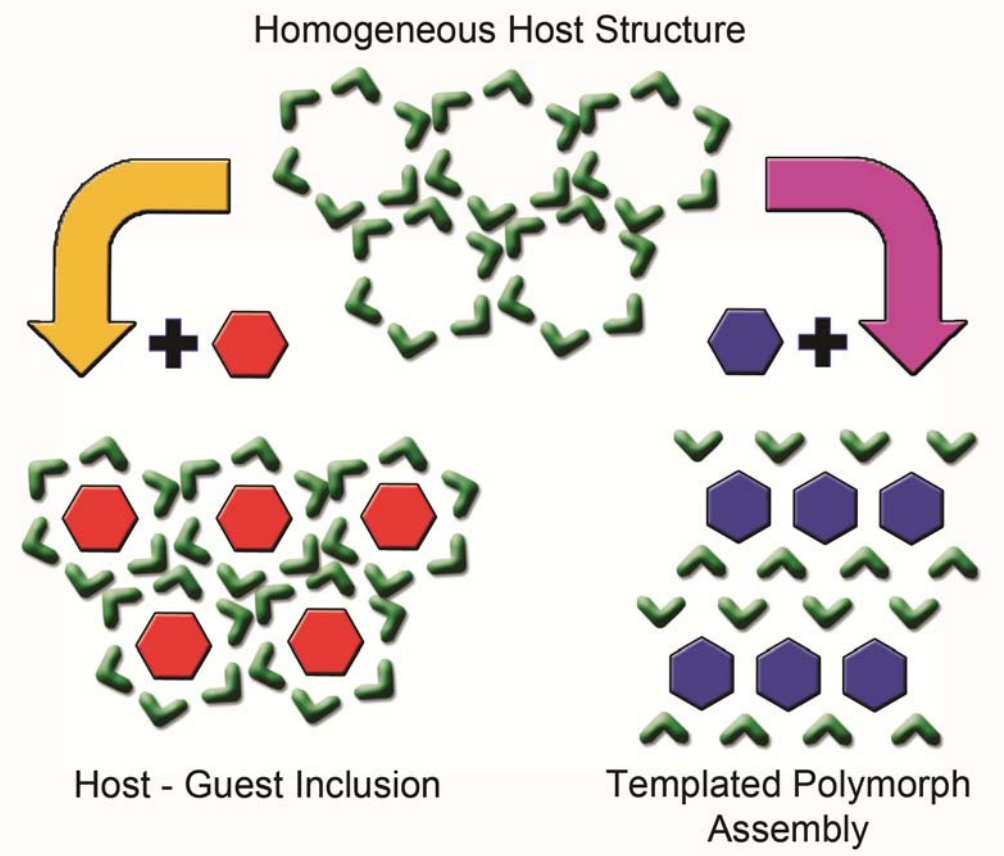

Figure 6.1. Assembly Motifs in Heterogeneous Molecular Self-Organization. An open porous network assembled from the host molecules (green boomerang shapes) is the prerequisite to host-guest inclusion (orange arrow). Here the ordering of the host molecules remains unchanged when the guests (red hexagons) are co-assembled. A templated polymorph assembly (pink arrow) occurs when the interactions with the added guests (blue hexagons) induce a new molecular ordering.

As an approach to predict the various local and global ordering motifs of Fréchet dendron self-organization, we developed an interaction-site model that condenses the essential molecular properties. Monte Carlo computations for this model successfully confirm that only basic properties of the molecular building blocks, namely geometry and a few salient weak interaction sites, encode these assembly motifs.[104-106] The predictive powers of the interaction site modeling also held for surfaces modifies with *n*-alkanes. In subsequent experiments we

could verify the resulting changes in pattern symmetry, orientation and hierarchical assembly.[105, 107]

Equipped with these foundations in the assembly principles of Fréchet dendrons, we sought to test the material's potential to create functional layers and focused on application in heterogeneous molecular assemblies. Recent efforts in molecular self-organization focus on these increasingly complex systems that are assembled from more than one molecular compound.[11, 108] The reported heterogeneous structures to date can be divided into two categories: host – guest inclusion (orange assembly pathway in figure 6.1), where the guest molecule are incorporated into pre-existing cavities with no resulting change to the host pattern, and templated polymorph assemblies (pink assembly pathway in figure 6.1), where the guest induces a new molecular ordering. Previously a molecular host species could only form assembly types of either one category. The missing link, a molecule that combines both assembly forms like the green boomerang shaped structure in figure 6.1, would enable the development of two-step processes and thus provide a new material functionality.

An approach to unify both assembly forms of heterogeneous self-organization would need to demonstrate three molecular orderings: A pure host structure containing cavities for possible selective guest inclusion, a host – guest assembly with unchanged unit cell parameters and a templated polymorph pattern which is not observed for the pure host compound. Finally, an explanation for the observed orderings should be provided.

6.1 Independent Host Pattern and Host – Guest Inclusion

This work takes heterogeneous molecular self-organization one step ahead of the latest results by De Feyter and co-workers, who showed an existing but still empty host pattern[109] and a templated assembly[16] from one molecular species. Here, the first compound, a Fréchet type dendron, is demonstrated that is able to organize in all three assembly forms: an empty host pattern with cavities, guest inclusion inside these pores and a templated new polymorph ordering.

At first, pure assemblies from four closely related Fréchet dendron molecules were studied in order to determine an appropriate host pattern with

open, and preferably empty, cavities as prerequisite for host – guest assembly. These Fréchet dendrons all contain three phenyl rings at their molecular core, the middle ring carrying an ester termination, and are equipped with two octyl chains on one side. The length of the decoration at the opposite end, and thereby the entire width of the molecule, varies from two dodecyl, two octyl and two butyl chains down to a simple alcohol group. More chemical details exemplified for the butyl decorated Fréchet dendron are given in chapter 5.1.

The assemblies of the four Fréchet dendron compounds, deposited on highly oriented pyrolytic graphite (HOPG) *via* solution casting from a hexane solution, were investigated using high resolution scanning tunneling microscopy at room temperature and under ambient conditions. Hexagonal structures were observed for all four molecules, see figures 6.1 a)-d) for the compounds in the order with decreasing size as listed above. The bright moieties in these STM measurements correspond to the molecular backbone. Three connecting dots are attributed to the three phenyl rings of one Fréchet dendron with a higher tunneling probability due to their π-electron system. The darker areas in the measurement are occupied by the less conductive alkane chains or represent empty areas.

It is immediately notable that the patterns in figures 6.2 a)-c) show an open porous network. Three of the molecules here assemble in a triangular fashion, while six of these triangles form a hexagon and build a honeycomb like pattern. In contrast, for the alcohol decorated Fréchet dendrons in figure 6.2 d) there are no cavities present. At a closer look at the dendrons decorated with dodecyl and octyl chains, the pores in figures 6.2 a) and b) do not appear to be empty and the observed contrast within is attributed to freely rotating molecules.

Figure 6.2 (next page). Hole Size Engineering. a)-d): STM images for four related Fréchet dendrons with decreasing molecular size show decreasing pore diameters. U_{Bias} = -800 mV and Current Setpoint: $|I_T|$ = 8 pA. e)-h): Corresponding MM energy minimizations confirm the interpretation of the molecular ordering. For the compound in c) and g) the cavities remain empty from self-inclusion, marking it a suitable candidate to study host – guest inclusion. See text.

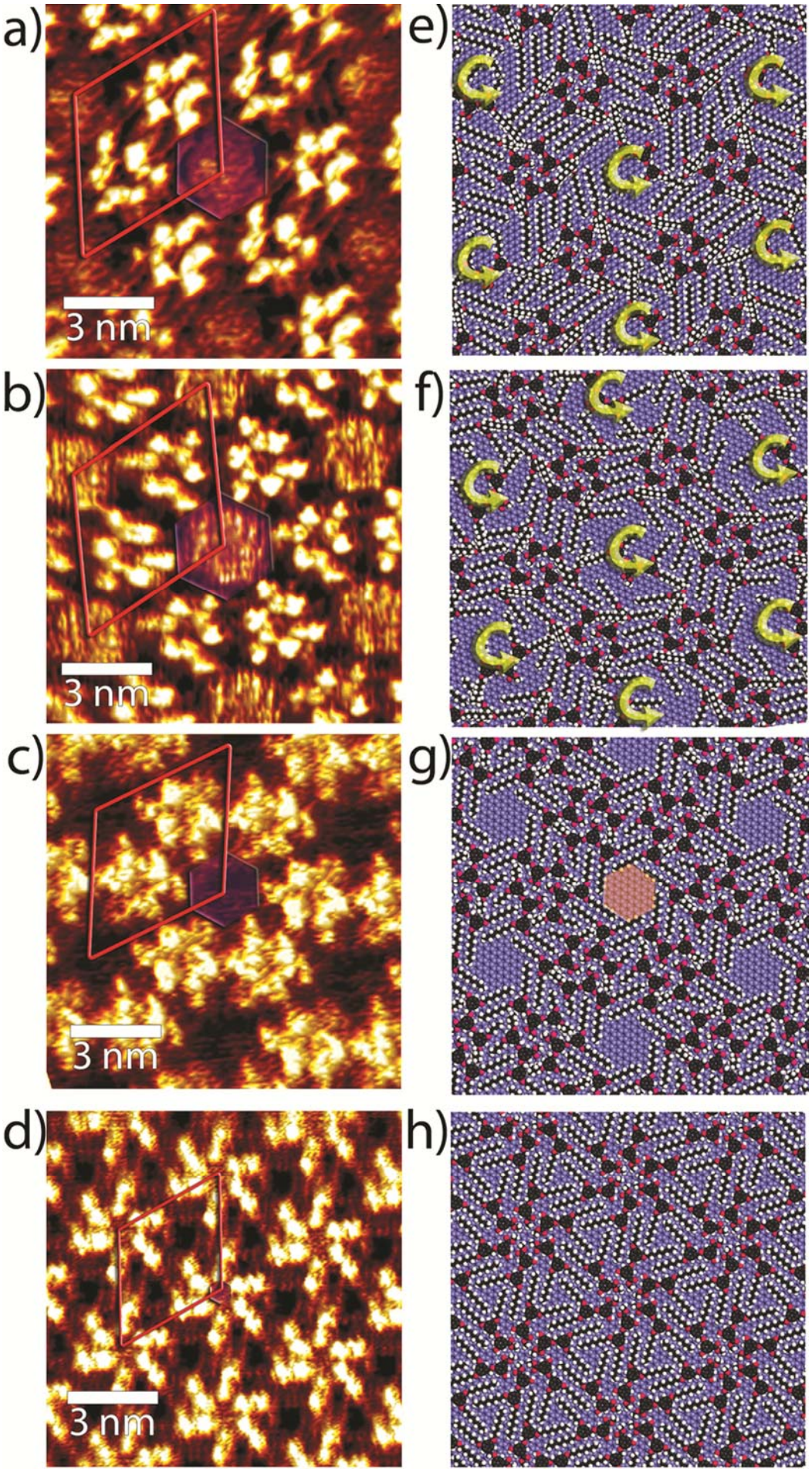
a)
3 nm
e)
b)
3 nm
f)
c)
3 nm
g)
d)
3 nm
h)

Corresponding molecular mechanics (MM) energy minimizations[7] for each of the four patterns were conducted to verify the interpretation of the molecular ordering. The depicted simulations in figures 6.2 e)-h) show a good fit to the measurements in figures 6.2 a)-d). When regarding the cavities of each pattern, the honeycomb structures for the dodecyl and octyl decorated molecules in figures 6.2 e) and f) allow the enclosure of a further Fréchet dendron while the cavities of the butyl decorated molecule, figure 6.2 g), are smaller and remain empty. The pattern for the alcohol decorated Fréchet dendron in figure 6.2 h) finally does not exhibit pores at all. Evaluating these observations, the Fréchet dendrons decorated with dodecyl and octyl chains were ruled out as suitable host compound for further study of heterogeneous self-organization due to their already filled cavities. Similarly the assembly of the alcohol decorated molecule was dismissed as it does not fulfill the prerequisite of a porous structure. The remaining molecule, the butyl decorated Fréchet dendron, however organizes in a porous network with empty cavities and thus represents the ideal candidate heterogeneous assemblies.

For a closer look at the honeycomb pattern of the butyl decorated Fréchet dendron the pore size in a high resolution image was determined to a diameter of 1.3 nm. The *p6* symmetric unit cell (a1 = a2 = 4.7 nm, ∢=60.8°) is shown in figure 6.3 a) alongside the corresponding MM energy minimization (enthalpy per area = 187.1 kJ mol^{-1} nm^{-2}). Again, the bright moieties in the measurement correspond to the molecular backbone while the darker areas in the measurement are occupied by the alkane chains of the Fréchet dendrons or represent the empty middle of the pores, as is illustrated by the MM energy minimization.

To realize heterogeneous assemblies for this Fréchet dendron compound, first adamantane molecules, a small saturated compound, see chapter 5.1, was added to the assembly. After letting the hexane solvent evaporate, the host pattern dimensions and unit cell parameters (a1 = a2 = 4.7 nm, ∢=60.4°) remain unchanged, see the high resolution STM image and corresponding MM energy minimization in figure 6.3 b). Now however, the bright contrast inside the pores indicates that guest molecules have been included. The MM simulation suggests that two adamantane molecules (yellow) could easily fit the available space.

[7] All simulations were performed by C. Rohr with Materials Studio 4.4. MM calculations employed the Forcite Plus module with a universal force field.[110] After placing the molecules on a fixed double layer of graphite in vacuum, repeating one unit cell with periodic boundary conditions, the assemblies were energy minimized to optimize the molecule–molecule as well as the molecule–substrate interactions.

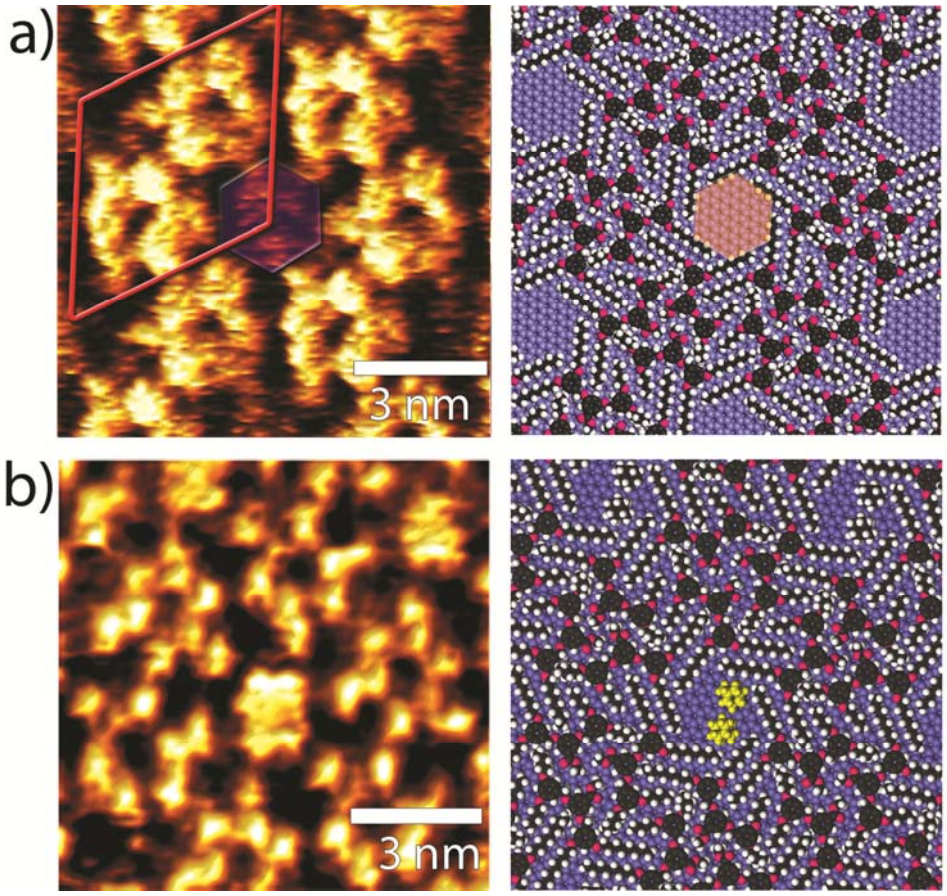

Figure 6.3. Host Pattern and Host – Guest Inclusion. a) High resolution STM image of one pore of the honeycomb pattern with marked unit cell and corresponding MM energy minimization of the molecular arrangement. The pores are empty, marking the structure an ideal candidate to study heterogeneous systems. b) STM image and MM energy minimization of adamantane inclusion within one pore. The co-adsorption of adamantane leaves the host pattern unchanged. Tunneling Bias: U_{Bias} = -700 to -800 mV and Current Setpoint: $|I_T|$ = 8 to 10 pA.

To determine the number of adamantane molecules that is actually included inside the pores, both MM and molecular dynamics (MD) simulations[8] were considered. The MM simulation suggests that at most three molecules would sterically fit within one pore of the host pattern, see figure 6.4 left. The molecules would then be localized at their specific adsorption site inside the pore due to steric reasons without being able to move, and the resulting shape of the

[8] MD simulations (Materials Studio 4.4) used a N-V-T ensemble at 298° K in 50.000 time steps of two fs.

pore filling should appear triangular in the STM image. However, the measurements show a six lobed structure, as the correlation averaged section in figure 6.4, middle, illustrates. Thus a molecular dynamics calculation simulating the trajectory of the center of mass of a single adamantane molecule was compared to the experimental results. The trajectory within the pore recreates the six lobed shape of the pore inclusions, compare figure 6.4, right, and the same results are achieved when two molecules are included in the simulations. Thus it was deduced that one or two adamantane molecules are incorporated inside the pores of the honeycomb host – guest network.

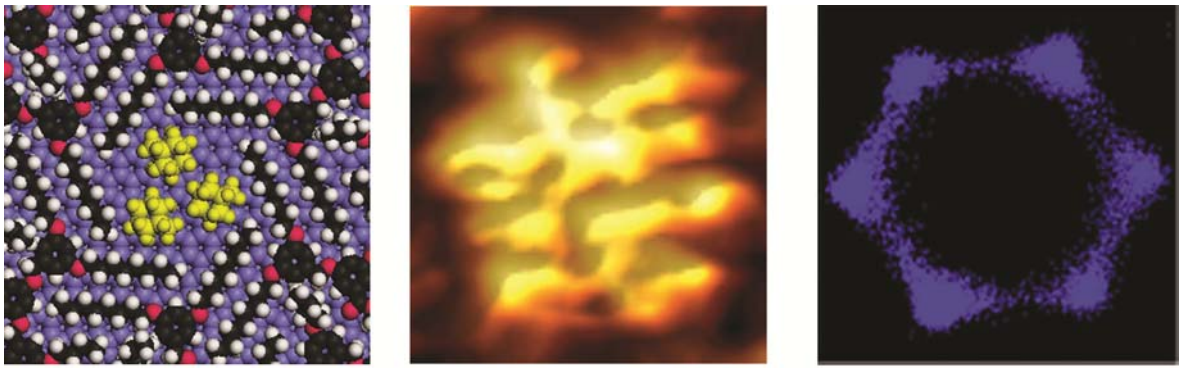

Figure 6.4. Dynamics of Adamantane Inclusions. Left: MM energy minimization displaying three included adamantane molecules inside a host pore. Middle: A correlation averaged STM image of the adamantane filled pore center shows a six lobed structure. Right: The trajectory of the center of mass gained from a molecular dynamics simulation of a single adamantane molecule recreates the six lobed shape.

6.2 The Templated Polymorph Assembly

When coronene is added to the Fréchet dendron assembly, always a distinctively different pattern is observed after solvent evaporation. The resulting structure does not depend on whether coronene is deposited in a successive droplet or in the same solution as the Fréchet dendrons.

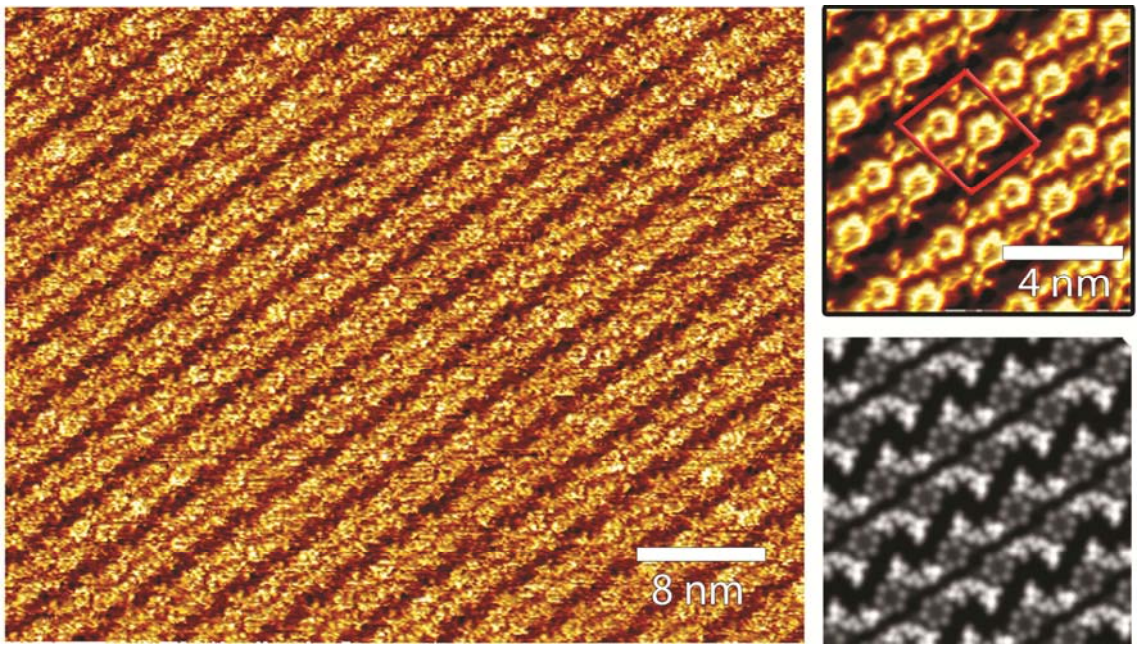

Figure 6.5. Templated Polymorph Assembly. Left: Large scale STM image of the new pattern that emerges when coronene is added to the Fréchet dendron assembly. Right: The high resolution close-up (top) with marked unit cell matches well to the DFT simulated STM-image of the integrated local density of states (ILDOS) with applied Gauss filter to simulate the effect of the extended tip (bottom). Tunneling Bias: U_{Bias} = -800 mV and Current Setpoint: $|I_T|$ = 8 pA.

A typical large scale measurement shows a row like assembly. In figure 6.5 left the rows are oriented from the lower left to the upper right corner of the image. The correlation averaged close-up on the right displays the *p2* symmetric unit cell (a1 = 2.6 nm, a2 = 3.4 nm, ∢ 81.2°). Below, the DFT[9] simulated STM image shows the calculated density contours convoluted with a Gaussian function to mimic the shape of the STM tip. Together with the MM energy minimization (enthalpy per area = 203.2 kJ mol^{-1} nm^{-2}), see figure 6.6 below, the simulations compare well to the measurements and support the interpretation of the molecular ordering in a new templated polymorph assembly.

[9] The energy-minimized MM simulations were used as input to derive the integrated local density of states (LDOS) by providing the atomic positions. The CASTEP module (Materials Studio 4.4) with Perdew–Wang '91 (PW91) generalized gradient approximation exchange correlation functionals (GGA) and a planewave basis set with an energy cutoff at 260 eV was used to calculate the STM images.[111] Density contours of a planar slice convoluted with a Gaussian function of a 2x a Pt d_z orbital in the LDOS were calculated to allow a comparison with the STM measurements.

6.3 Assembly Mechanism

Several possible causes were investigated to determine the reasons behind the change of assembly structure from host – guest inclusion to a templated assembly. As the pore sizes are comparable in diameter for both types of assembly patterns (1.30 nm and 1.35 nm, respectively), size selectivity[14] was excluded as a possible cause.

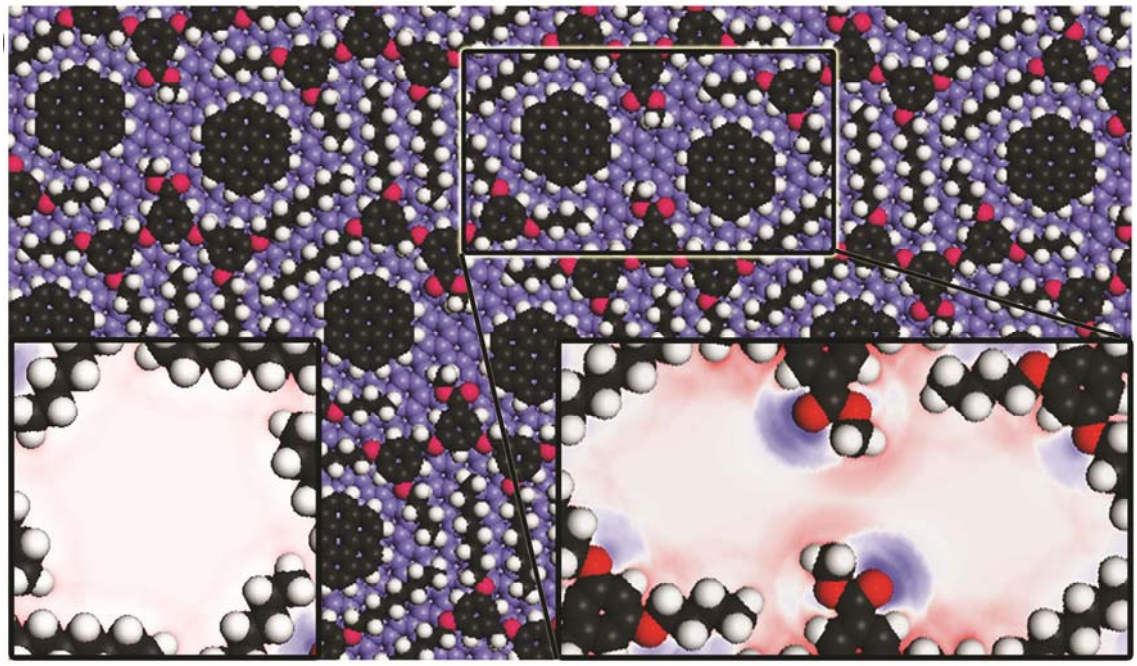

Figure 6.6. MM energy minimization of the templated assembly. The simulation fits well to the interpretation of the observed new ordering. Insets: Calculation of the electrostatic potentials inside the empty host-guest (left) and templated pores (right). See text.

Often the solvent is found to influence the observed molecular ordering, especially when the tip is immersed in the solvent/molecule solution during the measurement and images are obtained at the liquid – solid interface.[112, 113] In this case however the molecules were applied to the surface by solution casting, meaning the solvent evaporates before data is taken. For these cases we examined the solvent's influence on pure Fréchet dendron assemblies in previous studies. While in some cases the initially observed pattern was observed to depend on the polar and protic solvent properties, the thermodynamic end product observed over time remained the same. Therefore it can be concluded

that the intermolecular interactions dominate the solvent effect in cases where the solvent evaporates.[114] Thus they are considered of negligible impact on the here observed switching behavior.

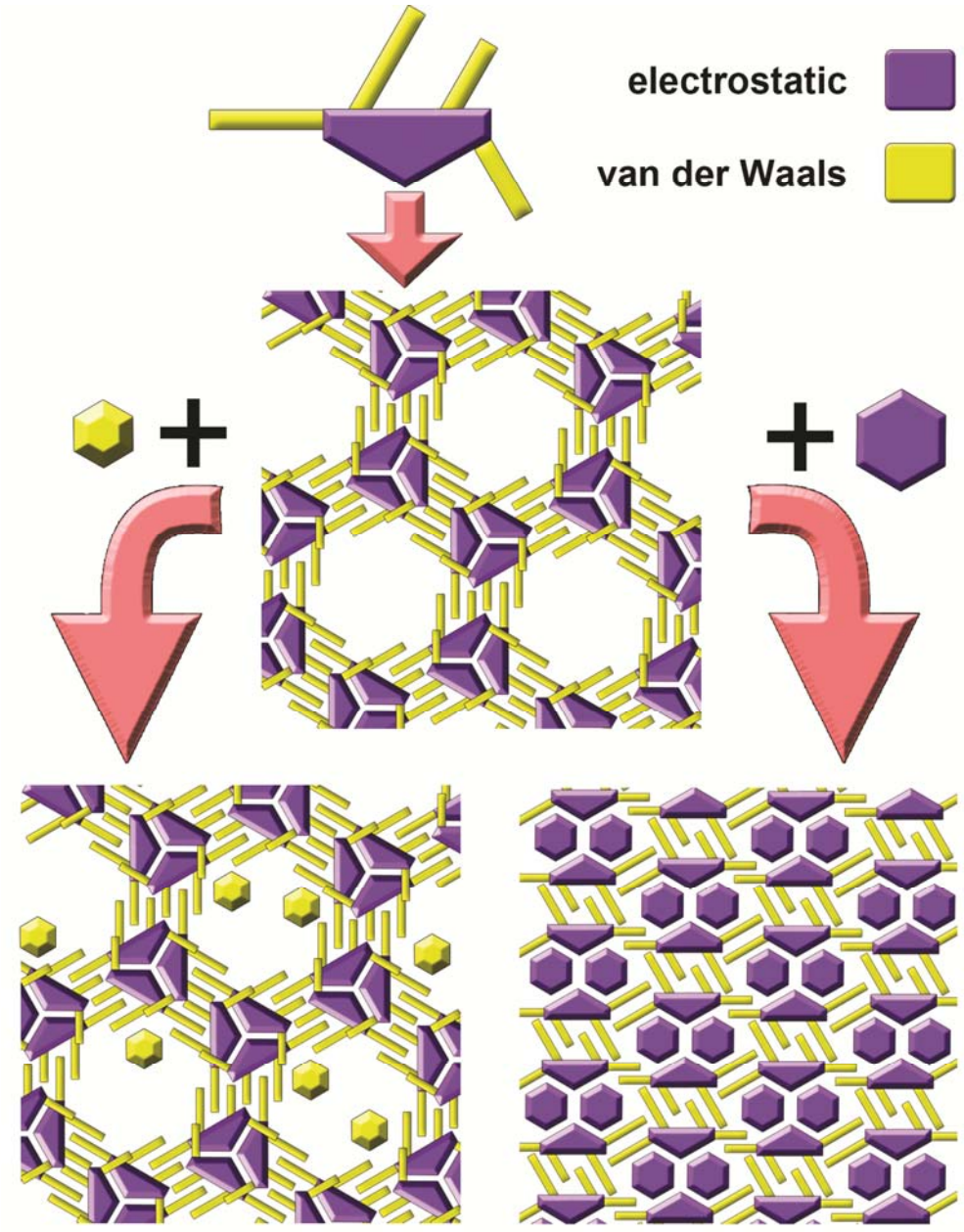

Figure 6.7. Separation of Interaction Types: Already within the host pattern the molecular parts interacting *via* van der Waals (yellow) or electrostatic forces (blue) are spatially separated. Added guest adamantane (yellow) interacts by van der Walls forces and is easily incorporated into the host pattern. Aromatic coronene (blue) is influenced by electrostatic forces and rearranges the ordering to create a new separation of the two interaction types.

Finally, MM energy minimizations were employed to calculate the respective enthalpies for both guests (adamantane and coronene) in both types of pores (host – guest and templated). While adamantane in the experimentally observed host – guest pattern gains 196.8 kJ mol^{-1} nm^{-2}, in the templated structure adamantane guests would only generate 183.5 kJ mol^{-1} nm^{-2}. Similarly, coronene gains 203.2 kJ mol^{-1} nm^{-2} in the experimentally observed templated pattern and is less favorable in the host – guest structure with only 199.8 kJ mol^{-1} nm^{-2}.[10] These results support the experiment findings yet do not clarify the mechanism responsible for the pattern selection.

The insets in figure 6.6 illustrate the differences in electrostatic potentials[11] inside both types of pores (host – guest and polymorph assembly). While the potential is nearly zero inside the pores of the Fréchet host pattern (left inset) a higher intensity was calculated for those of the templated assembly (right inset). Taking a closer look at the electronic properties of the incorporated guest molecules, the different interaction forces between guest and Fréchet dendrons attract attention. Adamantane interacts via van der Waals forces with the alkane chains surrounding the host pore. Polarizable coronene mainly interacts with its electrostatic environment forming dipole – induced dipole and maybe weak C-H…O hydrogen bonds.

The Fréchet dendron has two separated interaction regions, at the alkane chains *via* van der Waals and at the polar molecular core also *via* electrostatic forces. Looking at the pure Fréchet dendron assembly, these regions are spatially separated, see the illustration in figure 6.7. The cores of the Fréchet dendrons (blue) point towards each other while the interdigitation of the alkane chains (yellow) stabilize the molecular ordering. Saturated adamantane favors interactions with the alkane chains and thus can be incorporated into the host pores. The polarizable coronene however is influenced by the partial charges at the Fréchet cores. Thus the heterogeneous assembly process again separates the interaction regions marked in blue and yellow, compare figure 6.7. Consequently, it can be concluded that the electronic structure of the added guest molecule decides on the type heterogeneous pattern, inclusion in a host – guest system or a change to a new polymorph structure.

[10] To calculate the corresponding enthalpies for the structures not observed, one coronene was added in a cavity of the honeycomb pattern while four adamantanes (two per pore) were placed in the templated structure.

[11] Electrostatic potential calculations employed the Dmol[3] DFT module with a PW91 GGA functional (Materials Studio 4.4).

6.4 Conclusions

A Fréchet type dendron combines the two previously separated categories of heterogeneous molecular self-organization: host – guest inclusion and templated polymorph assembly. The decision for the respective ordering depends on the type of guest molecule. Saturated adamantane interacts via van der Waals with the alkane chains lining the pores of the Fréchet host pattern. Aromatic coronene is influenced by the polar Fréchet cores. Striving to separate these two types of interactions within the pattern, the molecules order in a new templated arrangement. The observation of the pure host assembly, host – guest inclusion and templated polymorph assembly unifies these different assembly mechanisms in one molecular compound, and thus links previously separated motifs in self-organization. This new material function now allows the design of two-step protocols for guest selective inclusion and subsequent tuning of unit cell parameters.

7 A Novel Glycan Cantilever Array Sensor

This chapter describes the first purely carbohydrate based glycan cantilever array sensor. Mannose functionalized active layers sensitively and specifically detect the generic lectin Concanavalin A (ConA) against an *in-situ*, nonspecific galactose reference. A further analysis and additional tests verify the quality of the layer composition and the galactose reference. Parts of these results have been published.[115]

Since the first application of cantilever array sensor in 1994 by R. R. Schlittler and co-workers,[22] the cantilever technique has demonstrated its potential as a very sensitive mass sensor and as powerful and label-free detector for biomolecular recognition processes.[24, 25] Most assays today employing the cantilever technique are based on the genome and the proteome,[56] while the glycome and carbohydrate – ligand interactions are still largely neglected. These carbohydrate structures however regulate the interactions of cells with the extracellular environment[36-38] and also have been found on the surfaces of bacteria, viruses and parasites.[39] With advantages like label-free detection and short measurement times the cantilever array technique could prove a valuable tool to advance the emerging field of carbohydrate based research and diagnostic applications.

To this end, a cantilever array sensor setup would need to be established for the detection of a generic carbohydrate binding protein. The carbohydrate active layers are to be designed, tested and improved. To demonstrate the value of the setup, the sensitivity, accurate concentration dependence and specific sample recognitions require testing. Finally, complementary measurements with

nonspecific binding partners and additional test assays should verify the quality of the sensor design and the carbohydrate active layer.

7.1 Specific Carbohydrate – Protein Detection Demonstrated with Concanavalin A in Nanomolar Sensitivity

Active layers of trimannoside (Tri-Man), nonamannoside (Nona-Man) and galactoside (Gal) equipped with thiol linkers were created on the cantilever surfaces by self-assembly. While the mannoside functionalized cantilevers serve as specific target for lectin binding, the galactoside cantilevers serve as inherent reference to determine the nonspecific signal. The carbohydrate coatings were formed in parallel within one array of eight individual cantilevers, at times with one or both mannosides present, see figure 7.1 for the last case.

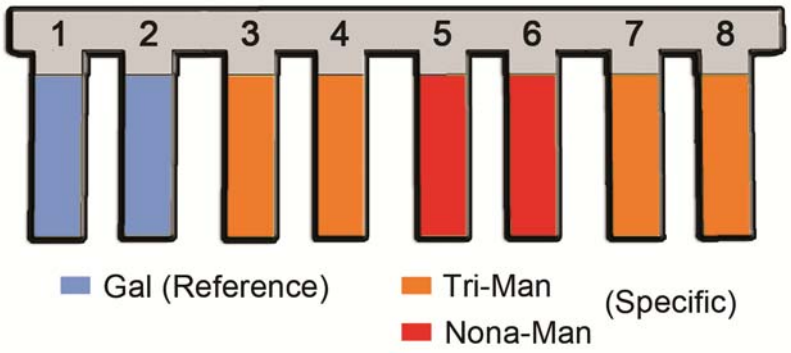

Figure 7.1. Functionalization of a Cantilever Array. The scheme illustrates how a typical array is coated with galactose reference (blue) and trimannose (orange) and nonamannose (red) specific layers.

As the sensor functionalization is often not achieved straight forward, the development of the corresponding protocols posed one of the major challenges for the following results. The details about the functionalization process and the determined protocols can be found in chapter 5.2.

An optimized density of the carbohydrate sensing layer is crucial to develop the maximum cantilever deflection upon protein binding and to minimize the contribution of nonspecific binding to the final signal size. For ConA, see

chapter 5.1, the largest signal sizes were achieved for incubation times between 10 to 15 minutes, longer incubation times up to 75 minutes did not improve the sensor signal. At the lower and upper ranges of the carbohydrate density the signal sizes slightly vary, as is discussed later in chapter 7.2.

For a typical injection of ConA sample, a negative deflection is apparent for all cantilevers with significantly larger signals for the mannose than for the galactose cantilevers. The nonamannose cantilevers undergo an even larger deflection than the trimannose cantilevers. For an array that was functionalized as described above, the *average* deflection was calculated for galactose, trimannose and nonamannose cantilevers and plotted against time. The resulting graphs clearly demonstrate that the sensor not only discerns galactose from mannose coatings, but also discriminates between the two mannose structures (tri- and nonamannose) *via* the signal size, see figure 7.2 upper panel. After an initial, transient positive deflection accompanied by slight disturbances during the sample injection (shaded area), followed by continuing negative deflections, the signals begin to level out towards the end of the sample where the running buffer returns to the measurement chamber. All three curves then continue in an almost horizontal fashion, only for the nonamannose cantilevers a very slight increase to a higher baseline can be observed.

Taking advantage of the *in-situ* reference cantilevers, the *differential* signal was calculated by subtracting the galactose reference signal from the two mannose signals. As could be expected, the *differential* nonamannose signal is considerably larger than the *differential* trimannose deflection, see figure 7.2 lower panel. After the end of the sample injection, both curves level with again the nona-mannose signal showing a slight baseline increase.

Due to its high affinity binding sites for mannosides, ConA recognizes the nonamannose and trimannose sensor molecules. Additional nonspecific binding can occur on other areas of the protein, the PEG linker or the cantilever surface, and also by low affinity binding of galactose to the protein binding pocket. The increased adsorption of ConA molecules on the sugar covered surfaces leads to a difference in surface stress between lower and upper side of the micrometer thin cantilever which is relieved by downward bending (so-called compressive surface stress).[116] Also protein – protein and protein - surface interactions as well as conformational changes upon protein binding can contribute to the surface stress and the cantilever bending.[117-119]

The larger nonamannose signal is attributed to increased multivalent (due to multivalent nonamannose) and multisite binding (due to the multiple binding pockets of ConA).[120] This effect is visible in the *average* as well as *differential* signals. The observed deflection for the galactose cantilevers is attributed to nonspecific binding events as are described above. Thus the nonspecific contribution to the binding is eliminated in the *differential* signals for nonamannose and trimannose. In other words, these *differential* signals correspond to the specific binding of ConA to the mannose coated cantilevers which is illustrated by the arrows indicating the total, nonspecific and specific signal in figure 7.2. The initial, transient positive deflections at the beginning of the sample injection are attributed to conformational changes that occur upon receptor binding.[119] When the buffer flow is stopped during the sample injection, the deflection signals quickly level, inferring binding equilibrium. Due to the continuous pull of the buffer flow this is not observed during regular experimental conditions.

Figure 7.2 (next page). Specific ConA Recognition and Sugar Discrimination.[12] Upper panel: *Averaged* deflections of identically functionalized cantilevers with galactose, trimannose and nonamannose coatings for a ConA sample of 2 mg/mL (19.2 µM) (shaded area). The nonamannose signal is about four times larger than the galactose reference, the trimannose signal about two times larger than the galactose reference. The larger mannose signals are attributed to the high affinity of ConA for mannoside moieties, increased multisite and multivalent binding is responsible for the larger nonamannose deflection. The galactose signals reflect nonspecific binding events. Lower panel: *Differential* signals were calculated by subtracting the nonspecific galactose reference from the specific mannose signals, see the respective arrows in the upper panel. Therefore the resulting deflection size corresponds to the contribution of the specific ConA – mannose binding, indicated by the arrows in the lower panel. Again the larger nonamannose signal, compared to the trimannose, reflects the propensity for multivalent and multisite binding of the protein. For further discussion see text.

[12] Measurement by A. Mader.

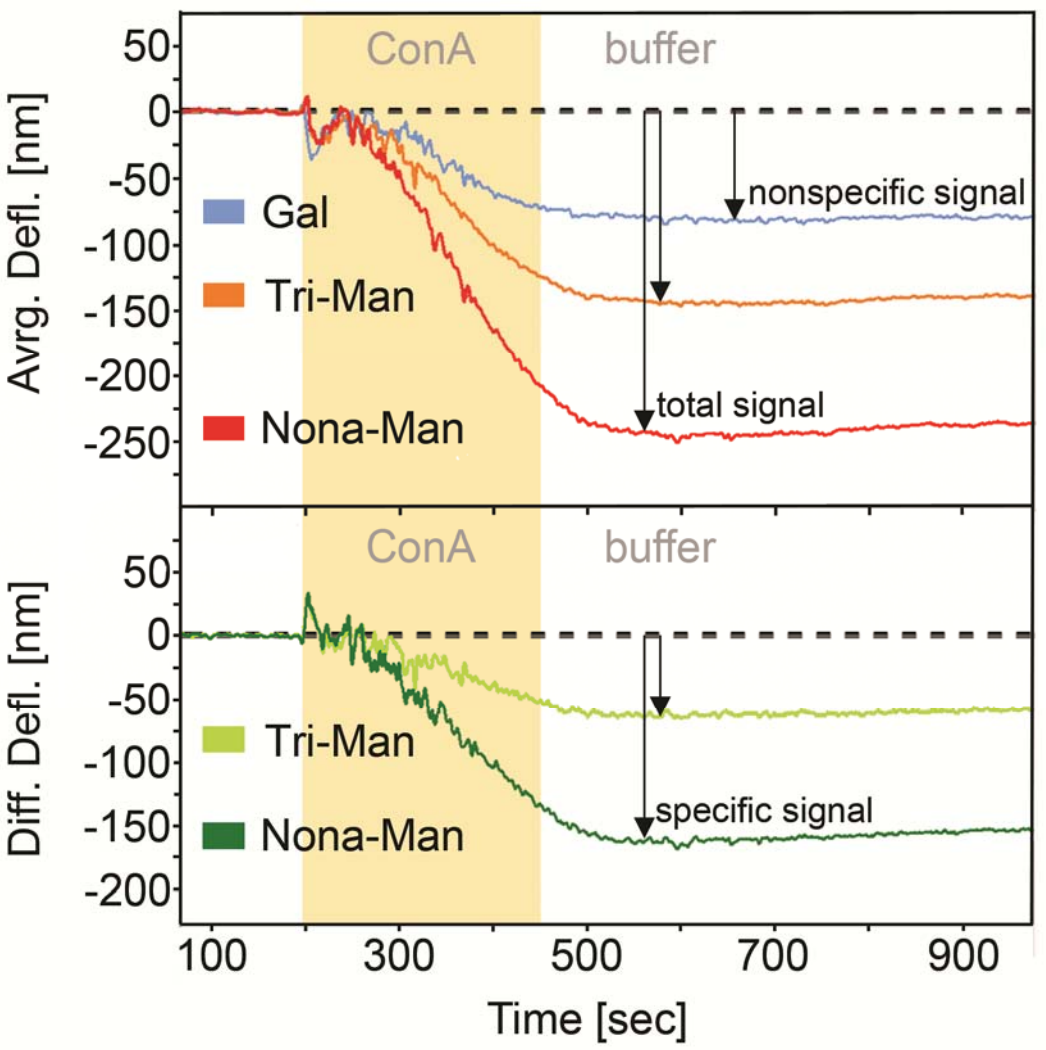

The quality of a sensor can be evaluated in terms of its sensitivity, the concentration dependence of the signal size and the specificity of the binding. In the following these three criteria are investigated for the detection of ConA with this glycan array sensor.

What is the limit of detection for ConA samples with this sensor?

The sensitivity of any sensor device is crucial for its practicability and future applications. To test the sensor's response to very low concentrations, ConA samples were diluted down to the nanomolar range. Even after a high concentration of 10 mg/mL (96.2 µM) was injected initially, in an immediately following experiment, very low concentration of only 1 µg/mL (9.6 nM) could be clearly detected for trimannose coated sensors. Figure 7.3 shows the two consecutive injections plotted overlaid for better comparability. To highlight the relevant section in figure 7.3, the inset enlarges the sensor signal detecting the

nanomolar protein concentration with a significant differential deflection for the ConA – trimannose binding. The observed resolution is attributed to the high affinity of ConA for mannoside structures.

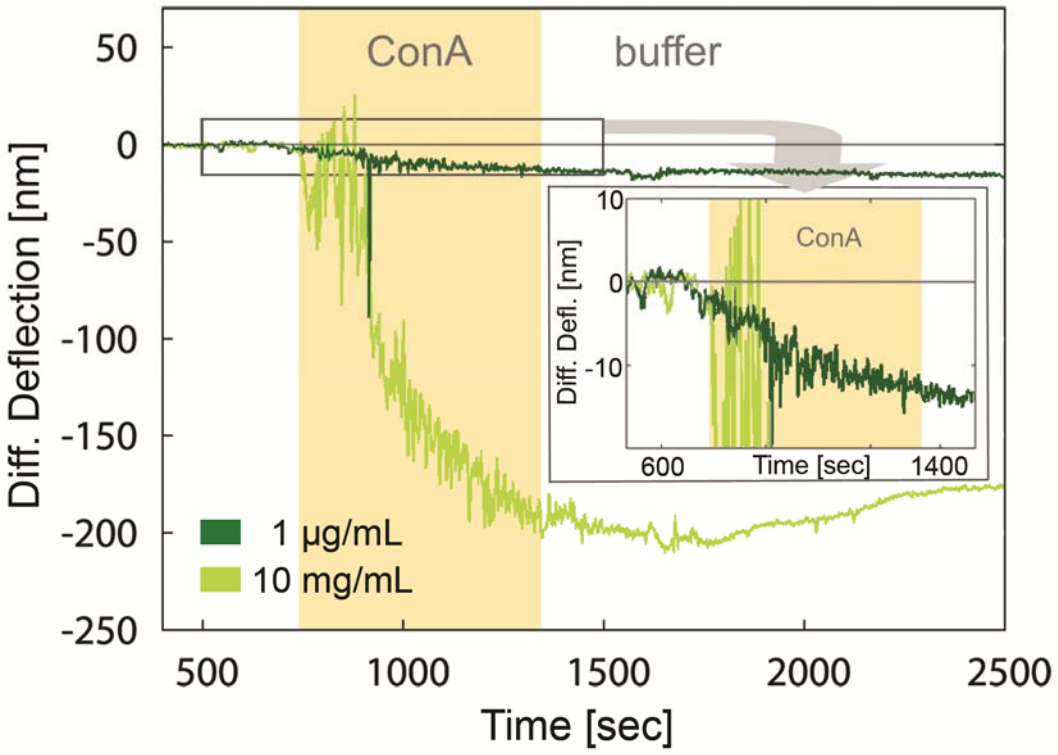

Figure 7.3. Sensitivity of the Cantilever Sensor for ConA Binding. After an injection of a very high concentration of 10 mg/mL (96.2 µM) a consecutive injection with only 1 µg/mL (9.6 nM) still yielded a distinct differential signal of for the ConA – trimannose recognition. The two curves were measured in sequence and overlaid in the figure for better comparability. The inset shows and enlargement of the relevant time frame. The sensors' observed sensitivity down to the nanomolar regime is attributed to the high affinity of ConA for the mannose covered cantilevers and agrees well with literature.

The demonstrated sensitivity of the cantilever sensor in the lower nanomolar regime indicates the good quality of the sensor surface functionalization. Already at the stage of the sensor's development achieved during this thesis, these results reach a limit of detection in the same order of magnitude or better as measurements performed on other comparable surface

bound sensing techniques like surface plasmon resonance (SPR, limit of detection: 560 nM ConA monomer), quartz crystal microbalance (QCM, limit of detection 90 nM ConA monomer) or glycan microarrays (limit of detection: 9.6 nM fluorescence labeld (FITC) ConA).[121, 122]

How well do the sensor signals reflect the affinity of the ConA – mannose binding?

First, a sensor's response should reflect the probed sample concentrations. Thus a series of six consecutive injections was conducted with increasing ConA concentrations, for consistency also on a trimannose and galactose functionalized array. There are two commonly used protocols for such concentration series: Either the individual steps are performed in direct succession or additional cleaning steps are included between consecutive experiments to remove the bound analyte. The first so-called non-regeneration protocol was employed here, as testing with cleaning agents like sodium dodecyl sulfate (SDS) or high salt concentrations showed no impact on the following signal sizes for protein detection. About 15 to 25 data points, depending on the actual protein concentrations used, could be acquired per array before unusually low signal sizes indicated surface saturation. This observation suggests a high carbohydrate ligand density on the cantilever surface compared to the offered protein concentrations,[123] see also the discussion in chapter 7.2. Consequently, no intermediate cleaning steps were included except the return of the running buffer. Figure 7.4 shows for the here conducted concentration series that the differential deflections increase with the respective concentration, the sensor consistently detects larger sample concentrations *via* larger signal sizes. The increasing signal sizes for concentrations over a very large concentration range of four orders of magnitude up to very high concentrations indicate that the sensor is operated far from the maximum binding concentration under comparable on- and off-rates.

The number of specific binding events on the sensor surface increases as larger sample concentrations are injected, explaining the continuously larger deflections. To quantitatively evaluate the concentration dependence, the maximum differential deflections were plotted against their respective concentration, see the inset in figure 7.4. A Langmuir isotherm analysis, see chapter 4.4, was applied to determine the dissociation constant K_d. The resulting K_d value of 15.3 µM is slightly larger than values obtained with quartz crystal

microbalance (QCM, 1.15µM) or surface plasmon resonance (SPR, 0.26 µM) methods.[121] This could indicate that the trimannose structures attached to the cantilever surface cannot bind ideally to the ConA proteins and could result from the sugars lying flat on the cantilever surface, as is also discussed in chapter 7.2. Conversely, if the sensing layers could be further optimized in future work, an even larger sensitivity as is demonstrated above could be realized.

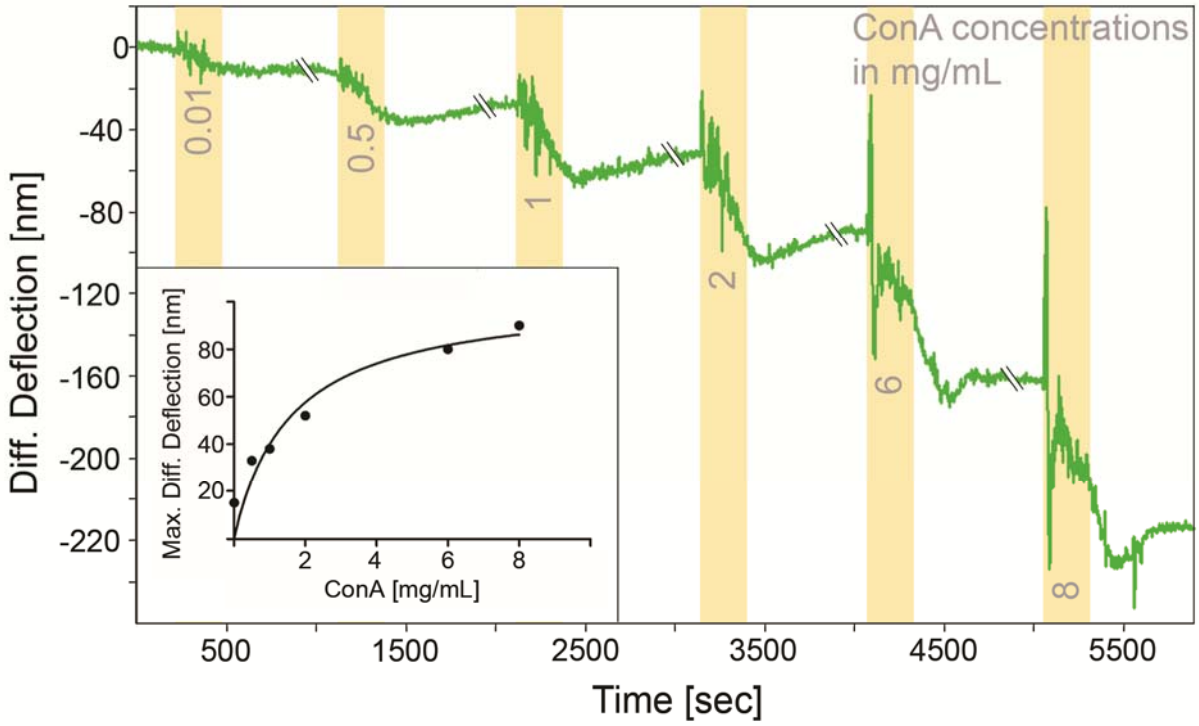

Figure 7.4. Concentration Dependence of the ConA Recognition and Dissociation Constant.[13] A series of six consecutive injections with increasing ConA concentrations shows corresponding, increasing signal sizes. The inset shows the maximum differential deflection plotted against the respective ConA concentration. A Langmuir isotherm analysis yielded a dissociation constant K_d for the system of 15.3 µM.

To evaluate the accuracy of individual signal sizes for consecutive measurements, 15 injections of 1 mg/mL (9.6 µM) were conducted under comparable conditions on nine independent cantilever arrays. Their mean signal sizes for nonamannose and trimannose cantilevers were 69 nm and 39 nm, with a standard deviation of 19% and 12%, respectively. For a new sensor these

[13] Measurement by A. Mader.

standard deviations is within an acceptable range, as also commercially available glucose sensors are allowed a deviation of 20% (FDA[14] recommendation). Once functionalized, the sensor could be dried, stored at -20°C and reused for many consecutive injections.

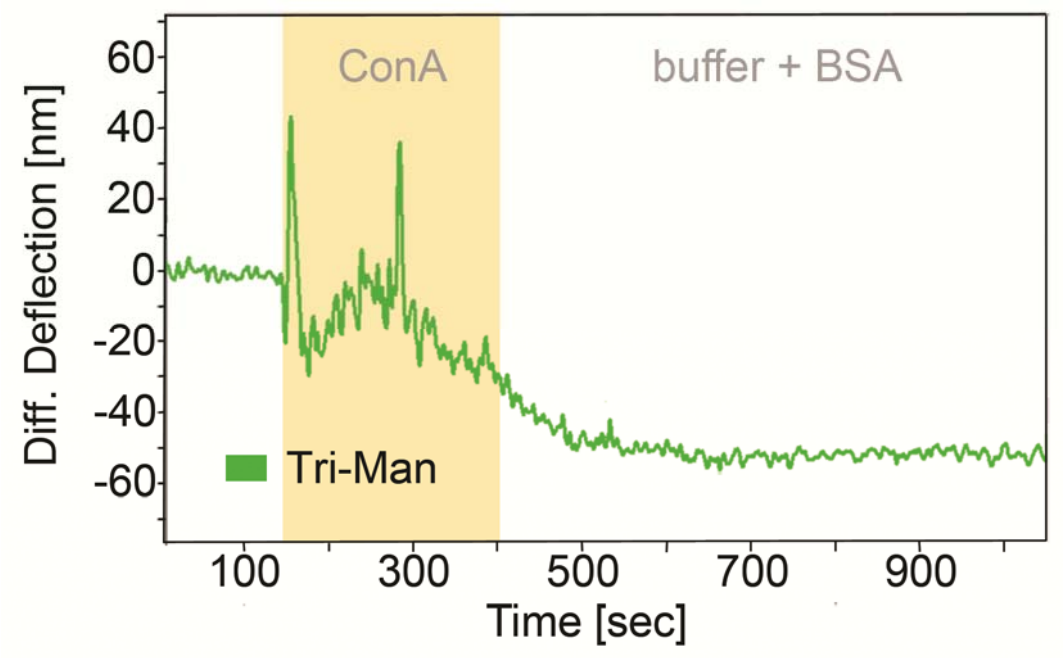

Figure 7.5. ConA Binding in BSA Background.[15] To imitate a more realistic sample background, nonspecific BSA (0.007 mg/mL; 0.1 µM) was added to the running buffer. An injection of ConA (2 mg/mL; 19.2 µM) yields a signal size comparable to measurement conditions with pure running buffer.

Are the ConA molecules recognized specifically by the mannose structures?

When aiming at more realistic applications, the sensor needs to be able to operate in a complex background and still specifically detect the target substance. To test the stability of the glycan cantilever array sensor, bovine serum albumin (BSA) (0.07 mg/mL; 1.0 µM) was added to the running buffer. An injection of 2 mg/mL (19.2 µM) ConA sample on a trimannose and galactose functionalized array resulted in consistent differential deflections compared to measurements in pure buffer, compare figure 7.4 and 7.5. The sensor is unperturbed by the added

[14] U. S. Food and Drug Association (FDA)
[15] Measurement by A. Mader.

BSA protein which demonstrates the robustness and lectin specificity of the sensor setup.

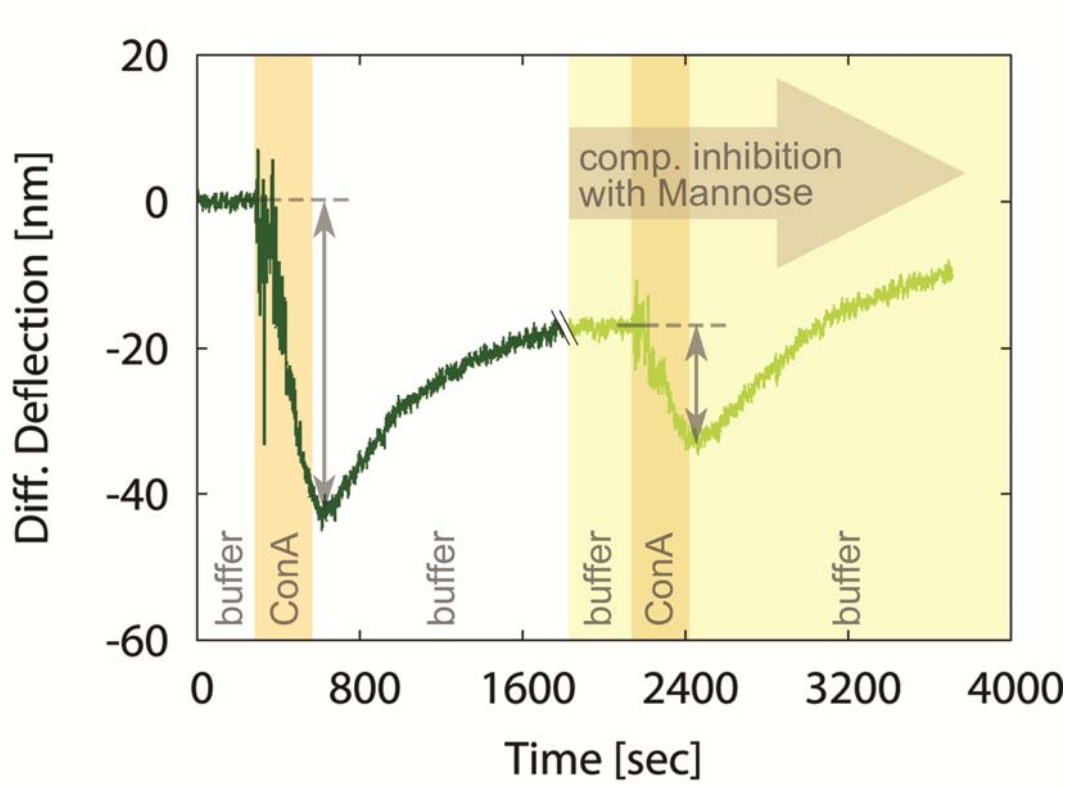

Figure 7.6. ConA Binding Specificity. After a reference injection of 1 mg/mL (9.6 µM) ConA sample, 100 mM free mannose was added to the running buffer to challenge the specificity of the protein – carbohydrate binding. A repeated injection of again 1 mg/mL (9.6 µM) resulted in about one third of the original signal size. The mannose dissolved in the buffer competes with the carbohydrates presented on the sensor surface, leading to fewer binding events on the sensor and consequently a smaller signal size.

Finally, the ConA – mannose binding was challenged by a competitive inhibition assay to demonstrate the specificity of the carbohydrate – protein complex. First a reference injection of 1 mg/mL (9.6 µM) was conducted. Then free mannose was added to the running buffer (100 mM) and a second measurement was conducted with identical sample concentration. The now observed differential deflection was reduced to about one third of the original size, see figure 7.6 for the two injections.

The free mannose dissolved in the buffer competes with the surface bound carbohydrates for binding to the ConA proteins. Thus less binding events occur on the sensor surface and in turn the deflection size is reduced. The successful competitive inhibition independently confirms the effectiveness of the cantilever array design and the selectivity of the protein binding to the mannosides anchored on the cantilever surface.

These results demonstrate the ability of the glycan cantilever array sensor to specifically detect the generic protein ConA down to nanomolar sensitivity. The following chapter aims at drawing additional conclusions from these results regarding the molecular interactions on the sensor surface.

7.2 Signal Origin, Strength and Evolution

The biomolecular processes which take place on the cantilever surface and induce the surface stress are complex and a comprehensive theoretical model is still elusive. Many physical and chemical effects like conformational changes, molecule – molecule and molecule – substrate interactions *via* van der Waals and electrostatic forces add to the observed cantilever bending.[117-119] Here the previously described results are evaluated in this light and combined with simple yet effective additional tests. Beyond the sensitivity and specificity of the sensor, the following paragraphs aim to verify the quality of the sensing layers by asking specific questions about the molecular mechanisms behind signal origin, strength and evolution that naturally follow the evaluation of the experimental data.

How are the carbohydrate molecules oriented on the cantilever surface?

An important question for the sensor's performance is if the carbohydrate molecules are freely accessible for protein recognition: Are the molecules standing upright or lying down? The slightly larger values for the dissociation constant derived for the ConA – trimannose binding in chapter 7.1 gave a first indication about a less than optimal binding efficiency. A further hint about the arrangement of the carbohydrate molecules can be gained by looking at the results of the competitive inhibition assay. Considering basic biochemistry, it is usually not expected that *mono*mannose dissolved in the buffer solution is able to inhibit multivalent *nona*mannose binding. However, the results here indicate otherwise as the sensor signal is clearly reduced in the presence of

monomannose, compare figure 7.6. Thus it can be inferred that the nonamannose structures used for this work are of lesser binding strength that means affinity, than would be expected and monomannose can successfully compete for protein binding. This observation could be explained by the carbohydrates lying flat on the cantilever surface. Thus, only parts of the whole structure would be exposed and available for binding, effectively reducing the multivalency and binding strength of the nonamannose carbohydrates.

Why are the very first injections of a newly prepared cantilever array not consistent?

After the preparation and functionalization of new cantilever arrays, often inconsistent signal sizes for the respective sample concentration are observed for the very first injections. Then, following injections compare well within acceptable standard deviations as described in chapter 7.1 for ConA detection (and later in chapter 8.1 for CV-N). This indicates that an intermediate step happens which optimizes the surface coating before reliable sensing experiments can commence. Possibly the proteins of the first injection irreversibly attach to any free spaces on the cantilever surface, effectively blocking these nonspecific binding sites for the following experiments.

How many experiments can be conducted on one cantilever array?

After about 15 to 25 injections per array, depending on the actual protein concentrations used, unusually low signal sizes indicated surface saturation. Injections with cleaning agents like sodium dodecyl sulfate (SDS) or high salt concentrations were not observed to influence the signal sizes of following protein experiments, see also the discussion of the concentration series in chapter 7.1. The increasing signal sizes for concentrations over a very large concentration range of four orders of magnitude up to very high concentrations indicate that the sensor is operated far from the maximum binding concentration under comparable on- and off-rates. These observations suggest a high carbohydrate ligand density on the cantilever surface so that consecutive injections require no intermediate cleaning step for ideal binding.[123]

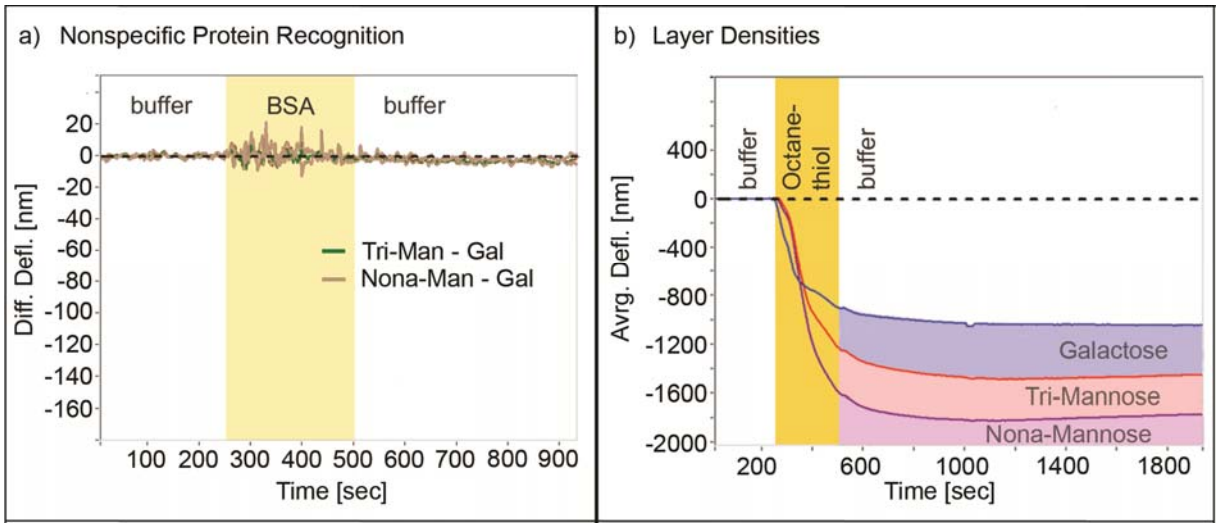

Figure 7.7. Nonspecific Adsorption and Layer Densities. a) Nonspecific BSA (0.063 mg/mL; 0.95 µM) was injected to test the sensor response for the three carbohydrate layers. No differential and thus specific response was recorded. b) An injection of the small thiolated molecule octanethiol (0.1 mM) indicates the number of available adsorption sites on the cantilever surface. Nonamannose cantilevers give the largest signals, followed by trimannose and galactose. This is presumably due to the increasing layer density in this order, resulting from the decreasing sugar group size.

How do sparse and dense active layers affect the sensor signal?

As described in chapter 7.1 for the functionalization of the arrays, shorter and longer incubation times, and thus sparse and dense layers for all carbohydrate structures, were tested. Counter intuition, more sparsely coated layers show a slightly larger signal in their average deflections than the denser coatings. The differential deflections however consistently show larger sizes for the denser coated cantilevers, as would be expected, as was also observed for the results in chapter 8.1. Therefore the larger average signals for sparse cantilevers are attributed to more nonspecific binding events on these surfaces due to the sparse coating which are eliminated in the differential signal. Longer functionalization times than 15 minutes reduced the specific signal and were not employed, as is described in chapter 7.1.

How do the layer densities between the different carbohydrate structures compare?

Due to the different sizes of the nonamannose, trimannose and galactose molecules, also the layers of the different mannose structures could differ even when prepared with equal incubation times. Consequently these layer densities, self-assembled under identical incubation times and conditions, were compared by their reaction to short thiolated alkanes. These molecules react very strongly with the gold coating of the cantilever surface and provide a good tool to access all available space not covered by the carbohydrates. An injection of octanethiol (0.1 mM) gave the largest signal for the nonamannose coating, followed by the trimannose and galactose layers, see figure 7.7 b). Comparing the carbohydrate structures, nonamannose has the largest head group of the three compounds, see chapter 5.1. Consequently it requires a larger distance between individual molecules during the self-assembly process, which in turn leads to a less dense functional layer and more free binding sites on the cantilever surface than is the case for the trimannose and the galactose molecules.

To determine if these differences in layer density show any impact on the recognition of much larger proteins, tests with BSA were conducted. BSA does not bind specifically to either carbohydrate, thus any differential signal would reflect only the increased nonspecific binding due to the differences layer density under the assumption that all carbohydrate moieties lead to the same amount of nonspecific protein attachment. After verifying the functionality of the sensor array for specific recognition, an injection of BSA (0.063 mg/mL; 0.95 µM) resulted in little to now differential deflection, see figure 7.7 a). The free inter-molecular space on the cantilever surface created during self-assembly is thus not accessible to the larger protein structures. Consequently, further steps for the passivation of these areas[34, 124] were deemed unnecessary.

Is galactose a good reference if it consistently shows a significant signal?

In contrast to other biomolecular interactions like for example avidin – biotin recognition or DNA hybridization, the specificity of the carbohydrate – protein binding is comparably low so that low affinity binding to other carbohydrate structures, like galactose in this case, may occur. To demonstrate these differences, a standard hybridization experiment of two single stranded DNA (ssDNA) sequences was performed.[125] A cantilever array was functionalized with the two thiolated ssDNA strands (77% homologous) Nl4-3

(sequence: GTT ACA ATA GGA AAA ATA GGA A) and Sf162 (sequence: CAT ACA ACA GGA AGA ATA ATA GGA G) for 40 minutes.

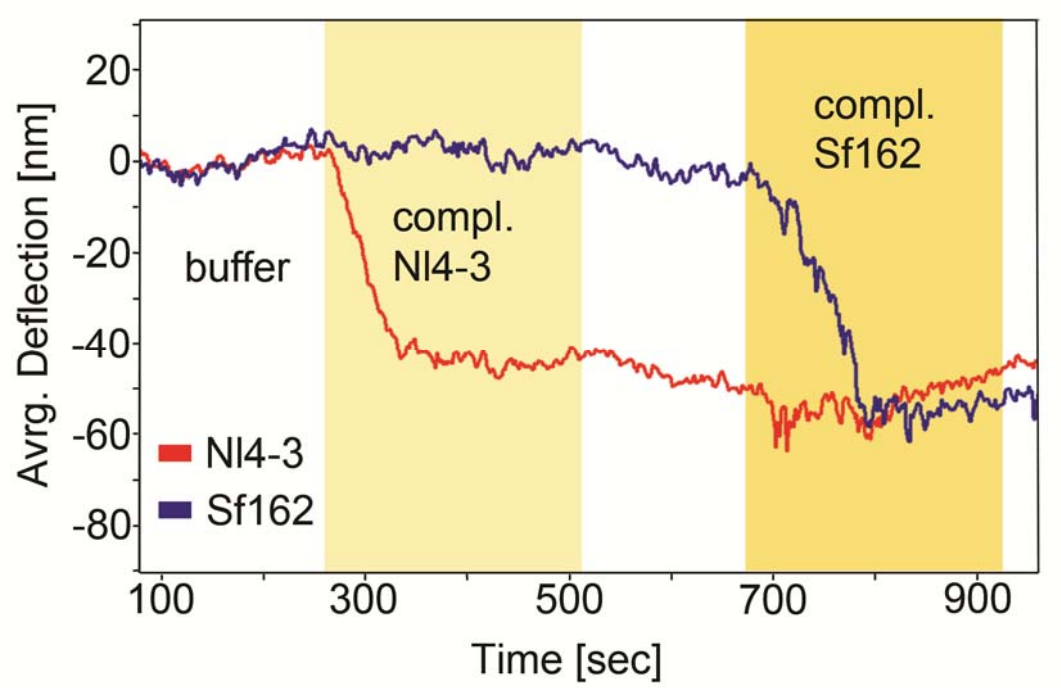

Figure 7.8. Hybridization of ssDNA strands. First an injection with the complementary of strand Nl4-3 results in a negative deflection of the Nl4-3 functionalized cantilevers (red), while the cantilevers with strand Sf162 maintain their base level. A following injection with the complementary to Sf162 induces also here a negative deflection (blue) and brings both signals to comparable levels.

Upon injection of the complementary to Nl4-3 (1 µM), only the cantilevers coated with thiol-Nl4-3 react and deflect downwards (red), while the cantilevers with thiol-Sf162 (blue) continue nearly undisturbed on their base level. A second injection with the complementary to Sf162 (1 µM) then shows nearly no influence on the Nl4-3 cantilevers (red) while now Sf162 coated sensors react and reach a comparable level of negative deflection (blue), see figure 7.8.

The negative deflections are attributed to the hybridization of the respective complementary strands. Charged side groups on the DNA double helix act repellant, inducing compressive surface stress and negative cantilever bending. No deflection and thus nonspecific binding is observed for the respectively other sequence. This infers a high specificity of the complementary sequences under these experimental conditions (T = 30° C).

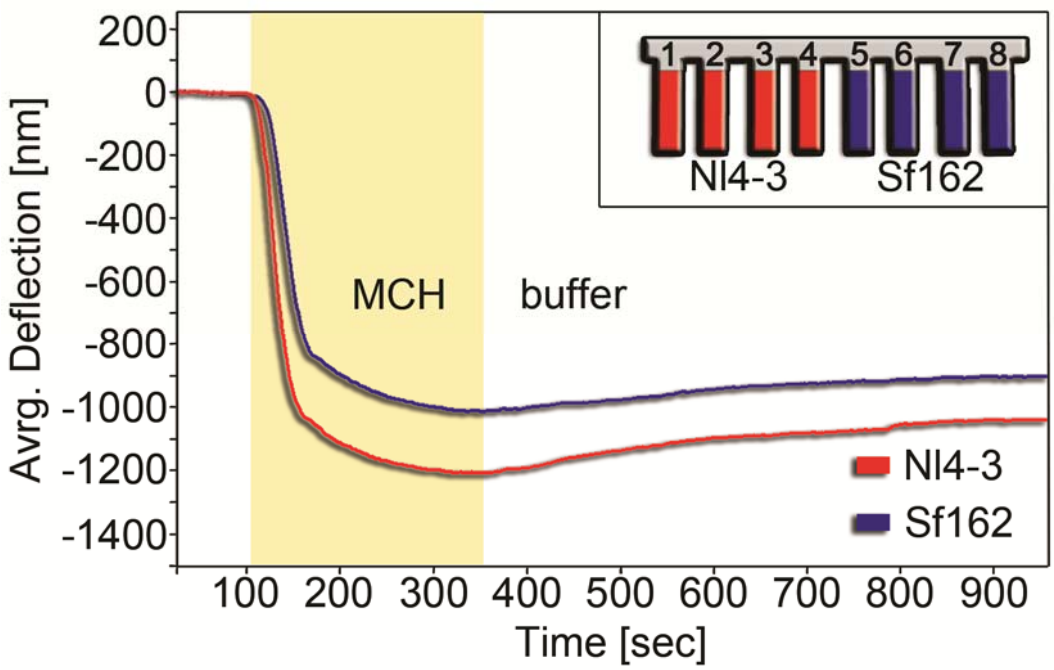

Figure 7.9. Layer Density of ssDNA Functionalized Array. An injection with mercaptohexanol (MCH, 0.1 mM) shows a larger signal for strand Sf162 than for strand Nl4-3, inferring a lesser density of the ssDNA layer. The inset shows the functionalization of the individual cantilevers of the array with strands Nl4-3 and Sf162.

The high specificity of the DNA hybridization is further attested to by looking at the layer densities for both ssDNA strands. A sample of a small thiolated alkane chain, in this case mercaptohexanol (MCH), was injected on the same array as used for the measurement shown in figure 7.8. All cantilevers deflect negatively, while the smaller average signal for Sf162 infers a denser layer, see figure 7.9. Thus, although the layer densities vary similar to those of the carbohydrate layers, compare figure 7.7, the ssDNA hybridization shows near to no nonspecific signal on the respective other cantilevers, as discussed above. This observation again underlines the high specificity of the ssDNA recognition.

In contrast to the high specificity of the DNA hybridization due to the specific base pair sequences, carbohydrate – lectin interactions allow more variation, ConA for example is known to also recognize glucose derivatives.[126] Thus, part of the signal observed for the galactose cantilever arrays upon injection of a ConA sample may stem from such nonspecific binding *via* the mannose binding site of the protein, as is also mentioned in chapter 7.1. As galactose also includes such interactions, in contrast to a non-carbohydrate

reference layer from alkanes or polyethylene glycol, it is an ideal reference for specific carbohydrate – protein interactions. When the galactose reference signal is subtracted from the mannose signal, the remaining differential signal almost ideally represents the aimed-at contribution of the purely specific binding.

These experiments and observations thoroughly test the glycan cantilever array sensor and give possible explanations for the processes taking place on the cantilever surface that could provide a first step towards a more complete understanding of the sensor response. They verify the quality of the sensor design and underline the specificity of the lectin recognition.

7.3 Conclusions

The results described in this chapter establish the first purely carbohydrate based cantilever array sensor for protein recognition. The glycan cantilever array sensor specifically and sensitively detects the generic protein ConA down to nanomolar concentrations. Additionally the sensor discriminates between different mannosides due to increased multisite and multivalent binding and indicates nonamannose and trimannose functional layers *via* larger and smaller sensor signals, respectively. Even after highest sample concentrations, ConA could be clearly detected down to 9.6 nM, representing a limit of detection comparable or better to similar methods. A Langmuir isotherm analysis applied to a series of consecutive injections of increasing sample concentrations determines the dissociation constant K_d to 15.3 µM slightly above literature values which was attributed to the fact that the carbohydrate structures are not ideally accessible for protein binding when attached to the cantilever surface. Measurements conducted in the background of BSA and a competitive inhibition assay with free mannose dissolved in the running buffer each independently confirm the specificity of the ConA – mannoside binding and the effectiveness of the sensor design.

To verify the quality and specificity of the layer design and aiming at a more complete understanding of the molecular interactions leading to the sensor signal, these experimental findings were further analyzed. As a result, the glycan cantilever array sensor might operate in the following way during a typical experiment:

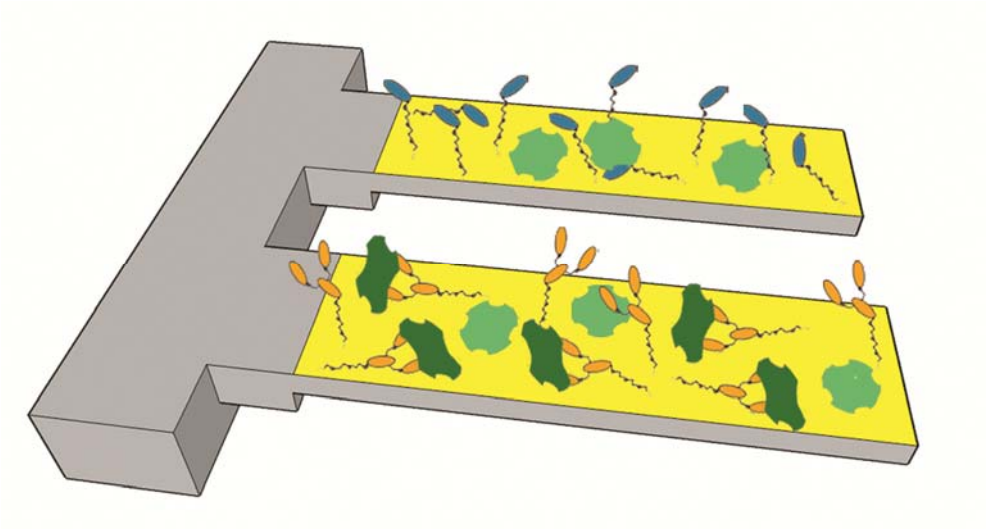

Figure 7.10. Model of the Molecular Processes on the Cantilever Surface. On a trimannose (orange) functionalized cantilever ConA proteins bind specifically (dark green) and nonspecifically (light green). On galactose (blue) coated cantilevers ConA binds nonspecifically to the galactose or the cantilever surface. See text.

After self-assembly on the gold coated array, the carbohydrate molecules lie down flat on the cantilever surface, see the cartoon representations for a trimannose and galactose cantilever in figure 7.10. The first protein injection irreversibly blocks nonspecific binding sites on the cantilever surface (light green ConA molecules in figure 7.10) so that consecutive experiments deliver consistent results for specific ConA recognition (dark green proteins in figure 7.10). Many subsequent injections can be performed before the sensor surface saturates. Up to the optimum carbohydrate density range, sparse cantilevers result in a slightly larger *average* signal, but a smaller *differential* deflection, due to increased nonspecific binding. The large nonamannose molecules assembly in the least dense layer, followed by trimannose and galactose, however this has almost no effect on protein recognition. To eliminate the contribution of the nonspecific binding, galactose cantilevers serve as an ideal reference for binding of mannose specific ConA.

In all, the cantilever array technique could be successfully introduced to carbohydrate – protein detection by demonstrating nanomolar sensitivity and a value for the dissociation constant of the mannose – ConA binding, both comparable to literature reports. The specificity of the recognition could be verified by competitive inhibition and a comparison to nonspecific BSA binding.

The next logical step now asks for the application of this sensor to the detection of clinically and biologically relevant proteins and pathogens.

8 Sensitive Detection of Anti-Viral Proteins and Pathogens with Glycan Cantilever Array Sensors

This chapter describes the application of the first glycan cantilever array sensor established in chapter 7 to the specific and sensitive detection of the anti-viral protein Cyanovirin-N (CV-N) down to picomolar concentrations. The recognition of a second anti-viral protein, Scytovirin (SVN), demonstrates the versatility of the sensor setup. In a second application the detection and discrimination of three different *Escherichia coli* (*E.coli*) strains down to a concentration of a few cells per sample unit successfully extend the sensor's capabilities from protein to pathogen detection. Parts of these results have been published.[115]

To be of value, the glycan cantilever array sensor established in chapter 7 needs to be applied to the detection of scientifically relevant systems. The most obvious step forward from detecting the generic protein ConA would involve the testing of proteins currently under clinical trial for diagnostic or therapeutic applications. A second field of interest that would profit from a low cost and fast sensing approach would lie in the detection of microorganisms and pathogens for environmental control and general health issues.

For a successful application of the system, the glycan cantilever array sensor would need to demonstrate a high sensitivity, concentration dependence and specificity for the detected proteins and bacterial samples.

8.1 Specific Detection of Anti-viral Cyanovirin-N down to the Picomolar Level

Cyanovirin-N (CV-N), an 11 kDa mannose isolated from cyanobacteria with potent anti-viral activity against Human Immunodeficiency Virus (HIV) was chosen as the first application for the glycan cantilever array sensor. CV-N has been shown to irreversibly bind to the nonamannose arms decorating gp120, the heavily glycosylated envelope protein of HIV, preventing the conformational changes necessary for HIV – cell fusion.[67, 69, 70] A need for accurate and sensitive sensor systems for CV-N detection has been voiced to determine and assess its therapeutic potential.[127]

To this end, CV-N is detected on trimannose and nonamannose cantilever sensors against a galactose reference. The cantilever arrays were prepared as described in chapters 7.1 and 5.2. Again both sparse and dense coatings were tested to optimize carbohydrate densities for CV-N recognition. As CV-N is of smaller size than ConA possibly denser layers are required.

The signals for a typical injection with CV-N (0.1 mg/mL; 9.1 µM) on a trimannose and galactose functionalized array were recorded and the *average* and *differential* deflections plotted against time. All cantilevers react with negative deflections, the trimannose cantilevers however give significantly larger signals as the galactose layers, similar as was described for ConA in chapter 7.1. For both carbohydrates, the more sparsely coated cantilevers result in a slightly larger *average*, see figure 8.1, upper panel. Also the *differential* deflections were derived as before by subtractin g the galactose from the trimannose deflections. As was discussed in chapter 7.2, now a larger signal is observed for the denser coating, see figure 8.1, lower panel. All curves show a slight upward trend after the sample (shaded area in figure 8.1) has ended.

The larger mannose deflections are attributed to the high affinity of CV-N to mannoside residues.[67, 70] Similar as for ConA, see chapter 7.1, also nonspecific binding to other areas of the protein, the PEG linker or the cantilever surface may contribute to the signal. The deflections of the galactose cantilevers are related to purely nonspecific binding events. The specific and nonspecific protein recognition on the cantilever surface induces surface stress and in turn the observed cantilever deflection.[117-119]

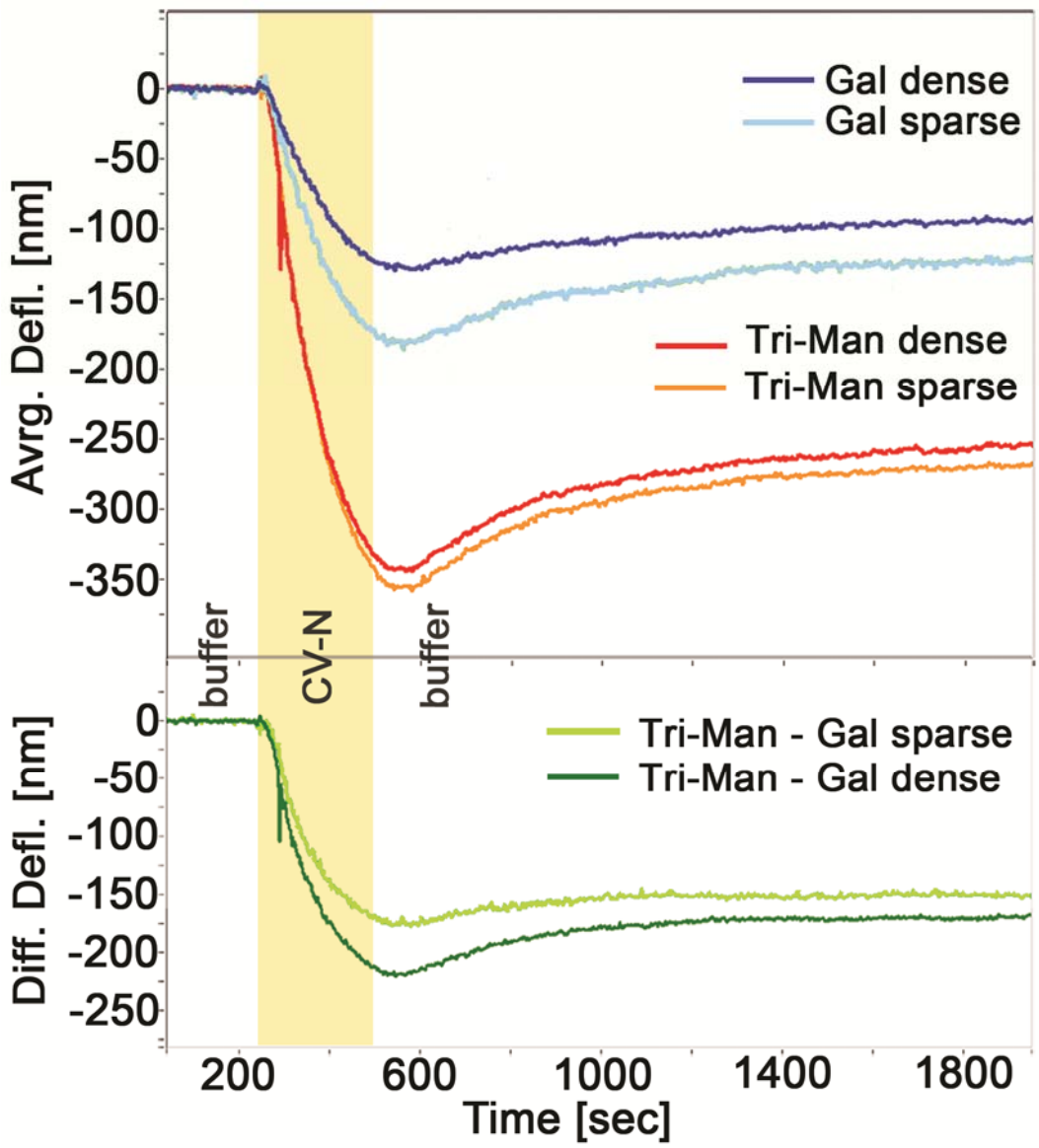

Figure 8.1. Detecting Cyanovirin-N. Upper panel: The *averaged* deflections of trimannose cantilevers in reaction to a CV-V sample of 0.1 mg/mL (9.1 μM) (shaded area) are about 3 – 4 times larger than the *averaged* deflections of the galactose reference signal. Lower panel: The corresponding *differential* deflection is assumed to reflect the specific binding. The slow recovery after return of the running buffer indicates the dissociation of nonspecific binding events. See text.

The larger *average* signals observed for the sparse layers are attributed to the less effective surface coating of the mannosides due to their larger monosaccharide headgroups in comparison to galactose. The resulting additional adsorption sites on the cantilever surface give rise to increased nonspecific

binding, which has also been explained in chapter 7.2. Since the *differential* signals represent only the specific part of the protein – carbohydrate recognition, here the denser coatings show the expected larger deflection. The observed upward deflection towards the end of the measurement may result from protein desorption due to the return of the running buffer.

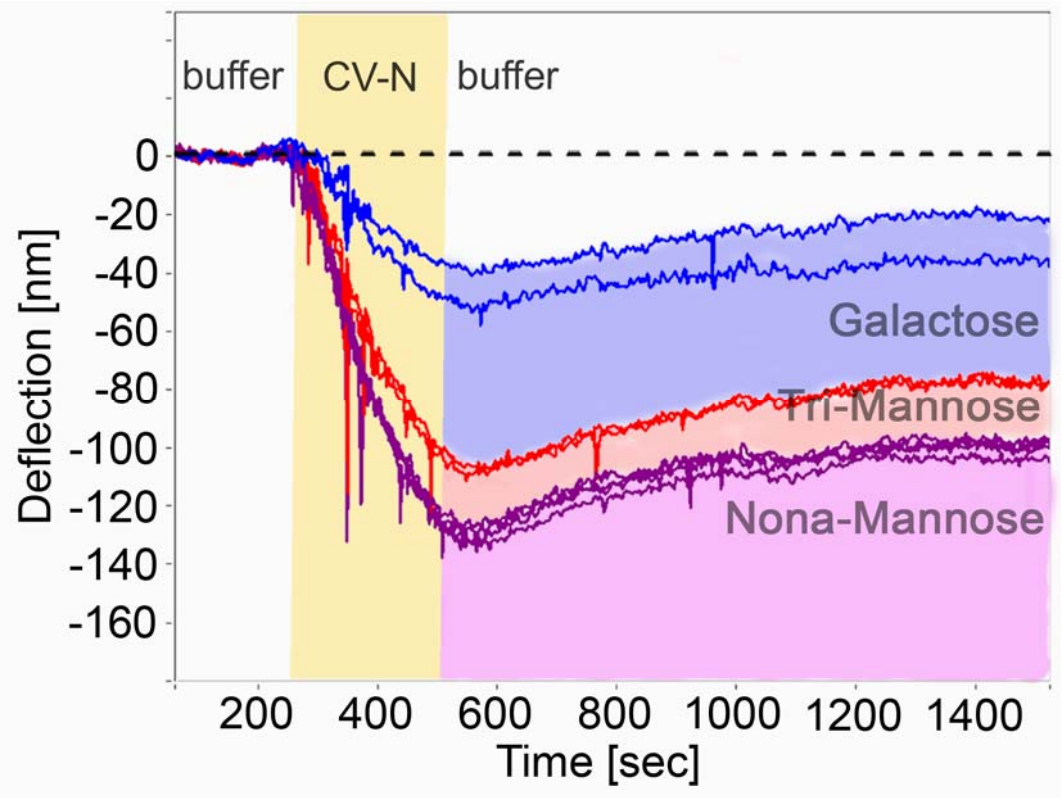

Figure 8.2 (next page). Sugar Discrimination by CV-N Binding. An array was functionalized with four nonamannose, two trimannose and two galactose cantilevers. Upon an injection of CV-N (0.1 mg/mL; 9.1 µM) the nonamannose cantilevers react about 20% stronger than the trimannose cantilevers, both clearly exceeding the galactose references. Due to increased multivalent and multisite binding, the sensor successfully discriminates between different oligomannose structures.

CV-N has been reported to have a high affinity to high mannose oligosaccharides.[67] Thus, a sensor was functionalized with nonamannose and trimannose as well as galactose cantilevers to test if these carbohydrates structures could be differentiated *via* the sensor signal. A sample injection with CV-N (0.1 mg/mL; 9.1 µM) resulted in deflections that were about 20% larger for

nonamannose than for trimannose cantilevers, and significantly smaller deflections for the galactose coatings, see figure 8.2. Presumably due to increased multisite and multivalent binding to nonamannose,[67] see chapter 5.1, more CV-N proteins bind to the nonamannose than to the trimannose sensors and induce the observed larger deflections. As discussed before, the signal for the galactose cantilevers is attributed to nonspecific protein binding. These results demonstrate that the sensor is able to discriminate CV-N recognition by different mannoside structures.

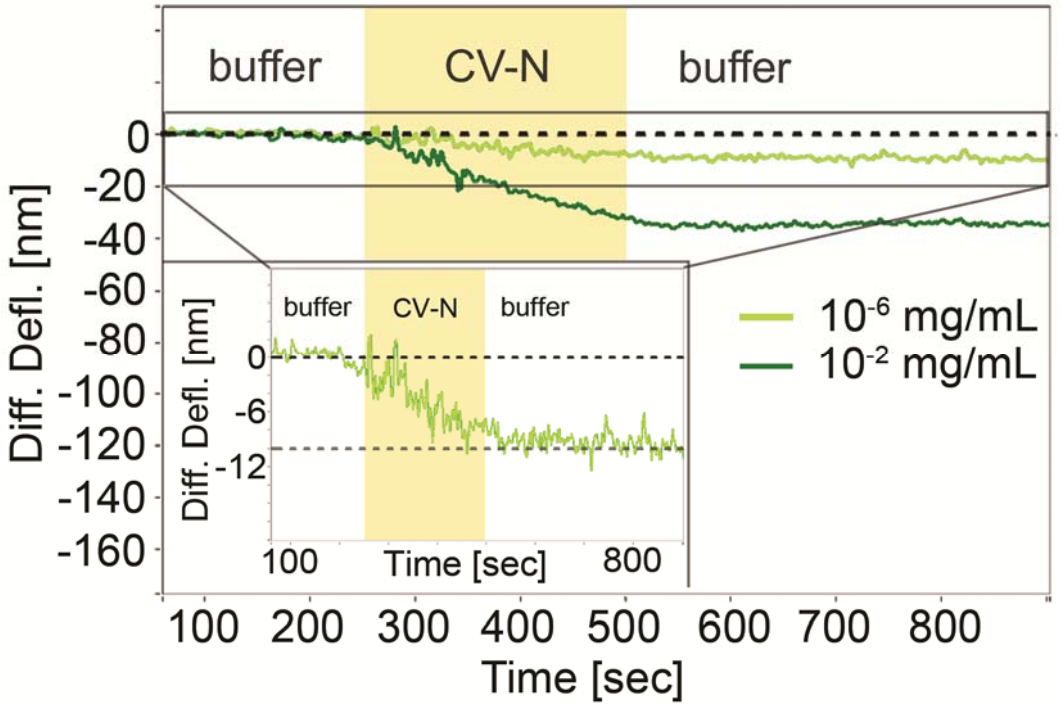

Figure 8.3. Sensitivity of CV-N Recognition. The sensor's sensitivity was successfully tested down to picomolar concentrations. Even after an injection of 10^{-2} mg/mL (0.9 µM) depicted by the dark green curve, the sensor shows a significant differential deflection, light green curve, for a concentration as low as 10^{-6} mg/mL (90.9 pM). The two injections were recorded in sequence but are overlaid here for comparability. The inset shows an enlargement of the picomolar resolution for better clarity. See text.

What is the limit of detection for CV-N proteins with this sensor?

To determine the sensor's sensitivity for very small amounts of protein, concentrations down to the picomolar range were tested. Even after a large

sample concentration of 10^{-2} mg/mL (0.9 µM), a subsequent injection with a very small concentration of 10^{-6} mg/mL (90.9 pM) resulted in a significant differential deflection of about 12 nm, see figure 8.3. Both injections are depicted overlaid for better comparability, while the inset again enlarges the injection with the small concentration to increase the graph's resolution. For CV-N recognition this experiment successfully demonstrates the sensor's sensitivity down to the picomolar regime. This low detection limit more than qualifies the sensor as tool in biological applications, as the relevant CV-N concentrations here lie in the nanomolar regime.[71, 127] The picomolar sensitivity of the glycan cantilever array sensor surpasses other cantilever assays that detect protein – protein binding[128, 129] and matches an immunosorbent competition assay especially developed for CV-N detection in plasma.[127]

How does the affinity of the CV-N binding reflected on the sensor signals?

For a detailed investigation of the sensor's performance, a series with increasing CV-N concentrations was conducted. Again larger differential deflection sizes were observed for larger sample concentrations, see figure 8.4. Comparing individual injections, an overview of six independent cantilever arrays showed that five out of six of the compared deflection sizes were reproducible within a standard deviation of 30%. With continuing preparation and handling experience the sensor performance improved and the standard deviations for the ConA signals discussed in chapter 7.1, which were derived after the CV-N experiments, already decreased to acceptable values below 20%.

To quantify the CV-N concentration dependence, a Langmuir isotherm, see chapters 4.4 and 7.1, was fitted to the results of the concentration series and plotted in the inset in figure 8.4. Three independent concentration series and subsequent Langmuir analyses yielded an average K_d value of (1.06 ± 0.69) µM for the CV-N – trimannose binding. As could be expected this value for a *tri*mannose is slightly better than a K_d value for a CV-N - *di*-mannoside binding that was published as 1.5 µM.[130] The sensor therefore accurately reproduces the binding affinity of the CV-N protein.

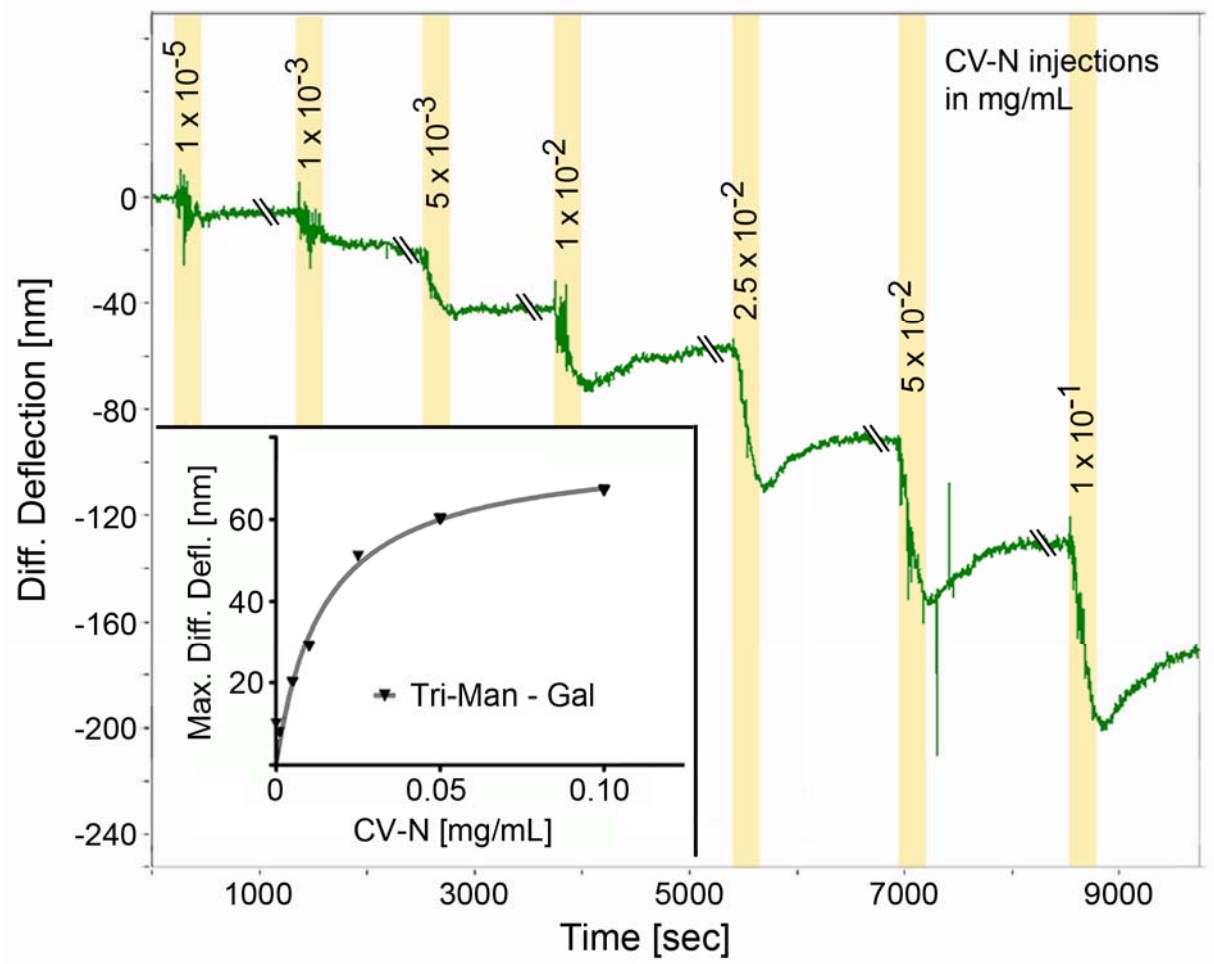

Figure 8.4. Concentration Dependence of CV-N Binding and Dissociation Constant. Increasing concentrations of CV-N samples were injected and the corresponding increasing signal sizes recorded. The inset shows the maximum differential deflections plotted against the respective concentration and fitted to a Langmuir isotherm to determine the dissociation constant K_d. See text.

Is CV-N specifically recognized by the mannose covered sensor surface?

The specificity of CV-N recognition by nonamannose and trimannose sensors was challenged by a competitive inhibition assay. First an injection (0.1 mg/mL; 9.1 µM) was performed in regular buffer. After adding free mannose (100 mM) to the running buffer a subsequent injection of the same concentration of 0.1 mg/mL (9.1 µM) then resulted in only about one third the original signal sizes for both carbohydrate structures, see figure 8.5. As was explained for the competitive inhibition with ConA in chapter 7.1, the free mannose competes with the mannosides on the sensor surface and thus reduces the binding events on the

cantilever surface and the resulting deflection. The reduction of the signal size in mannose buffer successfully verifies the specificity of the CV-N – carbohydrate binding.

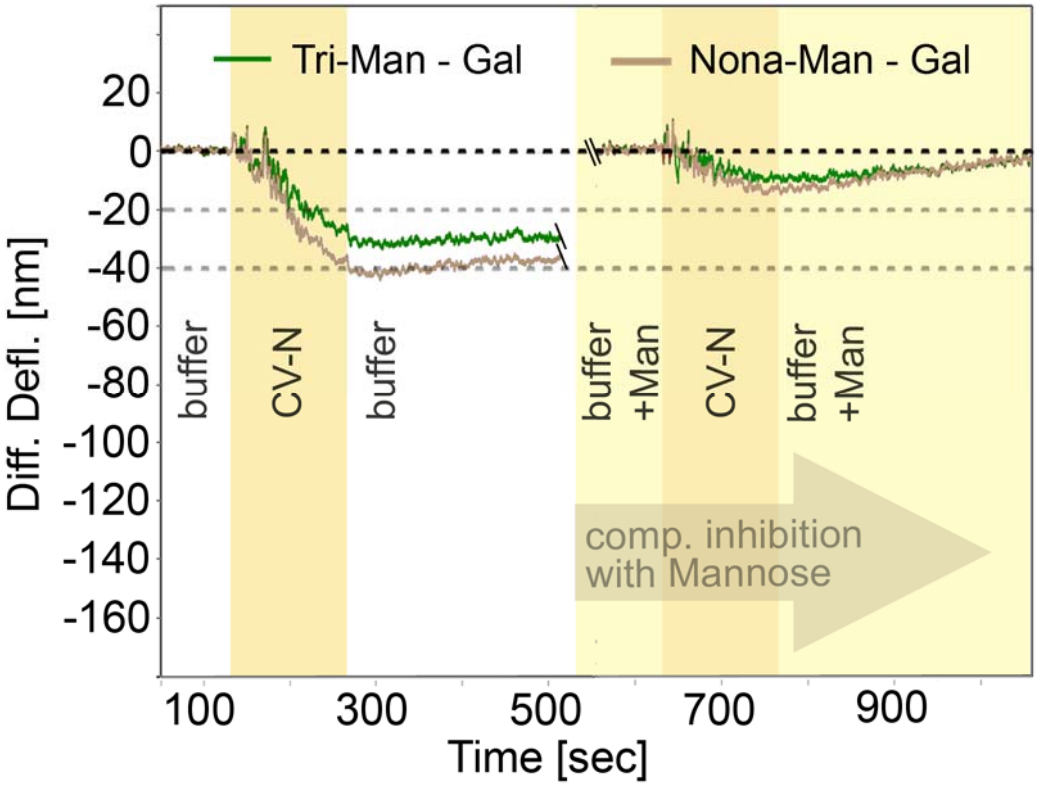

Figure 8.5. CV-N Binding Specificity. To confirm the specificity of the CV-N recognition, the binding is challenged with free mannose (100 mM) added to the running buffer. After a first reference injection (0.1 mg/mL; 9.1 μM), the differential deflection of a consecutive injection with the same CV-N concentration is reduced to about one third when mannose is added to the buffer. This reduction of the signal size confirms the specificity of the CV-N recognition. See text.

To examine the versatility and general usefulness of the sensor setup for lectin recognition, a second anti-viral protein currently under study for its potential to inhibit virus entry and thus HI-V infection, is tested. Scytovirin (SVN) is a 9.7 kDa protein isolated from the cyanobacterium *Scytonema varium* with high affinity for mannosides.[131] In contrast to CV-N, the binding mechanism for SVN has been reported to be distinctly different as both recognize different glycosidic linkages in high mannose oligosaccharides.[66]

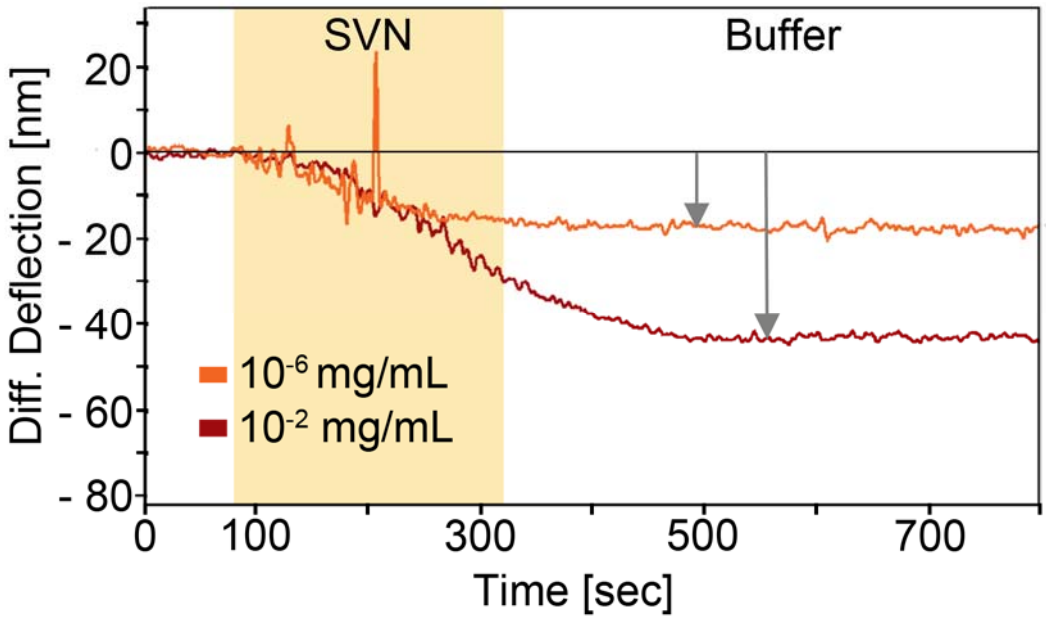

Figure 8.6. Detecting Scytovirin.[16] Two consecutive injections of SVN with a high (10^{-2} mg/mL; 1 µM) and a low concentration (10^{-6} mg/mL; 103 pM) were overlaid for comparison, see the two arrows for both concentrations. The sensor's ability to recognize SVN over four orders of magnitude, illustrates the generality of the sensor concept for the detection of clinically relevant proteins down to very low concentrations.

The differential signals of two subsequent injections of SVN with 10^{-2} mg/mL (0.9 µM) and 10^{-6} mg/mL (90.9 pM) were overlaid for comparison in figure 8.6. Two distinct signals were recorded that correspond in their size to the respective sample concentration. The cantilever bending is attributed to similar mechanisms of protein recognition and interactions as are described for ConA and CV-N in chapters 7.1 and 8.1, respectively. The observed sensitivity for SVN down to the picomolar level demonstrates that the sensor is able to successfully detect these proteins over a concentration range of four orders of magnitude. In combination, these results confirm the applicability of the method in detection assays for clinically relevant proteins that recognize different structural components of the carbohydrate sensing layers.

The glycan cantilever array sensor could be extended from the detection of the generic lectin ConA to the sensitive, concentration dependent and specific

[16] Measurement by A. Mader.

recognition of anti-viral CV-N. By successful detection of SVN, a second anti-viral protein, the generality of the sensor setup has been demonstrated. Thus a next logical step would be to test the sensor's potential in other areas where carbohydrate interactions dominate the recognition process, such as the detection of certain pathogens and bacteria.

8.2 Specific Detection of *Escherichia Coli* down to a few Cells per Sample

The sensitive recognition of microorganisms and pathogens is critical for environmental control and clinical applications.[5, 132] Traditional methods require several hours to days before the result becomes available,[133] here the short detection times of the cantilever sensor technique could provide a great advantage. To test the glycan cantilever array sensor setup established in chapter 7.1 for their potential, the recognition of three different strands of *Escherichia coli* (*E. coli*), see chapter 5.1, was investigated. All of these stands (ORN178, ORN206 and ORN208) recognize mannose via their phosphotransferase system (PTS). Additionally strand ORN178 is equipped with the mannose binding protein FimH at its pilii. ORN208 is equipped with the non-binding protein FimH*, while ORN206 contains no pilii at all. All of the measurements on E.coli recognition discussed in the following were performed by A. Mader for his diploma thesis.[78]

As a first feasibility test, a typical signal for a sample of *E.coli* strain ORN178 in an optical density (OD) of 0.05 on a cantilever array functionalized with nonamannose, trimannose and galactose was recorded and the *average* deflections plotted against time in figure 8.7, upper panel. All cantilevers reacted with compressive surface stress and corresponding negative deflections. The largest deflections were observed for the nonamannose layers, followed by trimannose and the considerably smaller signal of the galactose layers.

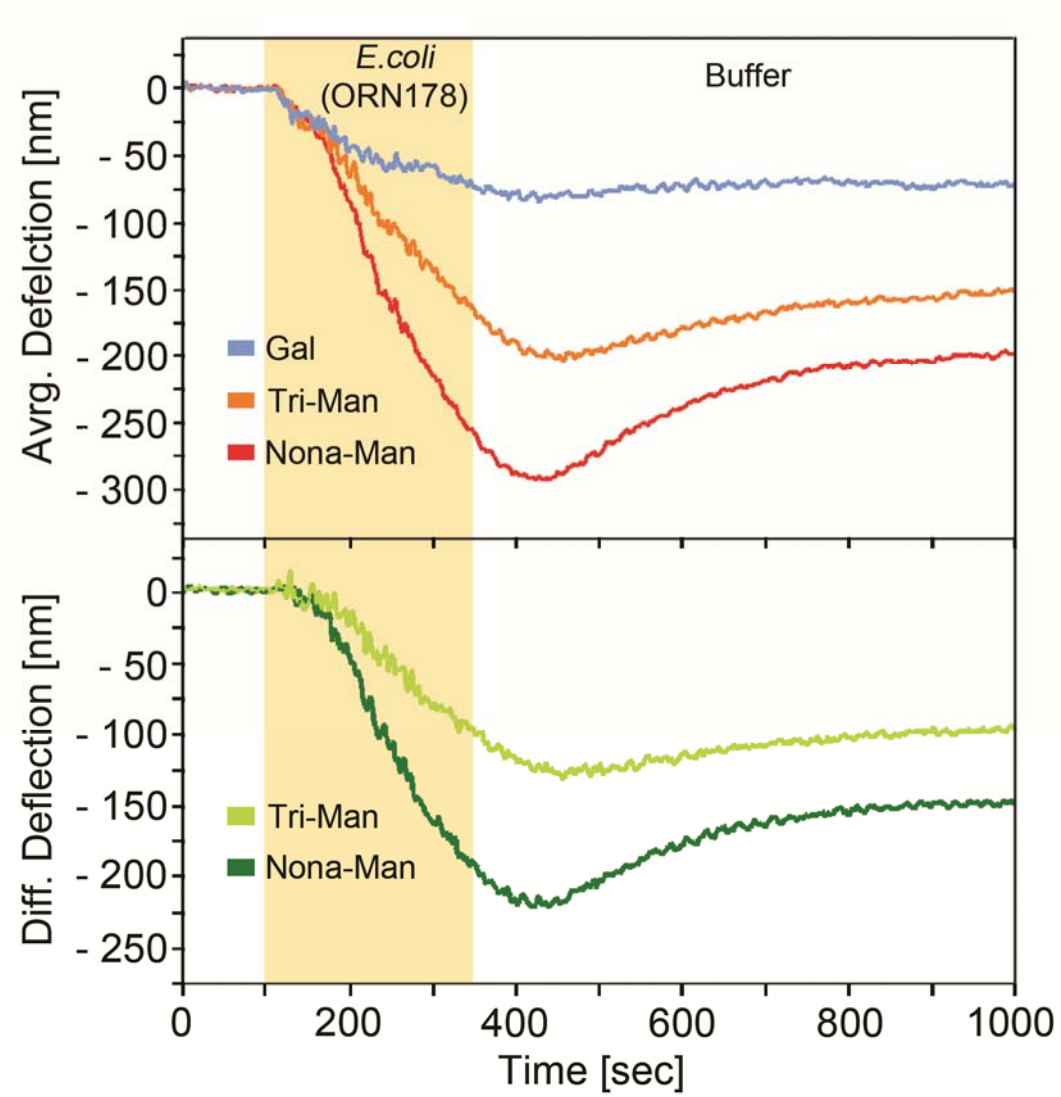

Figure 8.7. Specific Recognition of *E.coli* ORN178 and Carbohydrate Discrimination. Upper panel: A*veraged* deflections of galactose (Gal), trimannose (Tri-Man) and nonamannose (Nona-Man) cantilevers for an *E.coli* injection (shaded area) with an optical density (OD) of 0.05. The mannose sensors show significantly larger deflections than the galactose cantilevers, indicating specific binding by the mannose binding protein FimH at type I pilii. Due to increased multivalent and multisite binding, the nonamannose signal is stronger than the trimannose response, while the galactose signal is attributed to nonspecific binding. Lower panel: Corresponding *differential* deflection for nonamannose and trimannose recognition calculated by subtracting the galactose reference. The resulting signal representing the specific binding consistently shows a larger response for nonamannose than for trimannose cantilevers. See text.

The larger *average* signals for the mannose cantilevers can be explained by an increased number of binding events on these surfaces. This increased bacterial adhesion is attributed to the specific recognition of the FimH protein, which is located at the end of type I pilii, by the mannoside sensor coating. Additionally mannose binding *via* the phosphotransferase system (PTS) could contribute to the sensor signal, as the PTS is responsible for sugar uptake in *E.coli* and also contains mannose transporters. More multivalent and multisite binding events between nonamannose and bacterial cells increases the deflection for the nonamannose layers, similar as is described in chapters 7.1 and 8.1 for protein recognition. The galactose signal finally is attributed to nonspecific adhesion of bacteria on the galactose sugar moieties, the linker or the cantilever surface and possibly a less effective galactose transporter in the PTS system.[76] In all, the glycan cantilever array sensor successfully transduces the differences in binding strength of *E.coli* to the nonamannose, trimannose and galactose carbohydrate layers *via* larger and smaller cantilever deflection sizes.

Can different E.coli strains be differentiated?

To determine the versatility of the glycan cantilever array sensor for bacterial detection, the differential sensor signals for three *E.coli* strains differing in their mannose binding abilities, see also chapter 5.1, were compared on a nonamannose and galactose functionalized array. For this test, the related strains ORN178 (containing mannose binding FimH), ORN208 (containing nonbinding FimH*) and ORN206 (containing no pilii) were employed. Consecutive injections for each strain with an OD of 0.1 were recorded. The results are plotted in figure 8.8 overlaid on one timescale for better comparability.

The signal of mannose specific ORN178 resulted in a significantly higher deflection than that for ORN208. Strain ORN206 surprisingly gave the largest sensor response. The specific recognition of the nonamannose molecules by the FimH protein on the E.coli pilii as was described before leads to more binding events on the cantilever surface and consequently a larger signal for strain ORN178 than for strain ORN208. The signal for ORN208 in contrast is related to mannose recognition purely by the phosphotransferase system (PTS) of the *E.coli* cells.

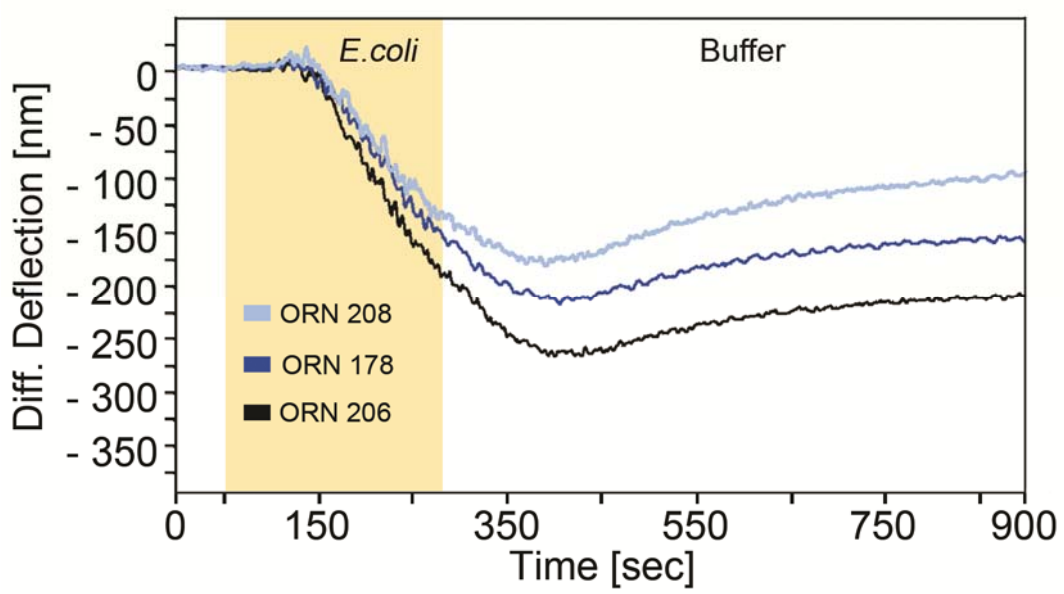

Figure 8.8. Differantiation of Three *E.coli* Strains. Differential deflections of a nonamannose cantilever sensor for three consecutive injections of the strains ORN178, ORN208 and ORN206 in this order with an OD of 0.1 plotted overlaid for better comparability. Strain ORN178 with mannose binding FimH shows a larger deflection than ORN208 with nonbinding FimH*. Conversely ORN206 shows an even larger signal, attributed to less steric hindrance due to the missing pilii.

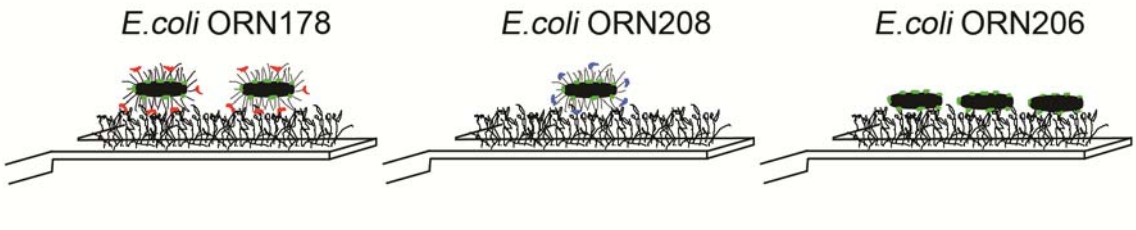

Figure 8.9. Schematic of *E.coli* Differentiation. Strain ORN178 can bind *via* the mannose specific FimH protein (red) at the end of its pilii, while in strain ORN208 the corresponding FimH* (blue) is rendered inactive. Both additionally recognize mannose *via* the sugar transporters of the PTS (green). Strain ORN206 does not contain obstructing pilii and thus binds in increasing number *via* the PTS transporters. See text.

The largest deflection that is observed for strain ORN206 could be explained by less steric repulsion due to the missing pilii, which could lead to increased binding on the cantilever surface *via* the mannose recognition of the PTS and a corresponding larger signal, compare the schematic representation in figure 8.9. Thus, the glycan cantilever array sensor is able to successfully discriminate three *E.coli* strains by their different equipment and accessibility of their respective mannose binding sites.

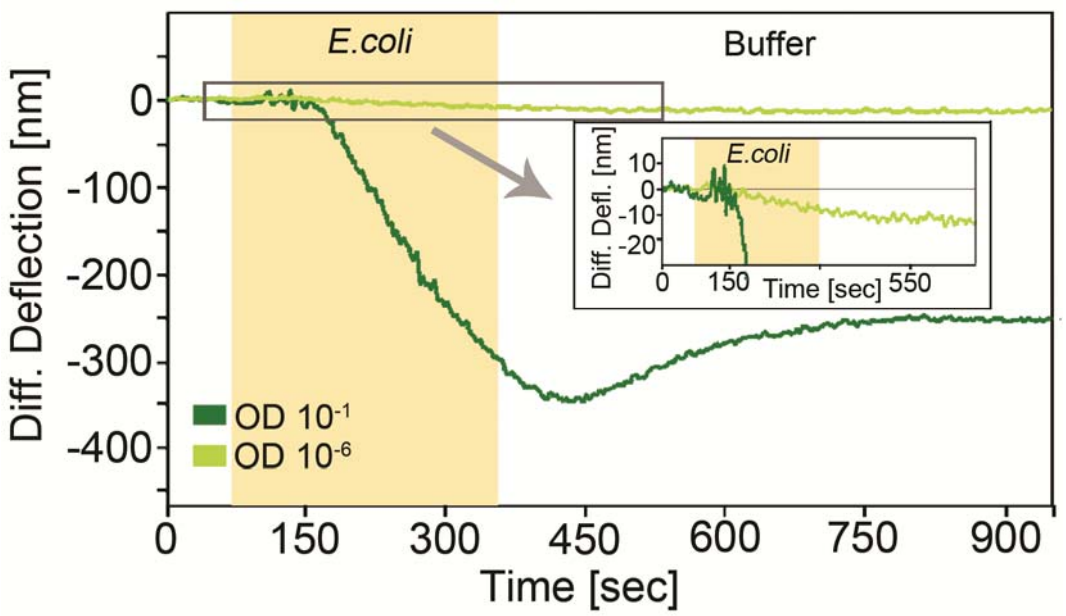

Figure 8.10. Sensitivity of *E.coli* Recognition. Even after an injection with high concentrations (OD 10^{-1}) the sensor detects a very low concentration (OD 10^{-6}) of strain ORN178, corresponding to about 200 cells per milliliter. Both sensor signals were overlaid for better comparability. The inset shows an enlarged section of the OD 10^{-6} injection, demonstrating the high sensitivity of the glycan cantilever array sensor for bacterial recognition.

What is the limit of detection for bacterial recognition?

The sensitivity of bacterial recognition was tested by comparing a high concentration of OD 10^{-1} from strain ORN178 with a subsequent measurement in an OD of only 10^{-6}, see figure 8.10. Even after these very high concentrations, the small sample concentration resulted in significant differential deflections. The enlarged representation depicted in the inset in figure 8.10 again demonstrates the sensor's high sensitivity down to very low bacteria concentrations.

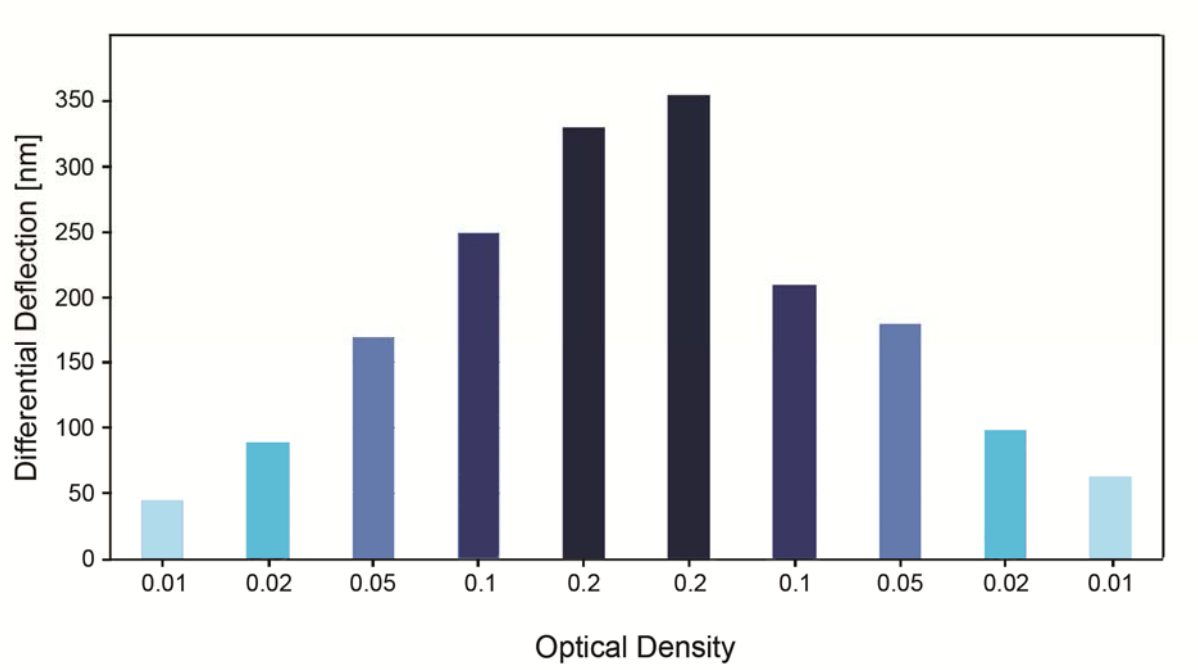

Figure 8.11. Concentration Dependence of Bacterial Recognition. The bar chart represents a series of experiments with increasing and decreasing concentrations of *E.coli* strain ORN208. Injections of the same concentrations, represented by the same color, deviate no more than 25% for the worst case and thus demonstrates the high reproducibility of the sensor response.

To determine the actual number of bacterial cells that are contained in these low sample concentrations, preliminary measurements showed that an optical density of 10^{-6} corresponds to about 200 cells per milliliter for this particular strain.[78] As a total sample volume of 100 µl was employed here, this means that only about 20 bacteria were available during the entire injection for binding to one of the eight individual cantilevers. Although further test are required to verify the exact cell count, already these result indicate an impressive limit of detection. Similar sensitivity could be obtained for the recognition of strain ORN208, so that the glycan cantilever array sensor offers a sensitivity that is one order of magnitude better than previously reported results for *E.coli* recognition with microarrays, piezoelectric excited cantilevers or carbohydrate functionalized quantum dots.[133-135]

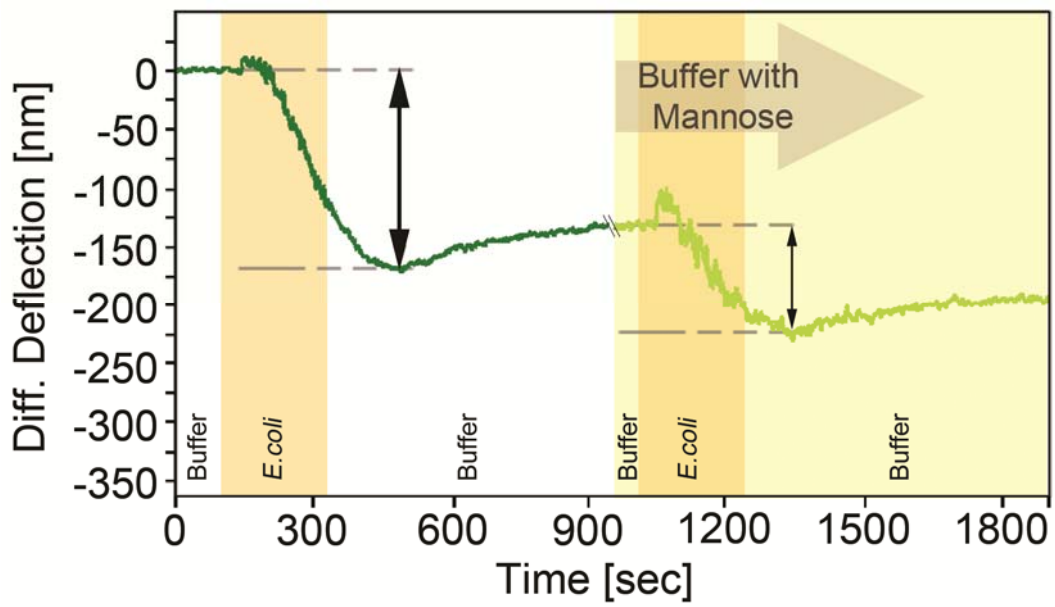

Figure 8.12. Specificity the *E.coli* – Nonamannose Binding. Following a reference injection with ORN178 (OD 0.05), free mannose (100 mM) was added to the running buffer and the experiment repeated with identical concentration (OD 0.05). For the second injection, the signal was reduced to about one half of the original size. The free mannose competes with the bacteria in solution, inhibiting *E.coli* binding to the cantilever surfaces and effectively reducing the signal size.

How good is the reproducibility of the signal size for specific E.coli *concentrations?*
A series of injections with increasing, followed by decreasing concentrations was performed to investigate the reliability of the signal sizes. The resulting differential deflections for each concentration, color coded in the bar chart depicted in figure 8.11, were in good agreement for each repetition. The overall evaluation of 25 signal pairs for identical concentrations showed a maximum deviation of 25%,[78] which compares well with the results reported for protein detection in chapters 7.1 and 8.1.

Are the bacteria specifically recognized by the glycan cantilever array sensor?

Finally, the specificity of the glycan cantilever array sensor for *E.coli* recognition was challenged by a competitive inhibition assay. First, an injection of strain ORN178 (OD 0.05) was performed to gain a reference signal size. Then, free mannose (100 mM) was added to the running buffer and the experiment

repeated with the identical bacteria concentration (OD 0.05). Now a signal size of only about one half was observed when compared to the previous reference injection, see figure 8.12. This signal reduction can be explained by the competition of the free mannose dissolved in the buffer with the mannosides on the cantilever surface. The resulting lower number of binding event in this situation consequently leads to the smaller observed deflection, effectively demonstrating the specificity of the glycan cantilever array sensor for *E.coli* recognition *via* its mannoside binding sites.

The specific detection and discrimination of three different *E.coli* strains down to only a few cells per sample volume extends the successful application of the glycan cantilever array sensor from protein recognition to mannose specific bacteria. This technique presents a first approach towards a low cost bacterial sensor with short processing times requiring no preliminary bacterial enrichment step that could easily be advanced to the detection of a broad range of other carbohydrate – pathogen interactions.

8.3 Conclusions

The specific and sensitive detection of the anti-viral lectin CV-N successfully expands the application of the glycan cantilever arrays to clinically relevant proteins. Larger and smaller sensor signals signify increased multisite and multivalent binding to nonamannose and trimannose functional layers, respectively, and thus allow the discrimination between different mannoside structures. Even after high sample concentrations, the sensor recognizes CV-N down to 90.9 pM which matches the limit of detection reported for an immunosorbent competition assay and easily allows the sensor's application in the biologically relevant regime of nanomolar concentrations. The dependence of the sensor signal on the sample concentration could be established *via* a concentration series, the corresponding Langmuir isotherm analysis resulted in an average K_d value of (1.06 ± 0.69) µM which agrees well with literature. A competitive inhibition assay with free mannose dissolved in the running buffer independently confirmed the specificity of the CV-N – mannoside recognition for this sensor design. In summary, the label-free detection and fast response times of the cantilever sensing method in combination with these results may provide

an advantage over immunosorbent and other techniques for pharmacokinetic studies of anti-viral proteins.

In a further study the glycan cantilever array sensor is extended to the sensitive and specific detection of bacteria. The three different *E. coli* strains ORN178, ORN208 and ORN206 can be discriminated according to their mannose binding ability *via* corresponding and reproducible deflection sizes. Samples with concentrations as low as approximately 20 cells per injection could be successfully detected, which is one order of magnitude better than other reported *E.coli* sensors. Finally, the specificity of the *E.coli* recognition could be verified by a competition assay with free mannose added to the running buffer. The glycan cantilever array sensor requires no sample pre or post processing and is characterized by simple sensor preparation and fast response times. In contrast, traditional techniques used for bacterial detection require culturing and post processing techniques like gel electrophoresis or polymerase chain reaction (PCR) for bacterial identification that altogether can take hours up to several days. The here demonstrated bacterial sensor thus offers a novel method for very sensitive, fast and accurate bacterial detection.

In conclusion, the glycan cantilever array biosensor developed in this work could be established by detailed experiments with the generic protein ConA and subsequently transferred to the sensitive and specific detection of mannose specific lectins and microorganisms critical for clinical and environmental safety applications. With advantages like label-free sensing, *in-situ* referencing and fast response times this technique may provide advantages or complementary support where such properties are critical in future applications.

9 Conclusions and Future Prospects

9.1 Heterogeneous Molecular Self-Organization

The use of multi component 2D molecular structures offers the convenient advantages of a bottom-up approach to surface functionalization. The first observation of all three forms of assembly, a pure host structure, host-guest inclusion and a templated polymorph pattern now unifies the different mechanisms of heterogeneous self-organization in only one molecular compound. This new material function opens up possibilities for two-step protocols that link the two previously separated motifs in heterogeneous self-organization. A variety of processes could be devised that allow switching between guest-selective inclusion and rearrangement of the pattern structure. The unity of two material functions in one compound could thus aid in areas of surface engineering where variable nano-patterning is desired. To this end, the shapes and properties of further guest molecules could be employed to influence and fine tune the molecular arrangement. As these experimental conditions seem critical to the assembly process, the use of substrates with different symmetries and work functions as well as solvents varying in their polar and protic properties could help to gain accurate control over the assembly mechanism and the resulting pattern function. In a more synthetic based approach the assembly properties of the Fréchet dendron molecules could be further exploited to act as adapter for functional groups linked to the molecular core. Thus various interaction sites could be engineered that act as specific receptors for guest components. Finally, as the understanding and control over the heterogeneous assembly mechanism progress, three, four or more component systems could aid in the development of molecular structures with very specific functions for applications in nano-engineering, catalysis or biosensing.

9.2 Glycan Cantilever Array Sensors

The here described glycan cantilever array sensor successfully establishes a new tool for the rapidly growing field of carbohydrate based research. The sensor sensitively and specifically detects mannose specific lectins and microorganisms of biological relevance. Using prerecorded fingerprints of certain bacterial species might enable screening for a variety of different microbes in complex sample background with this technique. Employing an extended set of high mannose oligosaccharides with different glycosidic linkages, detailed studies could be devised to learn more about the specific binding mechanisms of proteins and pathogens. The development of successful vaccines and prophylactic therapeutics from proteins like CV-N and SVN critically relies on such knowledge about the recognition processes. Other immunological active proteins like Dendritic Cell-Specific Intercellular adhesion molecule-3-Grabbing Non-integrin (DC-SIGN), which is currently under investigation in the group of Prof. Seeberger at the MPI Berlin for its ability to recognize and bind to mannose decorated viruses, could be studied with this device. Such assays in general could aid drug and vaccine development against mannose decorated pathogens like Human Immunodeficiency Virus (HIV), malaria parasites or anthrax spores.

Although the quality of the sensor setup has been demonstrated, the carbohydrate sensing layer might be further optimized by sophisticated blocking methods to better inhibit nonspecific binding and thereby further increase the sensitivity and signal reliability. Technical efforts into easy to handle system operation and fail-safe functionalization protocols could then enable the utilization of the technique in routine clinical and diagnostic applications.

A further effort should also be aimed at a detailed understanding of the origin of surface stress due to analyte interactions on the cantilever surface. Although the general principles are known and approaches exist to combine the various effects, additional details about the intermolecular interactions on the cantilever surface might provide a more general theoretical model. Such knowledge might aid the improvement of surface functionalization protocols and thus enhance the sensor quality. It might significantly advance the technique to be useful as standard lab equipment, similar as could be achieved for surface plasmon resonance (SPR) or quartz crystal microbalances (QCM).

9.3 Anti-Viral Protein and Bacteria Detection

To gain versatility, the current sensor setup comprised of a carbohydrate active layer and a lectin sample could be inverted so that now a protein coating embodies the sensing layer. Many reported cantilever based assays have proven the feasibility of a protein sensing layers for antigen – antibody recognition. Cells, viruses and microorganisms decorated with glycoconjugates could then be detected. Since many functions of these cell carbohydrates are yet unknown, such an assay could aid to clarify their significance and push the progress of vaccine and drug development.

As the biocompatibility of synthetic materials advances, implantable, miniaturized cantilever sensor chips might be envisioned for the continuous monitoring of metabolites. However, the properties of suitable readout methods, for example based on the piezoelectric effect, would first need to improve to ensure high sensitivity and reliability of the sensor signal.

In all, with a comparable performance like surface plasmon resonance (SPR) and quartz crystal microbalances (QCM) the glycan cantilever array sensor offers advantages like label-free sensing, *in-situ* referencing and fast response times that could serve well in future research focused or clinical laboratories for applications investigating binding mechanisms or in high sensitivity pathogen detection.

References

[1] Whitesides, G. M.; Ostuni, E.; Takayama, S.; Jiang, X. and Ingber, D. E. Soft Lithography in Biology and Biochemistry. *Annu. Rev. Biomed. Eng.* **2001,** 3, 335-373.

[2] Arlett, J. L.; Myers, E. B. and Roukes, M. L. Comparative Advantages of Mechanical Biosensors. *Nat Nano* **2011,** 6, 203-215.

[3] Fritz, J. Cantilever Biosensors. *Analyst* **2008,** 133, 855-863.

[4] Dover, J. E.; Hwang, G. M.; Mullen, E. H.; Prorok, B. C. and Suh, S.-J. Recent Advances in Peptide Probe-Based Biosensors for Detection of Infectious Agents. *J. Microbiol. Methods* **2009,** 78, 10-19.

[5] Buchapudi, K. R.; Huang, X.; Yang, X.; Ji, H.-F. and Thundat, T. Microcantilever Biosensors for Chemicals and Bioorganisms. *Analyst* **2011,** 136, 1539-1556.

[6] Camazine, S., *Self-Organization in Biological Systems*. Princeton University Press: Princeton, N.J. ; Oxford, 2001; p viii, 538 p., 8 p. of plates.

[7] Ortega Lorenzo, M.; Baddeley, C. J.; Muryn, C. and Raval, R. Extended Surface Chirality from Supramolecular Assemblies of Adsorbed Chiral Molecules. *Nature* **2000,** 404, 376-379.

[8] Barth, J. V. Molecular Architectonic on Metal Surfaces. *Annu. Rev. Phys. Chem.* **2007,** 58, 375-407.

[9] Rohr, C.; Balbás Gambra, M.; Gruber, K.; Constable, E. C.; Frey, E.; Franosch, T. and Hermann, B. A. Molecular Jigsaw: Pattern Diversity Encoded by Elementary Geometrical Features. *Nano Lett.* **2010,** 10, 833-837.

[10] Lehn, J. M. Toward Self-Organization and Complex Matter. *Science* **2002,** 295, 2400-2403.

[11] Bonifazi, D.; Mohnani, S. and Llanes-Pallas, A. Supramolecular Chemistry at Interfaces: Molecular Recognition on Nanopatterned Porous Surfaces. *Chemistry – A European Journal* **2009,** 15, 7004-7025.

[12] Theobald, J. A.; Oxtoby, N. S.; Phillips, M. A.; Champness, N. R. and Beton, P. H. Controlling Molecular Deposition and Layer Structure with Supramolecular Surface Assemblies. *Nature* **2003,** 424, 1029-1031.

[13] Lei, S.; Tahara, K.; Feng, X.; Furukawa, S.; De Schryver, F. C.; Müllen, K.; Tobe, Y. and De Feyter, S. Molecular Clusters in Two-Dimensional Surface-Confined Nanoporous Molecular Networks: Structure, Rigidity, and Dynamics. *J. Am. Chem. Soc.* **2008,** 130, 7119-7129.

[14] Schull, G.; Douillard, L.; Fiorini-Debuisschert, C.; Charra, F.; Mathevet, F.; Kreher, D. and Attias, A.-J. Single-Molecule Dynamics in a Self-Assembled 2d Molecular Sieve. *Nano Lett.* **2006,** 6, 1360-1363.

[15] Griessl, S. J. H.; Lackinger, M.; Jamitzky, F.; Markert, T.; Hietschold, M. and Heckl, W. M. Incorporation and Manipulation of Coronene in an Organic Template Structure. *Langmuir* **2004,** 20, 9403-9407.

[16] Furukawa, S.; Tahara, K.; De Schryver, F. C.; Van der Auweraer, M.; Tobe, Y. and De Feyter, S. Structural Transformation of a Two-Dimensional Molecular Network in Response to Selective Guest Inclusion. *Angew. Chem. Int. Ed.* **2007,** 46, 2831-2834.

[17] Bléger, D.; Kreher, D.; Mathevet, F.; Attias, A.-J.; Schull, G.; Huard, A.; Douillard, L.; Fiorini-Debuischert, C. and Charra, F. Surface Noncovalent Bonding for Rational Design of Hierarchical Molecular Self-Assemblies. *Angew. Chem. Int. Ed.* **2007,** 46, 7404-7407.

[18] Yoshimoto, S.; Honda, Y.; Ito, O. and Itaya, K. Supramolecular Pattern of Fullerene on 2d Bimolecular "Chessboard" Consisting of Bottom-up Assembly of Porphyrin and Phthalocyanine Molecules. *J. Am. Chem. Soc.* **2007,** 130, 1085-1092.

[19] Gong, J.-R.; Yan, H.-J.; Yuan, Q.-H.; Xu, L.-P.; Bo, Z.-S. and Wan, L.-J. Controllable Distribution of Single Molecules and Peptides within Oligomer Template Investigated by Stm. *J. Am. Chem. Soc.* **2006,** 128, 12384-12385.

[20] Ziegler, C.; Göpel, W.; Hämmerle, H.; Hatt, H.; Jung, G.; Laxhuber, L.; Schmidt, H. L.; Schütz, S.; Vögtle, F. and Zell, A. Bioelectronic Noses: A Status Report. Part Ii. *Biosens. Bioelectron.* **1998,** 13, 539-571.

[21] Miles, M. Probing the Future. *Science* **1997,** 277, 1845-1847.

[22] Gimzewski, J. K.; Gerber, C.; Meyer, E. and Schlittler, R. R. Observation of a Chemical Reaction Using a Micromechanical Sensor. *Chem. Phys. Lett.* **1994,** 217, 589-594.

[23] Carrascosa, L. G.; Moreno, M.; Álvarez, M. and Lechuga, L. M. Nanomechanical Biosensors: A New Sensing Tool. *TrAC, Trends Anal. Chem.* **2006,** 25, 196-206.

[24] Lang, H. P.; Hegner, M. and Gerber, C. Cantilever Array Sensors. *Mater. Today* **2005,** 8, 30-36.

[25] Waggoner, P. S. and Craighead, H. G. Micro- and Nanomechanical Sensors for Environmental, Chemical, and Biological Detection. *Lab Chip* **2007,** 7, 1238-1255.

[26] Zhang, J.; Lang, H. P.; Huber, F.; Bietsch, A.; Grange, W.; Certa, U.; McKendry, R.; Guntherodt, H. J.; Hegner, M. and Gerber, C. Rapid and Label-Free Nanomechanical Detection of Biomarker Transcripts in Human Rna. *Nat Nano* **2006,** 1, 214-220.

[27] Fritz, J.; Baller, M. K.; Lang, H. P.; Rothuizen, H.; Vettiger, P.; Meyer, E.; Güntherodt, H.-J.; Gerber, C. and Gimzewski, J. K. Translating Biomolecular Recognition into Nanomechanics. *Science* **2000,** 288, 316-318.

[28] Hansen, K. M.; Ji, H.-F.; Wu, G.; Datar, R.; Cote, R.; Majumdar, A. and Thundat, T. Cantilever-Based Optical Deflection Assay for Discrimination of DNA Single-Nucleotide Mismatches. *Anal. Chem.* **2001,** 73, 1567-1571.

[29] Park, J.; Ryu, J.; Choi, S. K.; Seo, E.; Cha, J. M.; Ryu, S.; Kim, J.; Kim, B. and Lee, S. H. Real-Time Measurement of the Contractile Forces of Self-Organized Cardiomyocytes on Hybrid Biopolymer Microcantilevers. *Anal. Chem.* **2005,** 77, 6571-6580.

[30] Gfeller, K. Y.; Nugaeva, N. and Hegner, M. Micromechanical Oscillators as Rapid Biosensor for the Detection of Active Growth of Escherichia Coli. *Biosens. Bioelectron.* **2005,** 21, 528-533.

[31] Skottrup, P. D.; Nicolaisen, M. and Justesen, A. F. Towards on-Site Pathogen Detection Using Antibody-Based Sensors. *Biosens. Bioelectron.* **2008,** 24, 339-348.

[32] Pera, I. and Fritz, J. Sensing Lipid Bilayer Formation and Expansion with a Microfabricated Cantilever Array. *Langmuir* **2006,** 23, 1543-1547.

[33] Ndieyira, J. W.; Watari, M.; Barrera, A. D.; Zhou, D.; Vogtli, M.; Batchelor, M.; Cooper, M. A.; Strunz, T.; Horton, M. A.; Abell, C.; Rayment, T.; Aeppli, G. and McKendry, R. A. Nanomechanical Detection of Antibiotic-Mucopeptide Binding in a Model for Superbug Drug Resistance. *Nat Nano* **2008,** 3, 691-696.

[34] Wu, G.; Datar, R. H.; Hansen, K. M.; Thundat, T.; Cote, R. J. and Majumdar, A. Bioassay of Prostate-Specific Antigen (Psa) Using Microcantilevers. *Nat Biotech* **2001,** 19, 856-860.

[35] Varki, A.; Cummings, R. D.; Esko, J. D.; Freeze, H. H.; Stanley, P.; Bertozzi, C. R.; Hart, G. W. and Etzler, M. E., *Essentials of Glycobiology*. 2nd ed.; Cold Spring Harbor Laboratory Press, USA: 2009.

[36] Lowe, J. B. Glycosylation, Immunity, and Autoimmunity. *Cell* **2001,** 104, 809-812.

[37] Kansas, G. S. Selectins and Their Ligands: Current Concepts and Controversies. *Blood* **1996,** 88, 3259-3287.

[38] Danishefsky, S. J. and Allen, J. R. From the Laboratory to the Clinic: A Retrospective on Fully Synthetic Carbohydrate-Based Anticancer Vaccines. *Angew. Chem. Int. Ed.* **2000,** 39, 836-863.

[39] Tamborrini, M.; Werz, D. B.; Frey, J.; Pluschke, G. and Seeberger, P. H. Anti-Carbohydrate Antibodies for the Detection of Anthrax Spores. *Angew. Chem. Int. Ed.* **2006,** 45, 6581-6582.

[40] Seeberger, P. H. and Werz, D. B. Automated Synthesis of Oligosaccharides as a Basis for Drug Discovery. *Nat. Rev. Drug. Discov.* **2005,** 4, 751-763.

[41] Seeberger, P. H. and Werz, D. B. Synthesis and Medical Applications of Oligosaccharides. *Nature* **2007,** 446, 1046-1051.

[42] Bertozzi, C. R. and Kiessling, L. L. Chemical Glycobiology. *Science* **2001,** 291, 2357-2364.

[43] Plante, O. J.; Palmacci, E. R. and Seeberger, P. H. Automated Solid-Phase Synthesis of Oligosaccharides. *Science* **2001,** 291, 1523-1527.

[44] Blixt, O.; Head, S.; Mondala, T.; Scanlan, C.; Huflejt, M. E.; Alvarez, R.; Bryan, M. C.; Fazio, F.; Calarese, D.; Stevens, J.; Razi, N.; Stevens, D. J.; Skehel, J. J.; van Die, I.; Burton, D. R.; Wilson, I. A.; Cummings, R.; Bovin, N.; Wong, C.-H. and Paulson, J. C. Printed Covalent Glycan Array for Ligand Profiling of Diverse Glycan Binding Proteins. *Proc. Natl. Acad. Sci. U. S. A.* **2004,** 101, 17033-17038.

[45] Fukui, S.; Feizi, T.; Galustian, C.; Lawson, A. M. and Chai, W. Oligosaccharide Microarrays for High-Throughput Detection and Specificity Assignments of Carbohydrate-Protein Interactions. *Nat Biotech* **2002,** 20, 1011-1017.

[46] Ratner, D. M.; Adams, E. W.; Disney, M. D. and Seeberger, P. H. Tools for Glycomics: Mapping Interactions of Carbohydrates in Biological Systems. *ChemBioChem* **2004,** 5, 1375-1383.

[47] Paulson, J. C.; Blixt, O. and Collins, B. E. Sweet Spots in Functional Glycomics. *Nat. Chem. Biol.* **2006,** 2, 238-248.

[48] Horlacher, T. and Seeberger, P. H. Carbohydrate Arrays as Tools for Research and Diagnostics. *Chem. Soc. Rev.* **2008,** 37, 1414-1422.

[49] Bardeen, J. Tunnelling from a Many-Particle Point of View. *Phys. Rev. Lett.* **1961,** 6, 57-&.

[50] Tersoff, J. and Hamann, D. R. Theory and Application for the Scanning Tunneling Microscope. *Phys. Rev. Lett.* **1983,** 50, 1998-2001.

[51] Hofer, W. A.; Foster, A. S. and Shluger, A. L. Theories of Scanning Probe Microscopes at the Atomic Scale. *Reviews of Modern Physics* **2003,** 75, 1287.

[52] Chen, C. J., *Introduction to Scanning Tunneling Microscopy*. Oxford University Press: New York ; Oxford, 1993; p xxii, 412 p., 31 p. of plates.

[53] Cyr, D. M.; Venkataraman, B.; Flynn, G. W.; Black, A. and Whitesides, G. M. Functional Group Identification in Scanning Tunneling Microscopy of Molecular Adsorbates. *The Journal of Physical Chemistry* **1996,** 100, 13747-13759.

[54] Kohn, W. Nobel Lecture: Electronic Structure of Matter-Wave Functions and Density Functionals. *Reviews of Modern Physics* **1999,** 71, 1253-1266.

[55] Crandall, S. H. and Lardner, T., *An Introduction to the Mechanics of Solids*. McGraw-Hill Science/Engineering/Math: 1999.

[56] Goeders, K. M.; Colton, J. S. and Bottomley, L. A. Microcantilevers: Sensing Chemical Interactions Via Mechanical Motion. *Chem. Rev.* **2008,** 108, 522-542.

[57] Stoney, G. G. The Tension of Metallic Films Deposited by Electrolysis. *Proceedings of the Royal Society of London. Series A* **1909,** 82, 172-175.

[58] Janssen, G. C. A. M.; Abdalla, M. M.; van Keulen, F.; Pujada, B. R. and van Venrooy, B. Celebrating the 100th Anniversary of the Stoney Equation for Film Stress: Developments from Polycrystalline Steel Strips to Single Crystal Silicon Wafers. *Thin Solid Films* **2009,** 517, 1858-1867.

[59] Brantley, W. A. Calculated Elastic Constants for Stress Problems Associated with Semiconductor Devices. *J. Appl. Phys.* **1973,** 44, 534-535.

[60] Shu, W.; Laue, E. D. and Seshia, A. A. Investigation of Biotin-Streptavidin Binding Interactions Using Microcantilever Sensors. *Biosens. Bioelectron.* **2007,** 22, 2003-2009.

[61] Sader, J. E. Surface Stress Induced Deflections of Cantilever Plates with Applications to the Atomic Force Microscope: Rectangular Plates. *J. Appl. Phys.* **2001,** 89, 2911-2921.

[62] Sushko, M. L.; Harding, J. H.; Shluger, A. L.; McKendry, R. A. and Watari, M. Physics of Nanomechanical Biosensing on Cantilever Arrays. *Adv. Mater.* **2008,** 20, 3848-3853.

[63] Stachowiak, J. C.; Yue, M.; Castelino, K.; Chakraborty, A. and Majumdar, A. Chemomechanics of Surface Stresses Induced by DNA Hybridization. *Langmuir* **2005,** 22, 263-268.

[64] Constable, E. C.; Graber, S.; Hermann, B. A.; Housecroft, C. E.; Malarek, M. S. and Scherer, L. J. The Introduction of Asymmetry into Alkyl-Decorated Fréchet-Type Dendrons. *Eur. J. Org. Chem.* **2008,** 2008, 2644-2651.

[65] Merz, L.; Güntherodt, H. J.; Scherer, L. J.; Constable, E. C.; Housecroft, C. E.; Neuburger, M. and Hermann, B. A. Octyl-Decorated Fréchet-Type Dendrons: A General Motif for Visualisation of Static and Dynamic Behaviour Using Scanning Tunnelling Microscopy? *Chemistry – A European Journal* **2005,** 11, 2307-2318.

[66] Ratner, D. M. and Seeberger, P. H. Carbohydrate Microarrays as Tools in Hiv Glycobiology. *Curr. Pharm. Des.* **2007,** 13, 173-183.

[67] Shenoy, S. R.; Barrientos, L. G.; Ratner, D. M.; O'Keefe, B. R.; Seeberger, P. H.; Gronenborn, A. M. and Boyd, M. R. Multisite and Multivalent Binding between Cyanovirin-N and Branched Oligomannosides: Calorimetric and Nmr Characterization. *Chem. Biol.* **2002,** 9, 1109-1118.

[68] Wang, J. L.; Cunningham, B. A. and Edelman, G. M. Unusual Fragments in the Subunit Structure of Concanavalin A. *Proceedings of the National Academy of Sciences* **1971,** 68, 1130-1134.

[69] Boyd, M.; Gustafson, K.; McMahon, J.; Shoemaker, R.; O'Keefe, B.; Mori, T.; Gulakowski, R.; Wu, L.; Rivera, M.; Laurencot, C.; Currens, M.; Cardellina, J., 2nd; Buckheit, R., Jr; Nara, P.; Pannell, L.; Sowder, R., 2nd and Henderson, L. Discovery of Cyanovirin-N, a Novel Human Immunodeficiency Virus- Inactivating Protein That Binds Viral Surface Envelope Glycoprotein Gp120: Potential Applications to Microbicide Development. *Antimicrob. Agents Chemother.* **1997,** 41, 1521-1530.

[70] Bolmstedt, A. J.; O'Keefe, B. R.; Shenoy, S. R.; McMahon, J. B. and Boyd, M. R. Cyanovirin-N Defines a New Class of Antiviral Agent Targeting N-Linked, High-Mannose Glycans in an Oligosaccharide-Specific Manner. *Mol. Pharmacol.* **2001,** 59, 949-954.

[71] Bewley, C. A. and Otero-Quintero, S. The Potent Anti-Hiv Protein Cyanovirin-N Contains Two Novel Carbohydrate Binding Sites That Selectively Bind to Man8 D1d3 and Man9 with Nanomolar Affinity: Implications for Binding to the Hiv Envelope Protein Gp120. *J. Am. Chem. Soc.* **2001,** 123, 3892-3902.

[72] Russell, P. W. and Orndorff, P. E. Lesions in Two Escherichia Coli Type 1 Pilus Genes Alter Pilus Number and Length without Affecting Receptor Binding. *J. Bacteriol.* **1992,** 174, 5923-5935.

[73] Harris, S. L.; Spears, P. A.; Havell, E. A.; Hamrick, T. S.; Horton, J. R. and Orndorff, P. E. Characterization of Escherichia Coli Type 1 Pilus Mutants with Altered Binding Specificities. *J. Bacteriol.* **2001,** 183, 4099-4102.

[74] Hamrick, T. S.; Harris, S. L.; Spears, P. A.; Havell, E. A.; Horton, J. R.; Russell, P. W. and Orndorff, P. E. Genetic Characterization of Escherichia Coli Type 1 Pilus Adhesin Mutants and Identification of a Novel Binding Phenotype. *J. Bacteriol.* **2000,** 182, 4012-4021.

[75] Deutscher, J.; Francke, C. and Postma, P. W. How Phosphotransferase System-Related Protein Phosphorylation Regulates Carbohydrate Metabolism in Bacteria. *Microbiol. Mol. Biol. Rev.* **2006,** 70, 939-1031.

[76] Bachmann, B. J. Pedigrees of Some Mutant Strains of *Escherichia Coli* K-12. *Bacteriol. Rev.* **1972,** 36, 525-557.

[77] Stolz, B.; Huber, M.; Marković-Housley, Z. and Erni, B. The Mannose Transporter of Escherichia Coli. Structure and Function of the Iiabman Subunit. *J. Biol. Chem.* **1993,** 268, 27094-27099.

[78] Mader, A. Biosensorik Für Biochemische Erkennungsprozesse. Diploma Thesis, Ludwig-Maximilians-Universität München, München, 2011.

[79] Batra, I. P.; Garcia, N.; Rohrer, H.; Salemink, H.; Stoll, E. and Ciraci, S. A Study of Graphite Surface with Stm and Electronic-Structure Calculations. *Surf. Sci.* **1987,** 181, 126-138.

[80] Pong, W. T. and Durkan, C. A Review and Outlook for an Anomaly of Scanning Tunnelling Microscopy (Stm): Superlattices on Graphite. *Journal of Physics D-Applied Physics* **2005,** 38, R329-R355.

[81] Cai, C.; Bösch, M.; Bosshard, C.; Müller, B.; Tao, Y.; Kündig, A.; Weckesser, J.; Barth Johannes, V.; Bürgi, L.; Jeandupeux, O.; Kiy, M.; Biaggio, I.; Liakatas, I.; Kern, K. and Günter, P., Self-Assembly Growth of Organic Thin Films and Nanostructures by Molecular Beam Deposition. In *Anisotropic Organic Materials*, American Chemical Society: 2001; Vol. 798, pp 34-49.

[82] Meyer, E.; Overney, R.; Brodbeck, D.; Howald, L.; uuml; thi, R.; Frommer, J. and ntherodt, H. J. Friction and Wear of Langmuir-Blodgett Films Observed by Friction Force Microscopy. *Phys. Rev. Lett.* **1992,** 69, 1777.

[83] De Feyter, S. and De Schryver, F. C. Self-Assembly at the Liquid/Solid Interface: Stm Reveals. *The Journal of Physical Chemistry B* **2005,** 109, 4290-4302.

[84] Deegan, R. D.; Bakajin, O.; Dupont, T. F.; Huber, G.; Nagel, S. R. and Witten, T. A. Capillary Flow as the Cause of Ring Stains from Dried Liquid Drops. *Nature* **1997,** 389, 827-829.

[85] Braun, T. and et al. Digital Processing of Multi-Mode Nano-Mechanical Cantilever Data. *Journal of Physics: Conference Series* **2007,** 61, 341.

[86] Binnig, G.; Rohrer, H.; Gerber, C. and Weibel, E. Surface Studies by Scanning Tunneling Microscopy. *Phys. Rev. Lett.* **1982,** 49, 57.

[87] Binnig, G. and Smith, D. P. E. Single-Tube 3-Dimensional Scanner for Scanning Tunneling Microscopy. *Rev. Sci. Instrum.* **1986,** 57, 1688-1689.

[88] Crommie, M. F.; Lutz, C. P. and Eigler, D. M. Confinement of Electrons to Quantum Corrals on a Metal-Surface. *Science* **1993,** 262, 218-220.

[89] Crommie, M. F.; Lutz, C. P. and Eigler, D. M. Imaging Standing Waves in a 2-Dimensional Electron-Gas. *Nature* **1993,** 363, 524-527.

[90] Bode, M. Spin-Polarized Scanning Tunnelling Microscopy. *Rep. Prog. Phys.* **2003,** 66, 523-582.

[91] Rosei, F.; Schunack, M.; Naitoh, Y.; Jiang, P.; Gourdon, A.; Laegsgaard, E.; Stensgaard, I.; Joachim, C. and Besenbacher, F. Properties of Large Organic Molecules on Metal Surfaces. *Prog. Surf. Sci.* **2003,** 71, 95-146.

[92] Hla, S. W. and Rieder, K. H. Stm Control of Chemical Reactions: Single-Molecule Synthesis. *Annu. Rev. Phys. Chem.* **2003,** 54, 307-330.

[93] Lorenzo, M. O.; Baddeley, C. J.; Muryn, C. and Raval, R. Extended Surface Chirality from Supramolecular Assemblies of Adsorbed Chiral Molecules. Nature 2000, 404, 376-379.

[94] Hermann, B. A.; Scherer, L. J.; Housecroft, C. E. and Constable, E. C. Self-Organized Monolayers: A Route to Conformational Switching and Read-out of Functional Supramolecular Assemblies by Scanning Probe Methods. Adv. Funct. Mater. 2006, 16, 221-235.

[95] Moresco, F.; Meyer, G.; Rieder, K. H.; Tang, H.; Gourdon, A. and Joachim, C. Conformational Changes of Single Molecules Induced by Scanning Tunneling Microscopy Manipulation: A Route to Molecular Switching. Phys. Rev. Lett. 2001, 86, 672-675.

[96] Morgenstern, K. Isomerization Reactions on Single Adsorbed Molecules. Acc. Chem. Res. 2009, 42, 213-223.

[97] Hofer, W. A. Challenges and Errors: Interpreting High Resolution Images in Scanning Tunneling Microscopy. Prog. Surf. Sci. 2003, 71, 147-183.

[98] Ramos, D.; Tamayo, J.; Mertens, J.; Calleja, M. and Zaballos, A. Origin of the Response of Nanomechanical Resonators to Bacteria Adsorption. J. Appl. Phys. 2006, 100, 106105-3.

[99] McKendry, R.; Zhang, J.; Arntz, Y.; Strunz, T.; Hegner, M.; Lang, H. P.; Baller, M. K.; Certa, U.; Meyer, E.; Güntherodt, H.-J. and Gerber, C. Multiple Label-Free Biodetection and Quantitative DNA-Binding Assays on a Nanomechanical Cantilever Array. Proc. Natl. Acad. Sci. U. S. A. 2002, 99, 9783-9788.

[100] Gruber, K.; Rohr, C.; Scherer, L. J.; Malarek, M. S.; Constable, E. C. and Hermann, B. A. A Versatile Fréchet-Dendron Compound Unifies Host-Guest and Templated Heterogeneous Self-Assembly. Adv. Mater. 2011, 23, 2195-2198.

[101] Rohr, C. Rules of Molecular Self-Organization: Emergence, Control and Predictability. Ph.D. Thesis, Ludwig-Maximilians-Universität München, München, 2011.

[102] Rohr, C.; Gruber, K.; Malarek, M. S.; Constable, E. C. and Hermann, B. A. Multi-Hierarchical Assembly Via Molecular Flexibility. submitted.

[103] Rohr, C.; Gruber, K.; Malarek, M. S.; Scherer, L. J.; Constable, E. C. and Hermann, B. A. Giving Ostwald´S Law of Stages a New Complexity Perspective. submitted.

[104] Rohr, C.; Gambra, M. B.; Gruber, K.; Constable, E. C.; Frey, E.; Franosch, T. and Hermann, B. A. Molecular Jigsaw: Pattern Diversity Encoded by Elementary Geometrical Features. *Nano Lett.* **2010,** 10, 833-837.

[105] Rohr, C.; Gambra, M. B.; Gruber, K.; Hohl, C.; Malarek, M. S.; Scherer, L. J.; Constable, E. C.; Franosch, T. and Hermann, B. A. Predicting the Influence of a P2-

Symmetric Substrate on Molecular Self-Organization with an Interaction-Site Model. *Chem. Commun.* **2011,** 47, 1800-1802.

[106] Balbás Gambra, M.; Rohr, C.; Gruber, K.; Hermann, B. A. and Franosch, T. Predicting Patterns for Molecular Self-Organization on Surfaces Using Interaction-Site Models. *submitted*.

[107] Rohr, C.; Gruber, K.; Malarek, M. S.; Scherer, L. J.; Constable, E. C. and Hermann, B. A. Surface Control of Chirality, Orientation and Hierarchical Assembly of Self-Organized Monolayers. *submitted*.

[108] Adisoejoso, J.; Tahara, K.; Okuhata, S.; Lei, S.; Tobe, Y. and De Feyter, S. Two-Dimensional Crystal Engineering: A Four-Component Architecture at a Liquid–Solid Interface. *Angew. Chem.* **2009,** 121, 7403-7403.

[109] Lei, S.; Tahara, K.; De Schryver, F. C.; Van der Auweraer, M.; Tobe, Y. and De Feyter, S. One Building Block, Two Different Supramolecular Surface-Confined Patterns: Concentration in Control at the Solid–Liquid Interface. *Angew. Chem. Int. Ed.* **2008,** 47, 2964-2968.

[110] Rappe, A. K.; Casewit, C. J.; Colwell, K. S.; Goddard, W. A. and Skiff, W. M. Uff, a Full Periodic Table Force Field for Molecular Mechanics and Molecular Dynamics Simulations. *J. Am. Chem. Soc.* **1992,** 114, 10024-10035.

[111] Clark, S. J.; Segall, M. D.; Pickard, C. J.; Hasnip, P. J.; Probert, M. I. J.; Refson, K. and Payne, M. C. *Z. Kristallogr.* **2005,** 220.

[112] Kampschulte, L.; Lackinger, M.; Maier, A.-K.; Kishore, R. S. K.; Griessl, S.; Schmittel, M. and Heckl, W. M. Solvent Induced Polymorphism in Supramolecular 1,3,5-Benzenetribenzoic Acid Monolayers. *The Journal of Physical Chemistry B* **2006,** 110, 10829-10836.

[113] Mamdouh, W.; Uji-i, H.; Ladislaw, J. S.; Dulcey, A. E.; Percec, V.; De Schryver, F. C. and De Feyter, S. Solvent Controlled Self-Assembly at the Liquid-Solid Interface Revealed by Stm. *J. Am. Chem. Soc.* **2005,** 128, 317-325.

[114] Höhl, C. Lösungsmittel-Induzierte Phasenvielfalt Selbstorganisierter Monolagen Von Fréchet-Dendronen Untersucht Mit Rastertunnelmikroskopie. Diploma Thesis, Ludwig-Maximilians-Universität München, München, 2008.

[115] Gruber, K.; Horlacher, T.; Castelli, R.; Mader, A.; Seeberger, P. H. and Hermann, B. A. Cantilever Array Sensors Detect Specific Carbohydrate–Protein Interactions with Picomolar Sensitivity. *ACS Nano* **2011,** 5, 3670-3678.

[116] Haiss, W. Surface Stress of Clean and Adsorbate-Covered Solids. *Rep. Prog. Phys.* **2001,** 64, 591.

[117] Moulin, A. M.; O'Shea, S. J.; Badley, R. A.; Doyle, P. and Welland, M. E. Measuring Surface-Induced Conformational Changes in Proteins. *Langmuir* **1999,** 15, 8776-8779.

[118] Dutta, P.; Tipple, C. A.; Lavrik, N. V.; Datskos, P. G.; Hofstetter, H.; Hofstetter, O. and Sepaniak, M. J. Enantioselective Sensors Based on Antibody-Mediated Nanomechanics. *Anal. Chem.* **2003,** 75, 2342-2348.

[119] Koeser, J. and et al. Time Resolved Analysis of Molecular Interactions Using Nanomechanical Cantilever Sensors. *Journal of Physics: Conference Series* **2007,** 61, 612.

[120] Dam, T. K.; Roy, R.; Das, S. K.; Oscarson, S. and Brewer, C. F. Binding of Multivalent Carbohydrates to Concanavalin a Anddioclea Grandiflora Lectin. *J. Biol. Chem.* **2000,** 275, 14223-14230.

[121] Zhang, Y.; Luo, S.; Tang, Y.; Yu, L.; Hou, K.-Y.; Cheng, J.-P.; Zeng, X. and Wang, P. G. Carbohydrate–Protein Interactions by "Clicked" Carbohydrate Self-Assembled Monolayers. *Anal. Chem.* **2006,** 78, 2001-2008.

[122] Park, S.; Lee, M.-r.; Pyo, S.-J. and Shin, I. Carbohydrate Chips for Studying High-Throughput Carbohydrate–Protein Interactions. *J. Am. Chem. Soc.* **2004,** 126, 4812-4819.

[123] Tang, Y.; Mernaugh, R. and Zeng, X. Nonregeneration Protocol for Surface Plasmon Resonance: Study of High-Affinity Interaction with High-Density Biosensors. *Anal. Chem.* **2006,** 78, 1841-1848.

[124] Braun, T.; Ghatkesar, M. K.; Backmann, N.; Grange, W.; Boulanger, P.; Letellier, L.; Lang, H.-P.; Bietsch, A.; Gerber, C. and Hegner, M. Quantitative Time-Resolved Measurement of Membrane Protein-Ligand Interactions Using Microcantilever Array Sensors. *Nat Nano* **2009,** 4, 179-185.

[125] Concentris GmbH. Application Note 03-LS. Detection of Specific DNA Sequences under Different Hybridisation Conditions. http://www.concentris.com (accessed May 2011).

[126] Lis, H. and Sharon, N. Lectins: Carbohydrate-Specific Proteins That Mediate Cellular Recognition. *Chem. Rev.* **1998,** 98, 637-674.

[127] Bringans, S. D.; O'Keefe, B. R.; Bray, M.; Whitehouse, C. A. and Boyd, M. R. Development of a Fluorescent Microplate Assay for Determining Cyanovirin-N Levels in Plasma. *Anal. Bioanal. Chem.* **2004,** 380, 269-274.

[128] Yue, M.; Stachowiak, J. C.; Lin, H.; Datar, R.; Cote, R. and Majumdar, A. Label-Free Protein Recognition Two-Dimensional Array Using Nanomechanical Sensors. *Nano Lett.* **2008,** 8, 520-524.

[129] Backmann, N.; Zahnd, C.; Huber, F.; Bietsch, A.; Plückthun, A.; Lang, H.-P.; Güntherodt, H.-J.; Hegner, M. and Gerber, C. A Label-Free Immunosensor Array Using Single-Chain Antibody Fragments. *Proc. Natl. Acad. Sci. U. S. A.* **2005,** 102, 14587-14592.

[130] Liang, P.-H.; Wang, S.-K. and Wong, C.-H. Quantitative Analysis of Carbohydrate−Protein Interactions Using Glycan Microarrays: Determination of Surface and Solution Dissociation Constants. *J. Am. Chem. Soc.* **2007,** 129, 11177-11184.

[131] Bokesch, H. R.; O'Keefe, B. R.; McKee, T. C.; Pannell, L. K.; Patterson, G. M. L.; Gardella, R. S.; Sowder, R. C.; Turpin, J.; Watson, K.; Buckheit, R. W. and Boyd, M. R. A Potent Novel Anti-Hiv Protein from the Cultured Cyanobacterium Scytonema Varium†. *Biochemistry* **2003,** 42, 2578-2584.

[132] Zourob, M.; Elwary, S. and Turner, A. P. F., *Principles of Bacterial Detection: Biosensors, Recognition Receptors and Microsystems*. 2008; Vol. XXXII, p 970.

[133] Disney, M. D. and Seeberger, P. H. The Use of Carbohydrate Microarrays to Study Carbohydrate-Cell Interactions and to Detect Pathogens. *Chem. Biol.* **2004,** 11, 1701-1707.

[134] Campbell, G. A.; Uknalis, J.; Tu, S.-I. and Mutharasan, R. Detect of Escherichia Coli O157:H7 in Ground Beef Samples Using Piezoelectric Excited Millimeter-Sized Cantilever (Pemc) Sensors. *Biosens. Bioelectron.* **2007,** 22, 1296-1302.

[135] Mukhopadhyay, B.; Martins, M. B.; Karamanska, R.; Russell, D. A. and Field, R. A. Bacterial Detection Using Carbohydrate-Functionalised Cds Quantum Dots: A Model Study Exploiting E. Coli Recognition of Mannosides. *Tetrahedron Lett.* **2009,** 50, 886-889.

List of Figures

Figure 4.1. Perturbation Approach at the Tip-Sample Interface.
Figure 4.2. The Tunneling Current.
Figure 4.3. Pure Bending of a Cantilever Beam.

Figure 5.1. Molecular Structures for Heterogeneous Self-organization.
Figure 5.2. Carbohydrate Structures for Sensing Layers.
Figure 5.3. Functionalization of a Cantilever Array Sensor.
Figure 5.4. Scheme of a Scanning Tunneling Microscope.
Figure 5.5. The Liquid Handling System of the Cantisens Research Platform.
Figure 5.6. Optical Readout Method for Cantilever Deflection.

Figure 6.1. Assembly Motifs in Heterogeneous Molecular Self-Organization.
Figure 6.2. Hole Size Engineering.
Figure 6.3. Host Pattern and Host – Guest Inclusion.
Figure 6.4. Dynamics of Adamantane Inclusions.
Figure 6.5. Templated Polymorph Assembly.
Figure 6.6. MM energy minimization of the templated assembly.
Figure 6.7. Separation of Interaction Types:

Figure 7.1. Functionalization of a Cantilever Array.
Figure 7.2. Specific ConA Recognition and Sugar Discrimination.
Figure 7.3. Sensitivity of the Cantilever Sensor for ConA Binding.
Figure 7.4. Concentration Dependence of the ConA Recognition and Dissociation Constant.
Figure 7.5. ConA Binding in BSA Background.
Figure 7.6. ConA Binding Specificity.

Figure 7.7. Nonspecific Adsorption and Layer Densities.
Figure 7.8. Hybridization of ssDNA strands.
Figure 7.9. Layer Density of ssDNA Functionalized Array.
Figure 7.10. Model of the Molecular Processes on the Cantilever Surface.

Figure 8.1. Detecting Cyanovirin-N.
Figure 8.2. Sugar Discrimination by CV-N Binding.
Figure 8.3. Sensitivity of CV-N Recognition.
Figure 8.4. Concentration Dependence of CV-N Binding and Dissociation Constant.
Figure 8.5. CV-N Binding Specificity.
Figure 8.6. Detecting Scytovirin.
Figure 8.7. Specific Recognition of *E.coli* ORN178 and Carbohydrate Discrimination.
Figure 8.8. Discrimination of three *E.coli* strains.
Figure 8.9. Schematic of *E.coli* Differentiation.
Figure 8.10. Sensitivity of *E.coli* Recognition.
Figure 8.11. Concentration Dependence of Bacterial Recognition.
Figure 8.12. Specificity the *E.coli* – Nonamannose Binding.

Publications

1. **Gruber, K**; Rohr, C.; Scherer, L. J.; Malarek, M. S.; Constable, E. C. and Hermann, B. A. A Versatile Fréchet-Dendron Compound Unifies Host-Guest and Templated Heterogeneous Self-Assembly. *Adv. Mater.* **2011**, 23, 2195-2198. DOI: 10.1002/adma.201100013

2. **Gruber, K**; Horlacher, T; Castelli, R; Mader, A; Seeberger, P. H. and Hermann, B. A. Cantilever Array Sensors Detect Specific Carbohydrate–Protein Interactions with Picomolar Sensitivity. *ACS Nano* **2011**, 5, 3670-3678. DOI: 10.1021/nn103626q

3. Rohr, C.; Balbás Gambra, M.; **Gruber, K.**; Constable, E. C.; Frey, E.; Franosch, T. and Hermann, B. A. Molecular Jigsaw: Pattern Diversity Encoded by Elementary Geometrical Features. *Nano Lett.* **2010**, 10, 833-837. DOI: 10.1021/nl903225j

4. Rohr, C.; Balbas Gambra, M.; **Gruber, K.**; Höhl, C.; Malarek, M. S.; Scherer, L. J.; Constable, E. C.; Franosch, T. and Hermann, B. A. Predicting the Influence of a p2-Symmetric Substrate on Molecular Self-Organization with an Interaction-Site Model. *Chem. Commun.* **2011**, 47, 1800-1802. DOI: 10.1039/C0CC03603J

5. **Gruber, K**; Hermann, B. A and Seeberger, P. H. Sensing Carbohydrate – Protein Interactions at Picomolar Concentrations Using Cantilever Arrays. *Angew. Chem. Int. Ed. DFG IYC Edition* **2011**, 50, A46-A51. DOI: 10.002/anie.201105813

6. Balbás Gambra, M.; Rohr, C.; **Gruber, K.**; Hermann, B. A. and Franosch, T. Predicting Patterns for Molecular Self-Organization on Surfaces using Interaction-Site Models. Submitted.

7. Rohr, C.; **Gruber, K.**; Malarek, M. S.; Scherer, L. J.; Constable, E. C. and Hermann, B. A. Trapping of Transient states: Giving Ostwald´s Law of Stages a new Complexity Perspective. Submitted.

8. Rohr, C.; **Gruber, K.**; Malarek, M. S.; Constable, E. C. and Hermann, B. A. Multi-Hierarchical Assembly via Molecular Flexibility. Submitted.

9. Rohr, C.; **Gruber, K.**; Malarek, M. S.; Scherer, L. J.; Constable, E. C. and Hermann, B. A. Surface Control of Chirality, Orientation and Hierarchical Assembly of Self-Organized Monolayers. Submitted.

10. Mader, A; **Gruber, K**; Horlacher, T; Castelli, R; Hermann, B. A; Seeberger, P. H.; Räder, J. O. and Leiser, M. Discrimination of *Escherichia coli* Strains using Glycan Cantilever Array Sensors. *Nano Lett.* **2012**, 12, 420-423. DOI: 10.1021/nl203736u.

Acknowledgments

This work would not have been possible without the valuable help and advice of several special people. In particular I want to thank…

- … my supervisor Bianca Hermann for introducing me to the scientific topics discussed here and the continuing support.
- … Joachim Rädler for adopting us into his group and taking over as my supervisor when that became necessary.
- … Stefan Thalhamer for writing the second opinion and the other members of my Ph.D. committee.
- … Carsten Rohr for the best working relationship, with lots of emergent properties.
- … Johannes Büttner for freely sharing his technical know-how and personal charm.
- … Andreas Mader for contributing the results on the *E.coli* detection during the course of his diploma thesis.
- … Madeleine Leisner for graciously supporting our work on the E.colis with know-how as well as valuable S1 lab space.
- … Peter Seeberger and Tim Horlacher for providing the carbohydrate samples and the fruitful collaboration.
- … Ed Constable, Michael Malarek and Lukas Scherer for providing the Fréchet dendrons.
- … the staff of the Walther-Meissner-Institute for the technical and administrative support.
- … the Elite Network of Bavaria for the Research Scholarship that ensured the financial basis and scientific freedom for this work.
- … last but not least my family and my partner for the incredible support throughout the years. I am very lucky to have you.